UNIVERSITY OF ALBERTA

MULTIMODE DAMPING OF SYNCHRONOUS GENERATOR TRANSIENTS USING SELF-TUNING CONTROL

BY

WILLIAM ERIC NORUM ©

A thesis submitted to the Faculty of Graduate Studies and Research in partial fulfillment of the requirements for the degree of Doctor of Philosophy.

DEPARTMENT OF ELECTRICAL ENGINEERING

EDMONTON, ALBERTA

FALL 1991

National Library of Canada
Canadian Theses Service

Ottawa, Canada
K1A 0N4

Bibliothèque nationale du Canada
Service des thèses canadiennes

The author has granted an irrevocable non-exclusive licence allowing the National Library of Canada to reproduce, loan, distribute or sell copies of his/her thesis by any means and in any form or format, making this thesis available to interested persons.

The author retains ownership of the copyright in his/her thesis. Neither the thesis nor substantial extracts from it may be printed or otherwise reproduced without his/her permission.

L'auteur a accordé une licence irrévocable et non exclusive permettant à la Bibliothèque nationale du Canada de reproduire, prêter, distribuer ou vendre des copies de sa thèse de quelque manière et sous quelque forme que ce soit pour mettre des exemplaires de cette thèse à la disposition des personnes intéressées.

L'auteur conserve la propriété du droit d'auteur qui protège sa thèse. Ni la thèse ni des extraits substantiels de celle-ci ne doivent être imprimés ou autrement reproduits sans son autorisation.

ISBN 0-315-70026-2

Canadä

UNIVERSITY OF ALBERTA

RELEASE FORM

NAME OF AUTHOR: William Eric Norum

TITLE OF THESIS: Multimode Damping of Synchronous Generator Transients
Using Self-Tuning Control

DEGREE: Doctor of Philosophy

YEAR THIS DEGREE GRANTED: Fall, 1991

Permission is hereby granted to the University of Alberta Library to reproduce single copies of this thesis and to lend or sell such copies for private, scholarly or scientific research purposes only.

The author reserves all other publication and other rights in association with the copyright in the thesis, and except as hereinbefore provided neither the thesis nor any substantial portion thereof may be printed or otherwise reproduced in any material form whatever without the author's prior written permission.

SIGNED: W. Eric Norum

ADDRESS: 9714 - 88th Avenue
Edmonton, Alberta

DATE: October 8, 1991

UNIVERSITY OF ALBERTA

FACULTY OF GRADUATE STUDIES AND RESEARCH

The undersigned certify that they have read, and recommend to the Faculty of Graduate Studies and Research for acceptance, a thesis entitled **Multimode Damping of Synchronous Generator Transients Using Self-Tuning Control**, submitted by William Eric Norum in partial fulfillment of the requirements for the degree of Doctor of Philosophy.

K. E. Bollinger (Supervisor)

Keith Stromsmoe

K. A. Stromsmoe

G. S. Christensen

S. L. Shah

RJ Fleming

R. J. Fleming (External Examiner)

Date: October 8/91

Abstract

This thesis presents techniques that allow a generalized minimum variance self-tuning power system stabilizer to damp the local and interarea oscillatory modes of a generator connected to a power generation and load pool. The multimode damping provided by the self-tuning power system stabilizer in response to stochastic and deterministic disturbances is described as are the effects of multivariable feedback.

The research reported in this thesis emphasized procedures for improving the identification portion of the adaptive control algorithm. This involved the development of frequency and time domain techniques to obtain models of the simulated power system. The sensitivity of the on-line identification algorithm within the self-tuning stabilizer was investigated using the models developed by the off-line studies as a reference. The improvement yielded by numerically stable techniques was studied using single and double precision implementations of both the conventional and factorized covariance update in the recursive least squares identification algorithm. Quantization effects of practical analog to digital and digital to analog converters were found to have little effect on the operation of the self-tuning stabilizer.

This research has led to the testing of the self-tuning stabilizer on a 400 MW thermal-powered synchronous generator. Results of preliminary field tests were encouraging and some examples are presented.

Acknowledgement

The author wishes to thank his supervisor, Professor K. E. Bollinger, for the encouragement, guidance and support given throughout this research project.

A special expression of gratitude is made to the author's family, in particular to Barbara, Carl and Stephen Norum, whose patience and understanding made this work possible.

Contents

1 Introduction **1**

1.1 Background to Power System Damping 1

1.2 Fixed-Parameter Stabilizer Tuning Methods 5

1.3 Generator System Identification 10

1.4 Adaptive Power System Stabilizers 14

1.5 Outline of this Thesis 20

2 Review of the Pertinent Theory **22**

2.1 Recursive Least Squares Parameter Identification 22

2.1.1 U-D Factorization of the Covariance Matrix 31

2.1.2 Exponential Forgetting 40

2.1.3 Restricted Exponential Forgetting 43

2.2 Generalized Minimum Variance Control 48

2.2.1 k-Step Ahead Output Predictor 49

2.2.2 Generalized Minimum Variance Control Strategy for Systems with Known Parameters 54

2.2.3 Self-Tuning Generalized Minimum Variance Control 60

2.3 Examples Illustrating Concepts and Algorithms 62

2.3.1 Example of U-D Factorization 62

2.3.2 Example of Self-Tuning GMV Control 65

3 Model of Power System for Simulation Studies 73

3.1 Mathematical Model of the Synchronous Generator 73

3.1.1 Mechanical Equations 76

3.1.2 Air-Gap Voltage 78

3.1.3 Open-Circuit Saturation Curve 79

3.1.4 Saturation Effects 81

3.1.5 Generator Block Diagram 83

3.1.6 Steady-State Generator Equations 84

3.2 Network Model and Generator Stator Equations 88

3.3 Turbine/Governor and AVR Models 94

3.4 Program Overview 97

3.4.1 Initial Conditions 97

3.4.2 Step by Step Simulation 99

3.4.3 Numerical Integration Algorithm 100

3.5 Two-Machine Infinite-Bus Test System 100

4 System Identification of the Two-Machine Infinite-Bus System 104

4.1 Frequency Response Model 105

4.2 Off-Line Time-Domain Identification 110

4.2.1 Least Squares Identification 110

4.2.2 Generalized Least Squares Identification 112

4.2.3 Excitation Shaping 114

5 Performance Studies of the Self-Tuning Power System Stabilizer 119

5.1 Identification Convergence Using Gaussian Load Disturbances Applied to the Equivalent Machine 120

5.2 Parameter Tracking During Change in Test Machine Operating Point 133

5.3 Suppression of Local and Interarea Modes Following Step Load Change 140

5.4 Suppression of Local and Interarea Modes Following Transient Fault Condition 146

5.5 Suppression of Local and Interarea Modes Following Transient Fault Condition Using Self-Tuning PSS with Multivariable Feedback 148

5.6 Effect of Analog to Digital and Digital to Analog Quantization on PSS Performance 153

5.7 Field Test Results 158

5.7.1 Implementing the Self-Tuning Algorithm on an Existing Digital PSS 158

5.7.2 Results of Preliminary Tests of the Self-Tuning PSS on a Coal-Fired Generator 159

6 Summary and Conclusions 165

6.1 Recommendations for Further Research 169

Bibliography 170

List of Figures

2.1 Covariance update using exponential forgetting. 44

2.2 Covariance update using restricted exponential forgetting. 46

2.3 Covariance traces for factored (a) and non-factored (b) covariance updates. 64

2.4 *A* polynomial coefficients identified by factored (a) and non-factored (b) covariance update algorithms. 66

2.5 *B* polynomial coefficients identified by factored (a) and non-factored (b) covariance update algorithms. 67

2.6 Disturbance transfer function after 2000 samples. 69

2.7 Disturbance transfer function after 100 samples. 72

3.1 Typical synchronous generator open-circuit characteristic curve 79

3.2 Synchronous generator model. 85

3.3 Synchronous generator steady-state vector diagram. 86

3.4 Generator equivalent circuit showing fictitious voltage and admittance for generator stator equations. 90

3.5 Block diagram and analog wiring diagram of Turbine/Governor type 3 (three-stage steam turbine and mechanical hydraulic governor). 95

3.6 Block diagram and analog wiring diagram of AVR type 2 (Simple static exciter). 96

3.7 Data flow in transient stability program. 97

3.8 Block diagram of two-machine infinite-bus test system. 101

4.1 Harmonic content of filtered PRBS excitation signal. 106

4.2 Frequency response (P_e/V_{stab}) of two-machine infinite-bus test system. 107

4.3 Frequency response ($P_e/P_{dist_{equiv}}$) of two-machine infinite-bus test system. 108

4.4 Comparison of frequency response (P_e/V_{stab}) of two-machine infinite-bus test system and 5-th order model obtained using batch least squares.111

4.5 Harmonic content of filtered, prewhitened PRBS excitation signal. . . 115

4.6 Harmonic content of electric power signal with filtered, prewhitened PRBS excitation. 115

4.7 Comparison of frequency response (P_e/V_{stab}) of two-machine infinite-bus test system and 5-th order model obtained using generalized least squares. 117

4.8 z-plane poles and zeros (P_e/V_{stab}) of 5-th order model obtained using generalized least squares. 118

5.1 Simulation conditions for self-tuning PSS tests with Gaussian noise applied to equivalent machine. 121

5.2 Spectrum of test machine electric power (a) and terminal voltage (b) with Gaussian noise applied to equivalent machine (PSS disabled). . 122

5.3 First element of parameter vector (a) and forgetting factor (b) from RLS using Kulhavý's variable forgetting factor. 124

5.4 Results of self-tuning PSS simulation with Gaussian noise applied to equivalent machine. a–Trace of covariance matrix, b–Prediction error, c–Forgetting factor, d–Spectrum of prediction error. 128

5.5 Parameter identification of self-tuning PSS simulation with Gaussian noise applied to equivalent machine. a–f_0, b–f_1, c–f_2, d–f_3, e–f_4. . . 129

5.6 Parameter identification of self-tuning PSS simulation with Gaussian noise applied to equivalent machine. a–g_0, b–g_1, c–g_2, d–g_3, e–g_4. . . 130

5.7 Spectrum of test machine electric power (a) and terminal voltage (b) with Gaussian noise applied to equivalent machine (PSS enabled). . 131

5.8 Frequency response (P_e/V_{stab}) of two-machine infinite-bus test system with fixed PSS. 132

5.9 Test machine transient response following change in test machine operating point. 135

5.10 Forgetting factor computed in response to change in test machine operating point. 136

5.11 Parameter identification of self-tuning PSS simulation with change in operating point of test machine. a–f_0, b–f_1, c–f_2, d–f_3, e–f_4. 138

5.12 Parameter identification of self-tuning PSS simulation with change in operating point of test machine. a–g_0, b–g_1, c–g_2, d–g_3, e–g_4. 139

5.13 Test machine transient response following step change in test machine electric power. 141

5.14 Forgetting factor computed in response to step change in test machine electric power. 142

5.15 Parameter identification of self-tuning PSS simulation with change in electric power of test machine. a–f_0, b–f_1, c–f_2, d–f_3, e–f_4. 144

5.16 Parameter identification of self-tuning PSS simulation with change in electric power of test machine. a–g_0, b–g_1, c–g_2, d–g_3, e–g_4. 145

5.17 Test machine transient response following transient fault condition. . 147

5.18 Test machine transient response following transient fault condition. . 151

5.19 Test machine transient response following transient fault condition. . 152

5.20 Parameter identification of self-tuning PSS simulation with Gaussian noise applied to equivalent machine and quantization of PSS input/output signals. a–f_0, b–f_1, c–f_2, d–f_3, e–f_4. 155

5.21 Parameter identification of self-tuning PSS simulation with Gaussian noise applied to equivalent machine and quantization of PSS input/output signals. a–g_0, b–g_1, c–g_2, d–g_3, e–g_4. 156

5.22 Frequency response (P_e/V_{stab}) of two-machine infinite-bus test system with fixed PSS. 157

5.23 Block diagram of equipment used for field tests of self-tuning PSS. . 161

5.24 Generator electric power and field voltage transients with no PSS. . . 162

5.25 Generator electric power and field voltage transients with self-tuning PSS. 163

List of Tables

2.1 Operation Count to Update $n \times n$ Covariance Matrix. 39

3.1 Two-machine infinite-bus test system parameter values. 102

5.1 Test machine variances with and without self-tuning PSS. 127

5.2 Test machine variances with and without quantization of PSS signals. 154

Glossary

ARMAX	Autoregressive moving average with exogenous input. A system model of the form $A(z^{-1})y(t) = B(z^{-1})u(t) + C(z^{-1})\xi(t)$.
AVR	Automatic Voltage Regulator.
Damping torque	Braking torque in phase with changes in machine rotor speed.
E_f	Generator field voltage.
FFT	Fast Fourier Transform.
GLS	Generalized least Squares.
GMV	Generalized Minimum Variance.
Infinite bus	A bus whose voltage and frequency remain constant regardless of the power flowing to or from it.
P	Covariance matrix or weighting vector.
P_e	Generator real electric power.
PRBS	Pseudo Random Binary Sequence.
PSS	Power System Stabilizer.
Q_e	Generator reactive electric power.
RLS	Recursive Least Squares.
Synchronizing torque	Braking torque in phase with changes in machine rotor angle.
V_{ref}	AVR reference voltage.
V_t	Generator terminal voltage.
z^{-1}	Backwards shift operator. $z^{-1}x(t) \equiv x(t-1)$
δ	Generator rotor angle relative to synchronous reference.
θ	Vector of model parameters.
ϕ	Vector of input/output samples.
ω	Generator rotor speed deviation from synchronous speed.

Chapter 1

Introduction

1.1 Background to Power System Damping

Modern electrical power generation and distribution systems are made up of many interconnected generators, each equipped with several control elements. An indication of the degree of interconnection can be found in [94] where it is noted that more than 40% of the power generated by major utilities is sold to other utilities. Security of supply is one factor leading to increased interconnection since the loss of a single generating unit or plant has less effect when that unit or plant makes up a smaller fraction of the available generation. Economic grounds encourage interconnection when a utility can purchase power from another more cheaply than it can generate that same power. An unfavorable effect of highly interconnected systems is the possibility of stability problems involving entire groups of generators[109].

Many direct and indirect factors contribute to the stability of synchronous generators. Stability encompasses the behavior of a generator to both transient, large scale, disturbances and to continuous, small scale, disturbances. Lightly-damped rotor oscillations are influenced by a number of factors, one being the setting of the generator's automatic voltage regulator (AVR). Generators are equipped with high-gain, fast-acting AVR's which enhance large scale stability by holding the generator in synchronism with the power system during large transient fault conditions. An adverse effect of these high-gain excitation systems is a decrease in the damping torque of the generators, leading to a system prone to oscillatory instability. Other factors contributing to this oscillatory instability are weak transmission lines between generators and loads, operation of generators at wide power angles as a result of heavy loading, and particular load characteristics. Counteracting these factors directly by building more transmission lines or adding generating capacity can be expensive or impractical since the characteristics of a given load may be impossible to change.

Underdamped rotor dynamics are characterized by several oscillatory modes originating from one or more generators interacting in a power pool. The modes can be grouped into three categories. The local mode of oscillation is the underdamped response of a single generator relative to the power system. A number of generators at a single generating station may exhibit oscillations relative to each other. These are referred to as the intermachine modes of oscillation. Low frequency interarea oscillations result when entire groups of generators exchange electromechanical energy. These poorly-damped, or even unstable, oscillations in the 0.2 to 0.8 Hz range place significant limitations on power transfer among utilities. In a paper presenting an approach to the analysis of interarea oscillatory modes, Pagola et. al [102] noted that increases in interconnection and power exchanges between distant geographic areas have made some power systems even more susceptible to interarea oscillations. The nature and source of these oscillations have been the focus of considerable attention by power engineers[61, 62, 66, 91, 94, 102, 126].

Since the early 1970's supplementary excitation controllers, commonly referred to as power system stabilizers (PSS's) have been added to generators to counteract the effect of the high-gain AVR's and other sources of negative damping. A PSS uses a generator's excitation system to provide a component of the electrical torque to damp rotor oscillations. Through this exchange of electromagnetic and mechanical energy the oscillatory mode of a generator can be effectively damped. The PSS feedback loop provides an economical way of enhancing the stability of a power system.

A PSS tuned only to reduce the local oscillatory mode could have a detrimental effect on the low frequency stability if the tuning procedure does not consider the interarea mode. Stabilizers capable of damping both the local and interarea oscillatory modes pose a challenge to researchers and power engineers.

The design and synthesis of PSS's are further complicated by the fact that the electric generator is a non-linear device whose characteristics, as seen by the PSS, vary with changes in generator loading and changes in the external network resulting from transmission line switching and load changes. Conventional, fixed-parameter, PSS's are usually tuned for a single operating point and may exhibit poor performance under different synchronous generator loading conditions. Constraints of time and system security during on-site commissioning make it impossible to test the operation of a PSS under all operating conditions. The number of variables makes it impossible to investigate every possible case using large scale power system simulations. Limitations of fixed parameter PSS's indicate a need for an adaptive PSS capable of tracking changes in the operating conditions of the generator to which it is attached. While several adaptive PSS strategies have been proposed [33, 34, 50, 54, 56, 57, 71, 74, 92, 116, 130], little attention has been paid to their ability to damp modes other than the local oscillatory mode. The research presented in this thesis investigates the multimode damping provided by an adaptive PSS.

The adaptive control strategy investigated in this thesis is an extension of that proposed by Gu [56, 57], Fan, Ortmeyer and Mukundan [50], and Xia and Heydt [130]. The main emphasis has been to develop and test improvements in the identification portion of the adaptive control algorithm and to investigate and develop improvements in the numerical stability of the implementation. A practical contribution of this thesis is the extension of the adaptive control algorithm to damp multiple modes as well as a presentation of the results of preliminary field tests of a PSS based on the adaptive algorithm.

The following section presents a review of techniques and test results presented by others in the field of synchronous generator stabilization. Design techniques for fixed-parameter PSS's are described which show some of the requirements and restrictions placed upon practical stabilizers. This is followed by an overview of methods used to obtain models of electric generators. The identification of such models is inherent either explicitly or implicitly in the operation of many adaptive control schemes. Pertinent adaptive PSS control strategies are then reviewed.

1.2 Fixed-Parameter Stabilizer Tuning Methods

This section reviews some of the many tuning strategies that have been proposed for obtaining settings for fixed-parameter PSS's. The review provides insight into some of the practical constraints that are imposed on PSS control strategies. The security of synchronous generator operation and practical limitations on control signal magnitudes are two of several factors that must be addressed.

A paper by de Mello and Concordia [44] in 1968 described the stabilization of a single generator supplying power through an external impedance to an infinite bus. A technique for stabilizing the generator through supplementary excitation control and a stabilizing method using shaft speed as the supplementary feedback signal were presented. The small signal model for which the PSS is designed was derived from a linearized model based on the machine reactances and time constants. The transfer function between shaft speed and the torque produced by the stabilizing signal was derived and a PSS which provided appropriate phase compensation over the frequency range of expected oscillations was synthesized. The effect of different loading conditions on the frequency response between the shaft speed and the stabilizing torque was shown. The PSS was designed as a compromise between the range of responses noted at the different loading conditions. Analog computer simulation results were presented and showed improved damping of the generator local mode in response to small step changes in the mechanical torque. The paper concluded that the compromise PSS provided significant damping but noted that in a real power system there are many modes of oscillation and that synthesis of a universal function adequate for the spectrum of possibilities remained a challenge.

A PSS design procedure based on pole-placement was presented in 1975 by Laha and Bollinger [81]. The transfer-function of the generator to be controlled was derived by fitting a straight-line approximation to the frequency response obtained by Fourier Transform analysis of wide bandwidth excitation signals applied to a large-scale power system simulation program. The state-space model of the generator was obtained from the transfer function thus obtained and the PSS was designed to place the closed-loop poles at locations which provided the desired response. The technique was shown to be effective in damping the local oscillatory mode of the generator for the loading conditions at which the frequency response was obtained.

Also in 1975, Bollinger, Laha, Hamilton and Harras [23] described a design method based on root locus techniques. The open-loop poles and zeros of the generator were determined from the frequency response between the voltage regulator input and the generator electric power measured while the generator was in operation. The PSS poles and zeros were then placed so as to move the generator's lightly-damped local mode s-plane poles to the left. Performance of the PSS in response to a disturbance was tested by disconnecting one of the other generators at the plant. Improved damping of of the local oscillatory mode over the uncompensated system was noted. Another application of this design method was reported in 1977 by Bollinger and Lalonde [25] in which the AVR settings for a 300 MW generator were derived. Settings derived from a generator model measured while the generator was operating were shown to provide a definite improvement in terminal voltage damping over the AVR tuned for open-circuit conditions. A phase-compensation tuning technique using frequency response data obtained by applying wide-bandwidth noise signals to a generator operating on-line was used by Bollinger, Winsor and Campbell [29] to design a stabilizer to damp power oscillations on a tie-line linking two large power pools. Of note is that the power flow from the tie-line itself was used as the supplementary feedback signal. Field test results showed improved damping of the tie-line power oscillations. More recently, the on-line frequency response measurement technique combined with the root locus controller design method described in [23] was used by Bollinger and Mistr [27] to design a PSS for a pumped storage plant. Step changes in the AVR reference signal showed that the PSS provided a definite improvement in the damping of the local oscillatory mode.

Eigenvalue and eigenvector analysis techniques for determining the generators which will provide greatest damping when equipped with PSS's and for determining the form of the stabilizer were described by de Mello, Nolan, Laskowski and Undrill [43] in 1980. The technique of de Mello et al. was extended by Abe and Doi [2] in 1983 and by Abdalla, Hassan and Tweig [1] in 1984. Further investigations of this method were performed by Lim and Elangovan [86] in 1985 and by Huang and Hsu [66] and by Yu and Li [132] in 1990.

The use of eigenanalysis methods to gain insight into the source and nature of interarea oscillations with a view to discovering effective ways to damp the modes has recently been the focus of considerable attention. Recent papers addressing this problem include ones by Rogers and Kundur [109], Pagola, Rouco, and Pérez-Arriaga [102], Sauer, Rajagopalan and Pai [112], and Mansour [94]. A method known as Prony analysis has also received considerable attention. The method is used to directly estimate the frequency, damping strength, and relative phase of modal components present in a given signal. It can be used to provide transfer functions for PSS design that produce a reduced-order model of a generator connected to a large system. The method is described by Hauer, Demeure and Scharf [61] and its application to PSS design is presented by Trudnowski, Smith, Short and Pierre [126].

Use of eigenanalysis to perform optimal regulator design was presented by Yu and Moussa [97, 133] in 1972 but the method was impractical in that it required full state feedback. Other papers describing the use of optimal output feedback techniques for PSS design include 1976 papers by Wilson, Raina and Anderson [129], and by Quintana, Zohdy and Anderson [107] and a 1982 paper by Okongwu, Wilson and Anderson [99]. The former paper employs non-linear output feedback and different coefficients depending on the operating point of the generator. The latter two papers used a linearized model of the generator as a basis for their design and both showed good damping of the local oscillatory mode.

A detailed analysis of tuning concepts and practical aspects of PSS design was presented by Larsen and Swann [83] in 1981. The advantages and disadvantages of shaft speed, terminal voltage frequency, electrical power and accelerating power as supplementary feedback signals are discussed. The conclusion reached is that either electrical or accelerating power is the most appropriate signal to be used. The paper continues with the description of a design procedure based on a combination of phase compensation and root locus techniques applied to the linearized model of the generator at some loading condition. The design procedure focuses on the damping of the local mode. It should be emphasized that the design procedure did not present a general method for damping both local and interarea modes. The effect of the stabilizer on the interarea mode was investigated through simulations of a three machine system only when the design had been completed. Simulations of the three machine system indicated that interarea damping in response to a transient fault condition was not reduced by the original PSS design. A modified PSS providing less local mode damping was shown to provide better interarea damping following a transient fault.

The choice of feedback signal from the synchronous generator for supplementary excitation control is a matter of considerable debate. Power system stabilizers using shaft speed, or changes in shaft speed, as the feedback signal are described in [1], [43], [44], [86] and [132]. Stabilizers using electric power as the feedback signal are described in [2], [23], [27] and [81]. Papers advocating the use of accelerating power, defined as the difference between the mechanical power supplied to the generator and the electrical power supplied by it, as the supplementary feedback signal were presented by de Mello, Hannett, and Undrill [42] in 1978, by de Mello, Hannett, Parkinson and Czuba [41] in 1982 and by Ishiguro, Tanaka, Shimomura, Maeda, Matsushita and Sugimoto [72] in 1986. A recent paper by Bollinger, Gu and Norum [20] compares electrical and accelerating power as feedback signals. Electrical power feedback was chosen for the research presented in this thesis but the adaptive control strategy could be applied to generators using accelerating power or shaft speed feedback as well.

1.3 Generator System Identification

Inherent in the synthesis of fixed-parameter stabilizers or in the operation of almost any adaptive stabilizer, either implicitly or explicitly, is some mathematical model of the generating unit to be controlled. In the case of the fixed-parameter stabilizer the model is used in the design procedure to derive the PSS parameters. For the adaptive stabilizer the model is updated as the operating conditions change and a new control strategy is calculated based on the updated model. The accuracy of the identification process is critical since it directly affects the damping provided by the adaptive controller.

A number of techniques have been proposed to establish the model of large electric generators and their excitation systems. The models have several applications, including large scale computer simulations of power systems[70] as well as their direct application to feedback controller synthesis[28]. The following paragraphs present a review of the literature in the field of on-line identification of generator models. Measurement methods which require that the generator be removed from service are described in [3], [9], [10], [40], [68], [69], [73], [77] and [119] but are not directly applicable to adaptive control strategies.

On-line frequency response tests of a generator using direct sinusoidal signal injection were performed by Manchur, Lee, Coultes, Griffin and Watson [93]. System response over a frequency range of 0.01 to 10.0 Hz was obtained. The transfer functions were then estimated from the measured frequency response. The actual method of deriving the transfer function parameters from the frequency response data was not reported. An alternative frequency response test method in which a second machine would be used to provide the source signal was proposed. An advantage claimed for the alternative method was its ability to provide better estimates of the machine's quadrature axis parameters. A method for determining the machine parameters from similar frequency response data was presented by Kazovskii and Lerner[75].

On-line measurement of the frequency response of a 60 MW hydroelectric generator using Pseudo-Random Binary Sequence (PRBS) excitation and Fast Fourier Transform (FFT) techniques was presented by Bollinger, Winsor and Cotcher [30]. The results of the FFT method were shown to compare well with those of the discrete sinusoid method. The ability of the method to operate in the presence of noisy data acquired from on-line tests was noted.

Application of the PRBS/FFT method was expanded to the individual responses of the voltage regulator components and machine by Bollinger, Khalil and Norum [22]. The paper presents practical suggestions for choice of sampling frequency and experimental conditions. Transfer functions were estimated from the frequency response using a trial and error technique. A direct transfer function parameter identification method based on the least squares technique applied to the input/output time series measurements was introduced and shown to give excellent parameter estimates of low-order, noise-free simulations.

An identification method based on an extended Kalman filter was used by Namba, Nishiwaki, Yokokawa and Ohtsuka [98] to estimate the parameters of a hydroelectric generator and its voltage regulator components. The system response was measured during transient conditions resulting from switching a tie-line in and out of service. No tests with other perturbing signals were reported. Problems with signal to noise ratios were noted but simulation studies using the identified parameters were shown to more accurately reflect the operation of the generator than were simulation studies using the design data provided by the manufacturer.

Barret, Colot, Herouard, Meyer, Michard and Monville [11] determined the frequency response of a 1080 MVA turbogenerator and its excitation system while the generator was in operation. The paper presents practical limitations on the variance of output signals for machines operating on-line and describes the concepts of pseudo-random ternary excitation and frequency response measurement from the signal spectral densities. Transfer functions and machine parameters were estimated from the frequency responses obtained by the application of sinusoidal signals to the voltage regulator reference input. Most of the tests were performed under no-load conditions. The tests under load conditions show considerably more scatter in the frequency response measurement as a result of the noise introduced from the rest of the power system. No estimate of the effect of this noise on the parameter estimates was made.

Bollinger, Khalil, Li and Norum [21] applied the least squares estimation technique introduced in [22] to simulated second and seventh order systems in the presence of noise and to a hydroelectric generator penstock system. The simulation studies show good parameter estimates even when a noise signal is added to the simulation.

Lang, Hutchison and Yee [82] used pseudo random ternary signal injection and correlation techniques to determine the impulse response of a small single-machine infinite-bus system. The system transfer function and machine parameters were derived from the impulse response obtained. The same method was applied to the open-circuited machine and the voltage regulator parameters were derived. System noise was reduced by averaging several acquisition records though the effect of the noise with fewer averages was not reported. The parameter estimates from the averaged data closely matched the theoretical values but no estimate of the parameter variances were reported.

Swidenbank, Boyd and Hogg [124] used pseudo random binary signal injection and recursive least squares identification to estimate the parameters of a 270 MW turbogenerator. The relatively poor match between the real system and model outputs seems to indicate that the system noise adversely affected the estimates. The 300 millisecond sampling period employed was considerably larger than that used by other researchers.

The recursive least squares technique is often employed as part of an adaptive control scheme. Papers describing this identification technique as part of an adaptive PSS are discussed in following section of this thesis.

A generalized least squares parameter estimation technique employing an observer to estimate unmeasurable generator signals was reported by Keyhani and Miri[76].

The method was applied to a noise-free computer simulation and good parameter estimates were obtained.

Sanchez Gasca, Bridenbaugh, Bowler and Edmonds [52] applied a trajectory sensitivity algorithm to data recorded under transient conditions to determine the parameters of a simulated single-machine infinite-bus system. Generalized least squared parameter estimates obtained from data acquired under similar circumstances is presented by Le and Wilson[84]. The disturbance in this case was a 10%, 100 millisecond step to the voltage regulator reference. Rapid decline in parameter accuracy in the presence of noise was noted. Tests with wider bandwidth perturbation signals were not reported.

Lee and Tan[85] used an iterative non-linear weighted least squares algorithm to derive the machine parameters from data acquired from a sudden three-phase short circuit applied to a machine operating at rated speed and no load. The method was applied to noise-free data from a simulation program and identified the parameters of a fifth-order model with great accuracy. In [21] and [22] the same algorithm was applied to on-line measurements of generator input/output signals. The algorithm was shown to provide a model whose response closely matched that of the system from which the data were acquired.

1.4 Adaptive Power System Stabilizers

A wide range of adaptive control strategies have been proposed for power system stabilization applications. In a 1987 review paper, Pierre [105] refers to over 90 papers in the field of adaptive power system control, including applications to adaptive load frequency control, combined governor and excitation control as well as primary (AVR) and supplementary (PSS) excitation control. Some of these adaptive supplementary excitation control publications are reviewed below.

An adaptive control scheme for the combined control of both prime mover and excitation control paths was described by Malik, Hope and El-Ghandakly [92] in 1978. The controller used a batch least squares identification technique using a sliding window of the three most recently acquired input/output samples to obtain a two-input, two-output, second-order model of the generator and derived an optimal control strategy based on the model. The algorithm was applied to a sixth-order model of a single-machine infinite-bus system and the response to a number of three-phase fault conditions was observed. A pseudo-random noise signal was applied to the generator output to ensure that the identification portion of the algorithm was continuously supplied with data. The published results show that the model identified by the algorithm was able to give a good estimate of the rotor angle and speed of the simulated machine. The damping provided by the controller was somewhat better than that obtained by a fixed-parameter stabilizer. The damping provided by dual excitation and governor control was shown to be better than that provided by excitation control alone.

A model-reference adaptive controller for a generator excitation path was described by Irving, Barrett, Charcossey and Monville [71] in 1979. Three state variables, namely changes in terminal voltage, changes in shaft speed and changes in electric power were used as inputs to the controller. No explicit model of the generator was derived in the algorithm. A state feedback vector was derived to match the output of the combination of the generator and a series-connected model to the output of a parallel model. This series-parallel combination was said to diminish the effects of sudden unmeasurable disturbances. Experimental results on a micro-alternator single-machine infinite-bus system show considerably better damping of the local oscillatory mode for the adaptive regulator over a conventional AVR/PSS combination.

An adaptive controller based on recursive least squares identification of a discrete-time, third-order model of the generator and a control strategy which shifted the closed-loop poles of the generator/controller combination towards the center of the unit circle was presented by Ghosh, Ledwich, Malik and Hope [54] in 1984. The algorithm was shown to be more effective in damping the local oscillatory mode of a single-machine infinite-bus simulation than was a conventional stabilizer or a stabilizer designed using LQ optimization techniques. The LQ controller and a direct pole assignment controller were dismissed as being too computationally intensive to be implemented in a practical adaptive controller. A minimum-variance control strategy was said to be unsuitable for excitation control as a result of its poor performance on non-minimum phase systems. The simulation studies ensured continuous excitation for identification by adding a pseudo-random noise signal to the output of the controller. An advantage of the pole shifting strategy is the single tuning value, namely the amount of shift towards the center of the unit circle, for adjusting the extent of the control action. The method provides no guarantee that the derived controller will not have unstable poles, however.

Further simulation results of the adaptive pole shifting technique were presented by Cheng, Chow, Malik and Hope [33] and by Cheng, Malik and Hope [34] in 1986. Here the technique has been improved to use a variable forgetting factor for the recursive least squares identification and an dynamic choice of the pole shifting factor based on control action limits. The action of the self-tuning stabilizer was shown not to conflict with similar stabilizers on other machines in a multi-machine simulation.

Adaptive control based on selection of a control strategy from a table of predetermined values is presented by Sharaf, Hogg, Abdalla and El-Sayed [116]. A controller based on an artificial neural network is presented by Hsu and Chen [65]. Both these methods suffer from the necessity to predetermine the action of the controller at all operating points, the former through the synthesis of the preselected controllers, and the latter through the training process of the network.

A novel rule-based control strategy was proposed by Hiyama [64] in 1990. The selection process for the rules was based on an optimization procedure at one operating point. Improved damping of the local oscillatory mode over a conventional stabilizer was noted at three operating points.

A self-tuning PSS based on a generalized minimum variance control strategy was present by Xia and Heydt [130] in 1983. A recursive least squares identification algorithm was used to identify a fourth-order discrete-time model of the generator. A fixed forgetting factor of unspecified value was employed to keep the identifier alert to changes in the system parameters. The problem of covariance matrix blowup associated with a fixed forgetting factor was circumvented by adding an uncorrelated, zero-mean noise signal to the controller output. The numerical advantages of matrix factorization methods to ensure the positive definiteness of the covariance matrix was noted but not implemented. The control action weighting of the generalized minimum variance control strategy was very small, leading to a control strategy similar to minimum variance control. Simulation studies of a single-machine infinite-bus system showed excellent parameter tracking at operating point changes. Good rotor damping is mentioned but no plots of this were shown.

In 1989, Gu and Bollinger [57] describe a generalized minimum variance self-tuning PSS similar to that described in [130]. The algorithm was improved by the addition of a variable forgetting factor to maintain the alertness of the identification while limiting covariance matrix blowup. No noise had to be added to the controller output. As in [130], a sampling frequency of 20 Hz was chosen, but in the cost function to be minimized control action variations were given nearly as much weight as output signal variations. Simulation results using a sixth-order nonlinear model of a single-machine infinite-bus system were presented. The response to step changes in mechanical torque and to a six-cycle three-phase fault with successful reclosing were shown. In all cases parameter tracking was fast and rotor damping was greatly improved over the generator not equipped with a stabilizer.

A multivariable version of the generalized minimum variance controller for combined control of the prime-mover and excitation control paths was presented in Gu's

PhD. thesis [56]. A detailed proof of the convergence properties of the multivariable self-tuning with variable forgetting factor generalized minimum variance control algorithm is given. Simulation studies of a single-machine infinite-bus system show improved local mode damping over a generator equipped with a conventional stabilizer.

Application of self-tuning generalized minimum variance control to a ten-machine simulated system was described by Fan, Ortmeyer and Mukundan [50] in 1990. Three signals, the terminal voltage, electric power and changes in shaft speed, were provided as inputs to each of the stabilizers. A dynamic goal pointing algorithm was used in which the reference point to which the system outputs are to be driven is calculated at each step as some fraction of the current output value. This was advocated to reduce control effort and overshoots during transient periods. The effect of this dynamic goal pointing were not compared with the effect of different control action weightings in the standard generalized minimum variance control algorithm. The response of the system under three different operating conditions and four different fault conditions was presented. Under all conditions the local mode damping of the systems equipped with adaptive stabilizers was better than that of the systems with conventional or no stabilizers.

The above review makes it clear that adaptive exciter control can provide improved generator performance over conventional control strategies. Only one of the techniques is said to be in operation on a full-scale power system[71], and none specifically addressed the problem of damping multiple oscillatory modes.

1.5 Outline of this Thesis

This thesis presents the results of research investigating self-tuning generalized minimum variance power system stabilizer strategies that address the damping of two oscillatory modes. This research is an extension of that presented by Gu [56]. Included in this extension are improvements to the identification portion of the adaptive control algorithm to provide better tracking of changes in the small-signal model of the generator arising from changes in operating conditions as well as improvements in numerical properties of the algorithm to make it practical for implementation on existing digital stabilizer hardware. The identification of a model of a generator exhibiting multiple oscillatory modes is studied. Simulation studies are used to investigate the multimode damping capabilities of an adaptive PSS. Results of preliminary field tests of the adaptive stabilizer are presented.

Chapter 2 presents the theory of the adaptive control techniques pertinent to the thesis. A description of the generalized minimum variance control algorithm for single-input single-output systems is given. The theory of the system identification process on which the self-tuning action of the controller is based is presented. Techniques which improve the parameter tracking and numerical stability of the identification portion of the algorithm are described. Examples showing the effects of these improvements are given.

The simulation program used to study the self-tuning controller is described in chapter 3. The mathematical model of the synchronous generator is presented and the method by which this model is coupled to the model of the power transmission network is described. The chapter concludes with a description of the simplified power system used for the studies presented in chapter 4.

In chapter 4 the results of a number of system identification techniques used to determine the characteristics of the simulated two-machine infinite-bus test system are shown. Both frequency-domain and time-domain models are obtained.

Chapter 5 presents the results of simulation studies investigating the performance of a simulated power system and the self-tuning PSS in response to a variety of stochastic and deterministic disturbances. The effect of analog to digital and digital to analog converter quantization and noise is shown in the following section. The simulation studies present the response of the self-tuning PSS to a number of different disturbances. The disturbances include a step load disturbance, a Gaussian load disturbance, a transient fault condition, and a change in the operating point of the test machine.

Chapter 5 concludes with a presentation of the results of preliminary field tests of the adaptive stabilizer. The self-tuning PSS was tested in existing digital stabilizer hardware connected to both steam and hydro-powered generators.

Chapter 6 presents the conclusions gleaned from the controller studies and recommends some directions for further research.

Chapter 2

Review of the Pertinent Theory

The chapter presents a review of theory and algorithms applicable to a class of self-tuning controllers. The two main components of the self-tuning controller are the Recursive Least Squares (RLS) parameter identification method by which a model of the process to be controlled is obtained, and the Generalized Minimum Variance (GMV) control strategy which computes the control action at each sampling interval. The application to a self-tuning PSS is described and examples illustrating some of the concepts are presented at the end of the chapter.

2.1 Recursive Least Squares Parameter Identification

The recursive least squares algorithm for system parameter identification is well-known and commonly used. A full derivation of the method is presented here since the algorithm is of fundamental importance to the self-tuning action of the controller. Detailed discussions of the convergence and statistical properties of the method can be found in [87], [88] and [118].

Application of the method to adaptive control systems is discussed in [39] and [55]. Improvements to the method are presented in [60], [78], [80], [111], [114], and [120]. A number of these improvements are discussed later in this chapter.

Recursive least squares identification is a member of a group of identification techniques known as prediction error methods in which the parameter estimate is adjusted to minimize the difference between the predicted output of the system and the actual output[4].

The least squares technique deals with models of the form,

$$y(t) = \phi^T(t)\theta \tag{2.1}$$

where,

$y(t)$ is some measurable quantity,

$\phi(t)$ is an n-vector of known quantities, commonly referred to as the vector of *regressors*, and,

θ is the n-vector of unknown parameters.

For the applications considered in this thesis the regressor values are previous samples of the plant output and control action.

The problem is to find an estimate $\hat{\theta}$ of the parameter vector θ from the measured values $y(1), \ldots, y(N)$ and $\phi(1), \ldots, \phi(N)$. The N measurements form a system of linear equations,

$$\begin{aligned} y(1) &= \phi^T(1)\theta \\ y(2) &= \phi^T(2)\theta \end{aligned}$$

$$\vdots$$

$$y(N) = \phi^T(N)\theta \tag{2.2}$$

This can be written compactly in matrix notation as,

$$Y = \Phi\theta \tag{2.3}$$

where Y is the $N \times 1$ vector of measured values and Φ is the $N \times n$ matrix of regressor values.

The equation errors, or *residuals*, are given by,

$$\varepsilon(t) = y(t) - \phi^T(t)\theta \tag{2.4}$$

or, in matrix form,

$$\varepsilon = Y - \Phi\theta \tag{2.5}$$

where ε is the $N \times 1$ vector of equation errors.

The *least squares estimate* of the parameters is the vector $\hat{\theta}$ which minimizes the sum of the squares of the equation errors,

$$V(\theta) = \frac{1}{2}\sum_{t=1}^{N}\varepsilon^2(t) = \frac{1}{2}\varepsilon^T\varepsilon \tag{2.6}$$

Substituting the expression for the equation errors from (2.5) into the above expression yields,

$$V(\theta) = \frac{1}{2}[Y - \Phi\theta]^T [Y - \Phi\theta]$$
$$= \frac{1}{2}\left[Y^T Y - Y^T\Phi\theta - \theta^T\Phi^T Y + \theta^T\Phi^T\Phi\theta\right] \quad (2.7)$$

The parameter vector which minimizes the cost function is found by first determining the derivative of the cost function with respect to the parameters,

$$\frac{\partial V(\theta)}{\partial\theta} = \frac{1}{2}\left[-Y^T\Phi - (\Phi^T Y)^T + (\Phi^T\Phi\theta)^T + \theta^T\Phi^T\Phi\right] \quad (2.8)$$

and then solving for the value of θ which sets the derivative to zero,

$$0 = -Y^T\Phi + \hat{\theta}^T\Phi^T\Phi$$
$$\hat{\theta} = (\Phi^T\Phi)^{-1}\Phi^T Y \quad (2.9)$$

The second derivative of the cost function with respect to the parameters is,

$$\frac{\partial^2 V(\theta)}{\partial\theta^2} = \Phi^T\Phi \quad (2.10)$$

which is non-negative, indicating that the solution of (2.9) does, in fact, minimize the cost function.

The statistical properties of the parameter estimate are derived subject to the assumption that the data are of the form,

$$y(t) = \phi^T(t)\theta_0 + e(t) \tag{2.11}$$

where θ_0 is the true parameter vector and $e(t)$ is a sequence of zero-mean white noise with variance r. In matrix form this is written as,

$$Y = \Phi^T\theta_0 + e \tag{2.12}$$

The difference between the parameter estimate $\hat{\theta}$, from (2.9), and the true parameter vector is,

$$\begin{aligned} \hat{\theta} - \theta_0 &= (\Phi^T\Phi)^{-1}\Phi^T Y - \theta_0 \\ &= (\Phi^T\Phi)^{-1}\Phi^T(\Phi\theta_0 + e) - \theta_0 \\ &= (\Phi^T\Phi)^{-1}\Phi^T e \end{aligned} \tag{2.13}$$

The covariance matrix of the parameter estimate $\hat{\theta}$ is given by,

$$E\left\{(\hat{\theta} - \theta_0)(\hat{\theta} - \theta_0)^T\right\} = E\left\{((\Phi^T\Phi)^{-1}\Phi^T e)(e^T\Phi(\Phi^T\Phi)^{-1})\right\} \tag{2.14}$$

where E is the expectation operator. The assumption of white noise means that,

$$E\left\{ee^T\right\} = rI \tag{2.15}$$

The Φ matrix is known and can be taken outside the expectation, so the expression for the covariance matrix reduces to,

$$E\left\{(\hat{\theta}-\theta_0)(\hat{\theta}-\theta_0)^T\right\} = r(\Phi^T\Phi)^{-1} \tag{2.16}$$

The derivation of the recursive form of the least squares identification technique begins by rewriting the expression for the parameter estimate, (2.9), at time t as,

$$\hat{\theta}(t) = \left[\sum_{s=1}^{t} \phi(s)\phi^T(s)\right]^{-1} \left[\sum_{s=1}^{t} \phi(s)y(s)\right] \tag{2.17}$$

From (2.16) the value of the covariance matrix at time t is,

$$P(t) = r\left[\sum_{s=1}^{t} \phi(s)\phi^T(s)\right]^{-1} \tag{2.18}$$

Expressed as an update from the previous sample, the covariance is,

$$P^{-1}(t) = P^{-1}(t-1) + \phi(t)r^{-1}\phi^T(t) \tag{2.19}$$

This expression requires a matrix inversion at each time step. The inversion can be eliminated by application of the matrix inversion lemma which states that,

$$[A+BCD]^{-1} = A^{-1} - A^{-1}B[C^{-1}+DA^{-1}B]^{-1}DA^{-1} \tag{2.20}$$

provided the inverses exist. Substitution of the corresponding values from (2.19) yields an expression requiring only a scalar division,

$$P(t) = P(t-1) - \frac{P(t-1)\phi(t)\phi^T(t)P(t-1)}{r + \phi^T(t)P(t-1)\phi(t)} \tag{2.21}$$

Combining (2.17) and (2.18), and taking the term at time t out of the summation yields,

$$\hat{\theta}(t) = \frac{P(t)}{r}\left[\sum_{s=1}^{t-1}\phi(s)y(s) + \phi(t)y(t)\right] \tag{2.22}$$

The parameters at time $t-1$ were,

$$\hat{\theta}(t-1) = \frac{P(t-1)}{r}\left[\sum_{s=1}^{t-1}\phi(s)y(s)\right] \tag{2.23}$$

Substituting the summation term from (2.23) into (2.22) yields,

$$\hat{\theta}(t) = \frac{P(t)}{r}\left[rP^{-1}(t-1)\hat{\theta}(t-1) + \phi(t)y(t)\right] \tag{2.24}$$

From (2.19) the covariance at time $t-1$ is,

$$P^{-1}(t-1) = P^{-1}(t) - \phi(t)r^{-1}\phi^T(t) \tag{2.25}$$

Substituting this value into (2.24) produces,

$$\hat{\theta}(t) = \frac{P(t)}{r}\left[r\left(P^{-1}(t) - \phi(t)r^{-1}\phi^T(t)\right)\hat{\theta}(t-1) + \phi(t)y(t)\right] \tag{2.26}$$

which reduces to,

$$\hat{\theta}(t) = \hat{\theta}(t-1) + \frac{P(t)}{r}\phi(t)\left[y(t) - \phi^T(t)\hat{\theta}(t-1)\right] \qquad (2.27)$$

From (2.27) two new values are defined,

$$\varepsilon(t) \triangleq y(t) - \phi^T(t)\hat{\theta}(t-1) \qquad (2.28)$$

$$K(t) \triangleq \frac{P(t)}{r}\phi(t) \qquad (2.29)$$

The term $\varepsilon(t)$ is a prediction error, being the difference between the measured output and the output predicted using the previous parameter values. The elements of the vector $K(t)$ are weighting factors, often referred to as the Kalman gains, that show how much the prediction error will adjust each element of the parameter vector.

Substituting the value of $P(t)$ from (2.21) into (2.29) yields,

$$K(t) = r^{-1}\left[P(t-1) - \frac{P(t-1)\phi(t)\phi^T(t)P(t-1)}{r + \phi^T(t)P(t-1)\phi(t)}\right]\phi(t) \qquad (2.30)$$

This reduces to,

$$K(t) = \frac{P(t-1)\phi(t)}{r + \phi^T(t)P(t-1)\phi(t)} \qquad (2.31)$$

The set of (2.21), (2.27), (2.28) and (2.31) form the recursive least squares identification algorithm. At each time step the following calculations are performed to update the parameter covariance $P(t)$ and the parameter estimate $\hat{\theta}(t)$,

$$\varepsilon(t) = y(t) - \phi^T(t)\hat{\theta}(t-1) \tag{2.32}$$

$$K(t) = \frac{P(t-1)\phi(t)}{r + \phi^T(t)P(t-1)\phi(t)} \tag{2.33}$$

$$P(t) = P(t-1) - K(t)\phi^T(t)P(t-1) \tag{2.34}$$

$$\hat{\theta}(t) = \hat{\theta}(t-1) + K(t)\varepsilon(t) \tag{2.35}$$

These equations are often presented with the r term in the denominator of (2.33) replaced by the value 1. This version of the Kalman gain calculation can be given two interpretations. The first is that the I/O regressor, ϕ, has been scaled so that the variance of the disturbance, $e(t)$ in (2.11), is, in fact, one. The second is that the covariance matrix, P, must be scaled by the variance of the disturbing signal in order to represent the statistical properties of the parameter estimate, $\hat{\theta}$. For example, if the I/O regressor has been scaled so that the variance of the disturbance signals is ρ, and if the recursive least squares identification is performed with the r term in the denominator of (2.33) set to 1, then the statistical properties of the parameter estimate $\hat{\theta}$ are given by P/ρ rather than by P.

One of these interpretations must be considered when implementing the algorithm, particularly when the initial value of the covariance matrix is being chosen. For example, if the incoming data are scaled down by a factor of 10, the algorithm will behave differently unless r is divided by a factor of 100, or the initial covariance estimate is multiplied by a factor of 100.

Several improvements to the recursive least squares identification algorithm have been proposed ([60], [78], [80], [111] and [120]). The following sections present modifications that improve its numerical properties and enable it to track parameters that change with time.

2.1.1 U-D Factorization of the Covariance Matrix

Implementations of the recursive least squares identification algorithm based directly on (2.32) through (2.35) are sensitive to computer roundoff[14, 15]. An improved implementation was presented by Bierman in 1976[15]. The improved implementation factors the covariance matrix so that factors of the covariance matrix, rather than the covariance matrix itself, are updated. This improves the numerical stability in two ways. The first improvement is due to the reduction in the numerical range of the variables involved in the computation of the covariance matrix. Numerical operations in the original algorithm involving numbers in the range of 10^{-N} to 10^{N} are replaced in the improved algorithm by operations involving numbers in the range of $10^{-N/2}$ to $10^{N/2}$. The improved algorithm thus requires only half the numerical precision to yield results as accurate as the original algorithm. The second improvement arises from the modification of the covariance update equation (2.34). A direct implementation of (2.34) involves the subtraction of values that may be nearly equal. This operation can cause considerable loss of accuracy when performed using finite-precision arithmetic. The accumulated loss of accuracy over several covariance updates can result in a covariance matrix that is no longer non-negative definite.

Replacing the covariance matrix update with an update of the factors of the covariance matrix ensures that the covariance matrix remains positive definite at all times. The improved algorithm is based on the decomposition of the covariance matrix into the factors,

$$UDU^T = P \tag{2.36}$$

where U is unit upper triangular and D is diagonal. The algorithm ensures that the elements of D remain positive and thereby ensures that the covariance matrix remains positive definite. The following paragraphs present a derivation of the algorithm.

In the following derivation accents are employed to provide a more compact notation. A tilde over a variable ($\tilde{\cdot}$) indicates the value prior to the update operation and a caret over a variable ($\hat{\cdot}$) indicates the value following the update. In this notation the covariance update (2.34) is written as,

$$\hat{P} = \tilde{P} - \frac{\tilde{P}\phi\phi^T\tilde{P}}{r + \phi^T\tilde{P}\phi} \tag{2.37}$$

Writing the covariance update equation in terms of the factored covariance yields,

$$\hat{U}\hat{D}\hat{U}^T = \tilde{U}\tilde{D}\tilde{U}^T - \frac{\tilde{U}\tilde{D}\tilde{U}^T\phi\phi^T\tilde{U}\tilde{D}\tilde{U}^T}{r + \phi^T\tilde{U}\tilde{D}\tilde{U}^T\phi} \tag{2.38}$$

Extracting some common factors and taking the transpose of some of the inner terms produces,

$$\hat{U}\hat{D}\hat{U}^T = \tilde{U}\left[\tilde{D} - \frac{\tilde{D}\tilde{U}^T\phi\left(\tilde{D}\tilde{U}^T\phi\right)^T}{r + \phi^T\tilde{U}\tilde{D}\tilde{U}^T\phi}\right]\tilde{U}^T \tag{2.39}$$

Two new vectors, a and b, and one scalar ζ_n, are defined as,

$$a = \tilde{U}^T\phi \tag{2.40}$$

$$b = \tilde{D}\tilde{U}^T\phi \tag{2.41}$$

$$\zeta_n = r + \phi^T\tilde{U}\tilde{D}\tilde{U}^T\phi \tag{2.42}$$

When written in terms of the vector components and the diagonal elements of $\tilde{D}$ the latter equation becomes,

$$\zeta_n = r + \sum_{i=1}^{n} a_i b_i = r + \sum_{i=1}^{n} \tilde{d}_i a_i^2 \tag{2.43}$$

Substituting (2.40), (2.41) and (2.42) into (2.39) yields,

$$\hat{U}\hat{D}\hat{U}^T = \tilde{U}\left[\tilde{D} - \zeta_n^{-1}bb^T\right]\tilde{U}^T \tag{2.44}$$

Defining the factorization of the term in brackets as,

$$\bar{U}\bar{D}\bar{U}^T = \tilde{D} - \zeta_n^{-1}bb^T \tag{2.45}$$

and substituting these values into (2.44) produces,

$$\hat{U}\hat{D}\hat{U}^T = \tilde{U}\bar{U}\bar{D}\bar{U}^T\tilde{U}^T \tag{2.46}$$

From this it can be seen that,

$$\hat{U} = \tilde{U}\bar{U} \quad \text{and} \quad \hat{D} = \bar{D} \tag{2.47}$$

Substituting these values into the left hand side of (2.44) yields,

$$\tilde{U}\bar{U}\hat{D}\bar{U}^T\tilde{U}^T = \tilde{U}\left[\tilde{D} - \zeta_n^{-1}bb^T\right]\tilde{U}^T \tag{2.48}$$

which reduces to,

$$\bar{U}\hat{D}\bar{U}^T = \tilde{D} - \zeta_n^{-1}bb^T \tag{2.49}$$

This simpler update can be performed in a numerically stable and computationally efficient fashion. The update is performed by taking,

$$c_n = -1/\zeta_n \tag{2.50}$$

and performing the backwards recursion for $j = n$ to $j = 1$,

$$\begin{aligned} \hat{d}_j &= \tilde{d}_j + c_j b_j^2 && (2.51) \\ c_{j-1} &= \frac{c_j \tilde{d}_j}{\hat{d}_j} && (2.52) \end{aligned}$$

$$\bar{U}_{ij} = \frac{c_j b_j b_i}{\hat{d}_j} \qquad i = 1, \ldots, j-1 \tag{2.53}$$

The update of the elements of the diagonal factor of the covariance matrix in (2.51) involves the addition of a positive term, and a negative term, since from (2.42) and (2.50) c_j is always negative. This form of computation can lose accuracy when the two terms are nearly equal and could possibly result in some of the elements of the diagonal factor becoming negative which would result in a negative-definite covariance. This difference computation can be avoided as follows. From the definition of b in (2.41) it can be seen that the elements of b are,

$$b_j = \tilde{d}_j a_j \tag{2.54}$$

Substituting this expression into (2.51) gives,

$$\hat{d}_j = \tilde{d}_j \left(1 + c_j \tilde{d}_j a_j^2\right) \tag{2.55}$$

This is then substituted into (2.52), the inverse is taken and the expression is rearranged to give,

$$\frac{1}{c_j} = \frac{1}{c_{j-1}} - \tilde{d}_j a_j^2 \tag{2.56}$$

This can be rearranged as,

$$\tilde{d}_j a_j^2 = \frac{1}{c_{j-1}} - \frac{1}{c_j} \tag{2.57}$$

Substituting this expression into (2.55) and simplifying yields,

$$\hat{d}_j = \tilde{d}_j \frac{c_j}{c_{j-1}} \tag{2.58}$$

From (2.43) and (2.50),

$$\frac{1}{c_n} = -\zeta_n = -\left(r + \sum_{k=1}^{n} \tilde{d}_k a_k^2\right) \tag{2.59}$$

Using the backwards recursion in (2.56), this can be expressed as,

$$\zeta_j = -\frac{1}{c_j} = -\left(r + \sum_{k=1}^{j} \tilde{d}_k a_k^2\right) \tag{2.60}$$

Replacing c_j and c_{j-1} in (2.58) with ζ_j and ζ_{j-1} allows the backwards recursion in (2.51) and (2.52) to be replaced by the initialization,

$$\zeta_1 = r + b_1 a_1 \tag{2.61}$$

$$\hat{d}_1 = \frac{r\tilde{d}_1}{\zeta_1} \tag{2.62}$$

and the forwards recursion from $j = 2, \ldots, n$,

$$\zeta_j = \zeta_{j-1} + b_j a_j \tag{2.63}$$

$$\hat{d}_j = \tilde{d}_j \frac{\zeta_{j-1}}{\zeta_j} \tag{2.64}$$

The update of the upper triangular factor of the covariance matrix, $\hat{U}$ can also be simplified. From (2.53) the update of the columns of $\bar{U}$ can be written as,

$$\bar{U} = I + \left[0 \;\; \lambda_2 b^{(1)} \;\; \lambda_3 b^{(2)} \;\; \cdots \;\; \lambda_n b^{(n-1)}\right] \tag{2.65}$$

where each column is the product of a scalar,

$$\lambda_j = \frac{c_j b_j}{\hat{d}_j} = -\frac{b_j}{\zeta_j \hat{d}_j} \tag{2.66}$$

and a column vector,

$$b^{(j)} = [b_1 \;\cdots\; b_j \;\overbrace{0 \;\cdots\; 0}^{n-j}]^T \tag{2.67}$$

Expressions (2.54) and (2.64) can be substituted into (2.66) to give the simpler expression,

$$\lambda_j = -\frac{a_j}{\zeta_{j-1}} \tag{2.68}$$

Combining (2.47) and (2.65) gives the updated upper triangular factor as,

$$\hat{U} = \tilde{U}\bar{U} = \tilde{U} + \left[0 \;\; \lambda_2 \tilde{U} b^{(1)} \;\; \lambda_3 \tilde{U} b^{(2)} \;\; \cdots \;\; \lambda_n \tilde{U} b^{(n-1)}\right] \tag{2.69}$$

Introducing the column vector,

$$K_{j+1} = \tilde{U} b^{(j)} \tag{2.70}$$

the expression for the updated upper triangular factor can be written as

$$\hat{U} = \tilde{U}\bar{U} = \tilde{U} + [0 \;\; \lambda_2 K_2 \;\; \lambda_3 K_3 \;\; \cdots \;\; \lambda_n K_n] \tag{2.71}$$

From the special structure of $\tilde{U}$ and $b^{(j)}$, and using $\tilde{u}_j$ to represent the j-th column of $\tilde{U}$, it can be seen that the update in (2.69) and (2.71) can be expressed as the recursion,

$$K_{j+1} = \tilde{U} b^{(j)} = K_j + b_j \tilde{u}_j \tag{2.72}$$

This recursive update requires a factor of n fewer operations than the direct update formed by computing $\bar{U}$ and $\tilde{U}\bar{U}$. The recursive update also yields the Kalman gain vector required for the parameter since from (2.33), (2.41) and (2.72),

$$\begin{aligned} K &= \frac{P\phi}{r + \phi^T P \phi} = \frac{\tilde{U}\tilde{D}\tilde{U}^T \phi}{\zeta_n} && (2.73) \\ &= \frac{\tilde{U} b}{\zeta_n} && (2.74) \\ &= \frac{K_{n+1}}{\zeta_n} && (2.75) \end{aligned}$$

The full U-D factored covariance update can thus be summarized as,

$$\begin{aligned} a &= \tilde{U}^T \phi && (2.76) \\ b &= \tilde{D} a && (2.77) \\ \zeta_1 &= r + a_1 b_1 && (2.78) \\ \hat{d}_1 &= \tilde{d}_1 r / \zeta_1 && (2.79) \end{aligned}$$

$$K_2 = [b_1 \ \underbrace{0 \cdots 0}_{n-1}] \tag{2.80}$$

followed by the recursion from $j = 2, \ldots, n$,

$$\zeta_j = \zeta_{j-1} + b_j a_j \tag{2.81}$$

$$\hat{d}_j = \tilde{d}_j \zeta_{j-1} / \zeta_j \tag{2.82}$$

$$\hat{u}_j = \tilde{u}_j - a_j K_j / \zeta_{j-1} \tag{2.83}$$

$$K_{j+1} = K_j + b_j \tilde{u}_j \tag{2.84}$$

The parameter update is performed as in (2.32), and (2.35) with the Kalman gain vector calculated as described in (2.75).

The U-D factored RLS implementation presented above provides greatly improved numerical properties with little increase in computational complexity[125]. Table 2.1 summarizes the operation counts required to perform a parameter and covariance update of an n parameter system using the unfactored and factored covariance update algorithms. For all but the smallest n, the operation counts are nearly identical.

Table 2.1: Operation Count to Update $n \times n$ Covariance Matrix.

Covariance Matrix	Operations		
	Additions	Multiplications	Divisions
Unfactored (P)	$1.5n^2 + 3.5n$	$1.5n^2 + 4.5n$	1
Factored (UDU^T)	$1.5n^2 + 1.5n$	$1.5n^2 + 3.5n$	$2n$

The operation counts noted in table 2.1 are slightly different than those reported in [14]. In [14] the algorithm was implemented to minimize the number of division operations, requiring n fewer divisions, but $2n$ more multiplications at each sampling interval. The computer on which the self-tuning PSS was implemented has a small ratio between the execution times of the division and multiplication instructions so the algorithm was adjusted to minimize the number of operations in general.

2.1.2 Exponential Forgetting

The RLS algorithm derived above has the deficiency that the covariance matrix, $P(t)$, continuously decreases as time progresses. The algorithm is unable to track parameter changes since all data since $t = 0$ are equally weighted. A method commonly employed to circumvent this problem is the application of exponential forgetting in which newer data are given more weight than older data[6]. The cost function to be minimized is then,

$$V(\theta) = \frac{1}{2}\sum_{t=1}^{N} \gamma^{N-t}\varepsilon^2(t) \tag{2.85}$$

where γ is the *forgetting factor* which discounts the effect of older data.

The derivation of the recursive identification algorithm with exponential forgetting begins by rewriting the summation form of the parameter estimation expression, (2.17), as,

$$\hat{\theta}(t) = \left[\sum_{s=1}^{t} \gamma^{t-s}\phi(s)\phi^T(s)\right]^{-1} \left[\sum_{s=1}^{t} \gamma^{t-s}\phi(s)y(s)\right] \tag{2.86}$$

The derivation proceeds as presented in the previous section.

The value of the covariance matrix at time t is,

$$P(t) = r\left[\sum_{s=1}^{t} \gamma^{t-s}\phi(s)\phi^T(s)\right]^{-1} \tag{2.87}$$

Breaking out the last term of the summation produces,

$$P(t) = r\left[\sum_{s=1}^{t-1} \gamma^{t-s}\phi(s)\phi^T(s) + \phi(t)\phi^T(t)\right]^{-1} \tag{2.88}$$

The covariance matrix at time $t-1$ is,

$$P(t-1) = r\left[\sum_{s=1}^{t-1} \gamma^{t-1-s}\phi(s)\phi^T(s)\right]^{-1} \tag{2.89}$$

Combining the last two equations gives the covariance at time t expressed as an update of the covariance at time $t-1$ as,

$$P^{-1}(t) = \gamma P^{-1}(t-1) + \phi(t)r^{-1}\phi^T(t) \tag{2.90}$$

Applying the matrix inversion lemma eliminates the matrix inversion required at each time step and results in the covariance matrix update expression,

$$P(t) = \frac{1}{\gamma}P(t-1) - \frac{\frac{1}{\gamma}P(t-1)\phi(t)\phi^T(t)\frac{1}{\gamma}P(t-1)}{r + \phi^T(t)\frac{1}{\gamma}P(t-1)\phi(t)} \tag{2.91}$$

which can be simplified to,

$$P(t) = \frac{1}{\gamma}\left[P(t-1) - \frac{P(t-1)\phi(t)\phi^T(t)P(t-1)}{\gamma r + \phi^T(t)P(t-1)\phi(t)}\right] \tag{2.92}$$

The remaining three equations making up the recursive least squares update at each time step are unchanged by the addition of the forgetting factor.

The exponential forgetting factor can also be applied to the U-D factored covariance matrix update. Applying the forgetting factor in this case is particularly efficient since the scaling in (2.92) need be applied only to the diagonal factor, D, of the covariance matrix and thus requires only n operations rather than the $n(n+1)/2$ operations of (2.92).

The application of a fixed forgetting factor to the covariance matrix poses a problem if the system is not continuously subjected to disturbances. In this case the covariance matrix can increase exponentially so that when some disturbance does affect the system the parameters vary wildly. A number of solutions to this problem of covariance 'blow-up' have been proposed. Among these are the placing of an upper limit on the trace of the covariance beyond which covariance updating is inhibited [55], holding the trace of the covariance matrix constant [55], and inhibiting covariance update when incoming data carry little information [120]. In 1981 Fortescue et al.[51] proposed a variable forgetting factor whose value was determined at each sampling interval based on the information contained in the current regressor vector. This method has been employed in a number of adaptive PSS algorithms [33, 34, 50, 56, 57]. The method handles the case of nonuniform information distribution in time, but does not address the problem of nonuniform distribution in parameter space. In [60] and [79] it is noted that variable forgetting factor of [51] may cause problems when applied to systems whose input signal is formed from the feedback of the system output. A forgetting method that avoids these problems is discussed in the following section.

2.1.3 Restricted Exponential Forgetting

When the excitation signal used for system identification is derived from feedback of the system output the information content of the regressor vector is not uniform in all directions of the parameter space. The application of exponential forgetting in this situation can lead to poor parameter identification. The problem can be illustrated using a two-dimensional example in which the parameter vector $\hat{\theta}$ has two components, θ_1 and θ_2. A plot of the confidence limits of the parameter values is given by the solution of,

$$(\theta_e - \hat{\theta}(t))P^{-1}(t)(\theta_e - \hat{\theta}(t)) = \text{constant} \tag{2.93}$$

The solution, θ_e, of (2.93) forms an ellipse in the $\theta_1\theta_2$ plane where the center of the ellipse is the current parameter estimate. The size of the ellipse indicates the uncertainty of the estimate in a particular direction. The problem caused be exponential forgetting is shown in figure 2.1. The long arrow joining the centers of the ellipses shows the direction of the Kalman gain vector. The ellipse decreases in size in the

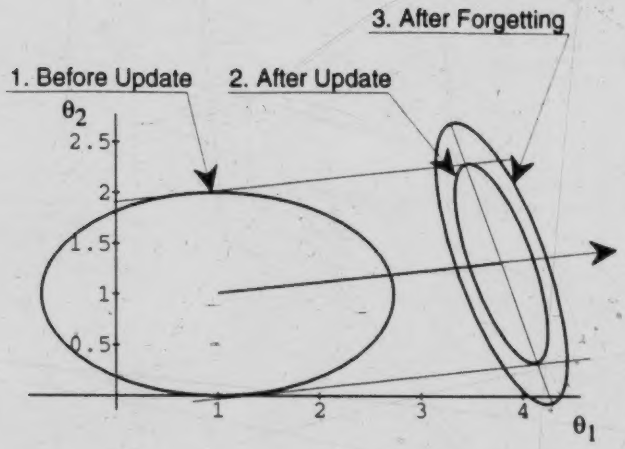

Figure 2.1: Covariance update using exponential forgetting.

direction of this vector. The exponential forgetting factor subtracts information, thus expanding the ellipse, in all directions. If, over a period of time, the incoming data contains information in only one direction, the covariance ellipsoids will become very large in the directions orthogonal to the incoming data. This condition arises when the excitation signal used for identification is computed as a feedback from the output signal. This is exactly the case when the identification is being performed as part of a self-tuning controller. When the excitation conditions change as a result of a change in disturbances affecting the plant, or as a result of a change in the plant parameters, the large covariance elements can cause the identified parameters to jump far from their desired values. This phenomenon of occasional large excursions in the parameter values is referred to in the literature as 'parameter bursting'.

An improved forgetting scheme, referred to as restricted exponential forgetting has been proposed by Hägglund [60] and Kulhavý [78, 79, 80]. The premise of the restricted exponential forgetting scheme is that information is forgotten only in the direction that new information is added.

The original inverse covariance update expression with no forgetting and assuming unit variance of the disturbance is (2.19),

$$P^{-1}(t) = P^{-1}(t-1) + \phi(t)\phi^T(t) \tag{2.94}$$

Application of an exponential forgetting factor, γ to this yields,

$$P^{-1}(t) = \gamma\left(P^{-1}(t-1) + \phi(t)\phi^T(t)\right) \tag{2.95}$$

The restricted exponential forgetting covariance update is given by,

$$P^{-1}(t) = P^{-1}(t-1) + \gamma'\phi(t)\phi^T(t) \tag{2.96}$$

Where γ' is calculated from the forgetting factor as,

$$\gamma' = \gamma - \frac{1-\gamma}{\phi^T P \phi} \tag{2.97}$$

The effect of the restricted exponential forgetting method on the same two-dimensional system is shown in figure 2.2. It can be seen that the forgetting in the direction of the Kalman gains is the same as that provided by exponential forgetting,

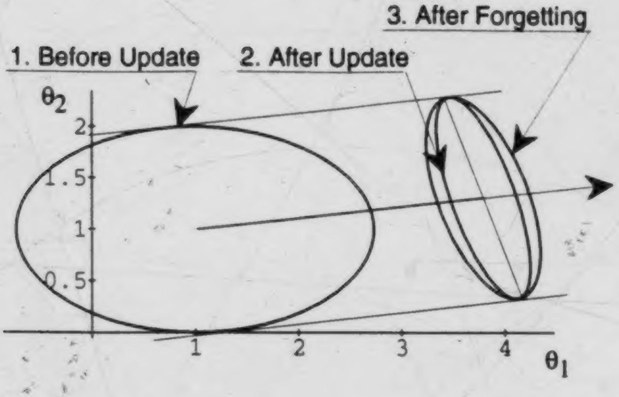

Figure 2.2: Covariance update using restricted exponential forgetting.

but that information is neither added nor subtracted in the orthogonal direction.

The implementation of restricted exponential forgetting is particularly convenient since the only change in the covariance update expression (2.33) or (2.78)-(2.79) is the replacing of r with γ'^{-1}. The forgetting can thus be applied with no more calculations than those involved with the original covariance update. The only additional calculations are the two subtractions and one division involved in calculating γ'.

In [80] a method for computing a forgetting factor that varies with the information contained in the present sample is described. At each step the following calculations are performed,

$$\epsilon(t) = y(t) - \phi^T(t)\theta(t) \tag{2.98}$$

$$\zeta(t) = \phi(t)^T U(t-1)D(t-1)U^T(t-1)\phi(t) \tag{2.99}$$

$$\eta(t) = \frac{\epsilon(t)\epsilon(t)}{\Lambda(t)} \tag{2.100}$$

$$\begin{aligned}
\epsilon_N^2 &= \frac{(\nu(t)+1)\eta}{1+\zeta(t)+\eta(t)} && (2.101)\\
\gamma(t+1) &= \left[1+(1+\rho)\left(\ln(1+\zeta(t))+\frac{\zeta(t)}{1+\zeta(t)}(\epsilon_N^2(t)-1)\right)\right]^{-1} && (2.102)\\
\Lambda(t+1) &= \gamma(t+1)\left[\Lambda(t)+\frac{\epsilon(t)\epsilon(t)}{1+\zeta(t)}\right] && (2.103)\\
\nu(t+1) &= \gamma(t+1)[\nu(t)+1] && (2.104)\\
\gamma'(t) &= \gamma(t+1)-\frac{1-\gamma(t+1)}{\zeta(t)} && (2.105)
\end{aligned}$$

The value $\gamma'^{-1}(t)$ is then used in the place of r in the covariance update expressions (2.78) and (2.79). The parameter update equation becomes,

$$\hat{\theta}(t) = \hat{\theta}(t) + \frac{U(t-1)D(t-1)U^T(t-1)\phi(t)}{1+\zeta(t)}\epsilon(t) \tag{2.106}$$

An alternative method for computing the forgetting factor at each sampling interval was proposed by Sripada and Fisher [120]. The forgetting factor is computed as,

$$\gamma_t = 1 - \frac{1+\zeta(t)-\sqrt{(1+\zeta(t))^2-\frac{4\|P(t-1)\phi(t)\|^2}{\mathrm{tr}\ P(t-1)}}}{2} \tag{2.107}$$

The above two methods for computing the forgetting factor were evaluated in simulation studies of a self-tuning PSS. Results are presented later in this thesis.

Another method for discounting the effect of old information in least squares identification was proposed by Salgado, Goodwin and Middleton [111]. The method does not easily permit the update of the factorized covariance matrix though, and was not evaluated.

2.2 Generalized Minimum Variance Control

This derivation of the generalized minimum variance control algorithm parallels that presented by Clarke and Gawthrop [35] which itself is an extension of Åström and Wittenmark's minimum variance regulator [5, 7, 63].

The system to be controlled is linear, time-invariant, has a single input, a single output and is subjected to random disturbances. It is described by the ARMAX (autoregressive, moving average with exogenous input) difference equation,

$$\sum_{i=0}^{n} a_i y_{t-i} = \sum_{i=0}^{n} b_i u_{t-k-i} + d + \sum_{i=0}^{n} c_i \xi_{t-i} \tag{2.108}$$

At a particular instant of time t, u_t is the system input, y_t is the system output, and ξ_t is the value of an unmeasurable, uncorrelated, zero-mean, random sequence disturbing the system. The system is of order n with an inherent delay of k sampling intervals and operates around a constant output level d. It is conventional to set the values of a_0 and c_0 to 1 and to scale the b coefficients and the variance of the disturbance sequence ξ_t accordingly. This model is more often expressed in terms of polynomials in the backwards shift operator z^{-1} as,

$$A(z^{-1})y_t = z^{-k}B(z^{-1})u_t + d + C(z^{-1})\xi_t \tag{2.109}$$

The coupling of the disturbance is minimum phase so the roots of $C(z) = 0$ are within the unit circle.

The cost function to be minimized is the expectation of the weighted control action u_t, and weighted deviations of the system output y_t from the setpoint w_t,

$$I = E\left\{\left(\sum_{i=0} p_i y_{t+k-i} - \sum_{i=0} r_i w_{t-i}\right)^2 + \left(\sum_{i=0} q'_i u_{t-i}\right)^2\right\} \tag{2.110}$$

The cost function can also be written in terms of polynomials in the backwards shift operator,

$$I = E\left\{(P(z^{-1})y_{t+k} - R(z^{-1})w_t)^2 + (Q'(z^{-1})u_t)^2\right\} \tag{2.111}$$

Fortescue, Kershenbaum and Ydstie [51] expand on this with P, Q' and R as ratios of polynomials in the backwards shift operator.

A special case of the cost function results when all the weighting parameters but p_0 are zero. The controller minimizing this cost function is known as the minimum variance regulator [7, 8] and operates by predicting the system output k steps ahead and choosing u_t so as to set the prediction to zero. The controller minimizing the cost function in the case of general weighting parameters is referred to as the generalized minimum variance controller.

2.2.1 k-Step Ahead Output Predictor

The generalized minimum variance control strategy is based on the minimization of the expected value of a number of terms. One of the terms includes the value of the system output k steps in the future. A method for predicting this value is the subject of the following paragraphs.

As noted in the previous section the system can be expressed as,

$$A(z^{-1})y_t = z^{-k}B(z^{-1})u_t + d + C(z^{-1})\xi_t \tag{2.112}$$

This can be expressed more concisely by dropping the (z^{-1}) notation from the polynomials. The system output is then expressed as,

$$y_t = z^{-k}\frac{B}{A}u_t + \frac{d}{A} + \frac{C}{A}\xi_t \tag{2.113}$$

The output at k steps in the future is given by applying the shift operator z^k to the right hand side of this equation and noting that $z^k d \equiv d$ since d is constant,

$$y_{t+k} = \frac{B}{A}u_t + \frac{d}{A} + z^k\frac{C}{A}\xi_t \tag{2.114}$$

The last term of this expression can be split into two components, the first being the effect of future disturbances and the second the effect of disturbances up to and including time t,

$$z^k\frac{C}{A}\xi_t = z^k E'_k\xi_t + \frac{F'_k}{A}\xi_t \tag{2.115}$$

The polynomial $E'_k(z^{-1})$ is the first k terms of the quotient $C(z^{-1})/A(z^{-1})$ and $z^{-k}F'_k(z^{-1})$ is the remainder.

The two components of the disturbance are defined as,

$$e_{t+k} \triangleq z^k E'_k\xi_t \tag{2.116}$$

$$e_t \triangleq \frac{F'_k}{A}\xi_t \tag{2.117}$$

Substituting these values into (2.114) yields,

$$y_{t+k} = \left[\frac{B}{A}u_t + \frac{F'_k}{A}\xi_t + \frac{d}{A}\right] + e_{t+k} \tag{2.118}$$

Define $y^*_{t+j|t}$ as the optimal (in the least squares sense) predictor of the system output y at time $t+j$, given input and output samples up to, and including, time t. The actual output at time $t+k$ is then the predicted output plus the effect of disturbances occurring between time t and time $t+k$. This can be expressed by,

$$y^*_{t+k|t} \triangleq y_{t+k} - e_{t+k} \tag{2.119}$$

Substituting the value of y_{t+k} from (2.118) into (2.119) produces,

$$y^*_{t+k|t} = \frac{B}{A}u_t + \frac{F'_k}{A}\xi_t + \frac{d}{A} \tag{2.120}$$

From (2.116), the effect of future disturbances is given by,

$$e_{t+k} = z^k E'_k \xi_t \tag{2.121}$$

Taking the time shift out of both sides gives,

$$e_t = E'_k \xi_t \tag{2.122}$$

Taking (2.119) and shifting it back k steps in time yields,

$$y^*_{t|t-k} = y_t - e_t \tag{2.123}$$

Merging the last two equations produces,

$$\xi_t = \frac{y_t - y^*_{t|t-k}}{E'_k} \tag{2.124}$$

Substituting this value into the expression for the predicted output, (2.120), yields,

$$y^*_{t+k|t} = \frac{B}{A}u_t + \frac{F'_k}{E'_k A}(y_t - y^*_{t|t-k}) + \frac{d}{A} \tag{2.125}$$

Grouping the predictions on the left hand side gives,

$$y^*_{t+k|t} + \frac{F'_k}{E'_k A}y^*_{t|t-k} = \frac{B}{A}u_t + \frac{F'_k}{E'_k A}y_t + \frac{d}{A} \tag{2.126}$$

Expressing the time shift in the second term on the left hand side as the application of z^{-k} and placing both left hand terms over a common denominator produces,

$$\frac{E'_k A y^*_{t+k|t} + z^{-k} F'_k y^*_{t+k|t}}{E'_k A} = \frac{B}{A}u_t + \frac{F'_k}{E'_k A} y_t + \frac{d}{A} \tag{2.127}$$

Rearranging some terms in the numerator of the left hand side of (2.127) to reflect the effect of past and future disturbances, as shown in (2.115), yields,

$$C = E'_k A + z^{-k} F'_k \tag{2.128}$$

The numerator of the left hand side of (2.127) can thus be written as,

$$\frac{C}{E'_k A} y^*_{t+k|t} = \frac{B}{A}u_t + \frac{F'_k}{E'_k A} y_t + \frac{d}{A} \tag{2.129}$$

Multipling both sides by $E'_k A$ produces,

$$C y^*_{t+k|t} = E'_k B u_t + F'_k y_t + E'_k d \tag{2.130}$$

Since d is a constant the expression $E'_k d$ can be replaced by the term $\gamma_k d$, where γ_k is the sum of the first k terms of the E polynomial,

$$\gamma_k = \sum_{i=0}^{k-1} e_i \tag{2.131}$$

Substituting this term in (2.130) results in the recursive expression for the k-step ahead predictor.

$$Cy^*_{t+k|t} = F'_k y_t + E'_k B u_t + \gamma_k d \tag{2.132}$$

The term recursive applies since the estimate $y^*_{t+j|t}$ is required to determine the value of $y^*_{t+j+1|t}$. The recursion begins by calculating $y^*_{t+1|t}$ and continues till $y^*_{t+k|t}$ (where k is the system delay) has been determined.

2.2.2 Generalized Minimum Variance Control Strategy for Systems with Known Parameters

The derivation of the generalized minimum variance control strategy begins by substituting the value of the system output from (2.119) into the cost function (2.111), producing the expression,

$$I = E\left\{(P(y^*_{t+k|t} + e_{t+k}) - Rw_t)^2 + (Q'u_t)^2\right\} \tag{2.133}$$

The only non-deterministic component of this expression is the error term, e_{t+k}, which is uncorrelated with the other terms. It can thus be separated from the other terms and the expectation operator can be dropped from those terms. The expression for the cost function then becomes,

$$I = (Py^*_{t+k|t} - Rw_t)^2 + (Q'u_t)^2 + E\left\{(Pe_{t+k})^2\right\} \tag{2.134}$$

The polynomial P is time-invariant and the disturbances are ergodic so the expectation can be replaced by the variance of the random sequence, Pe_{t+k}, as follows,

$$I = (Py^{*}_{t+k|t} - Rw_t)^2 + (Q'u_t)^2 + \sigma^2 \tag{2.135}$$

The goal is to choose a control action u_t that will minimize the value of this cost function. To that end the partial derivative of the cost function with respect to u_t is taken,

$$\frac{\partial I}{\partial u_t} = 2(Py^{*}_{t+k|t} - Rw_t)\frac{\partial y^{*}_{t+k|t}}{\partial u_t} + 2q'_0Q'u_t \tag{2.136}$$

The partial derivative on the right side of this expression can be formed from the k-step ahead prediction expression, (2.132), as,

$$\frac{\partial y^{*}_{t+k|t}}{\partial u_t} = \frac{e_0 b_0}{c_0} \tag{2.137}$$

The first coefficient of the E polynomial, e_0, is a_0/c_0, and both of these coefficients are equal to 1, so the partial derivative of the cost function can be written as,

$$\frac{\partial I}{\partial u_t} = 2(Py^{*}_{t+k|t} - Rw_t)b_0 + 2q'_0Q'u_t \tag{2.138}$$

The partial derivative of (2.138) with respect to u_t is positive so the cost function is minimized when (2.138) is set to zero. This gives the control strategy,

$$Py^{*}_{t+k|t} - Rw_t + \frac{q'_0Q'}{b_0}u_t = 0 \tag{2.139}$$

Substituting a new polynomial Q, defined as $q_0'Q'/b_0$, into (2.139) yields the expression for the control action,

$$Py^*_{t+k|t} - Rw_t + Qu_t = 0 \tag{2.140}$$

An alternative method of computing the control action can be formed by defining two new auxiliary signals in terms of the setpoint, control action, and real and predicted outputs,

$$\begin{aligned} \alpha^*_{t+k|t} &\triangleq Py^*_{t+k|t} - Rw_t + Qu_t && (2.141) \\ \alpha_{t+k} &\triangleq Py_{t+k} - Rw_t + Qu_t && (2.142) \end{aligned}$$

From (2.119) the real system output can be written as the sum of the predicted output and an error term as,

$$y_{t+k} = y^*_{t+k|t} + e_{t+k} \tag{2.143}$$

Substituting (2.143) into (2.142) gives,

$$\alpha_{t+k} = Py^*_{t+k|t} + Pe_{t+k} - Rw_t + Qu_t \tag{2.144}$$

Combining (2.141) and (2.144) gives,

$$\alpha_{t+k} = \alpha^{*}_{t+k|t} + Pe_{t+k} \tag{2.145}$$

The error term e_{t+k} in (2.143) is uncorrelated with the prediction $y^{*}_{t+k|t}$. Another function can be defined in terms of this error term and the first k coefficients of the P polynomial as,

$$\epsilon_{t+k} = \sum_{i=0}^{k-1} p_i e_{t+k-i} \tag{2.146}$$

Substituting (2.146) into (2.145) yields,

$$\alpha_{t+k} = \alpha^{*}_{t+k|t} + \epsilon_{t+k} \tag{2.147}$$

From (2.147) it can be observed that $\alpha^{*}_{t+k|t}$ is the optimal least squares predictor of α_{t+k}. Defining another cost function as the variance of the auxiliary signal, as,

$$J = E\left\{(\alpha_{t+k})^2\right\} \tag{2.148}$$

and then substituting the values of ϵ_{t+k} and $\alpha^{*}_{t+k|t}$ into (2.148) yields,

$$J = E\left\{(\alpha^{*}_{t+k|t} - Pe_{t+k})^2\right\} \tag{2.149}$$

The polynomial P is time-invariant and the disturbances are ergodic so the expectation can be replaced by the variance of the random sequence. The same expectation can be seen in (2.135). The prediction term is deterministic and can thus be removed from the expectation. The cost function can thus be expressed as,

$$J = \alpha^*_{t+k|t} + \sigma^2 \tag{2.150}$$

$$J = Py^*_{t+k|t} - Rw_t + Qu_t + \sigma^2 \tag{2.151}$$

Taking the partial derivative of (2.151) with respect to u_t yields,

$$\frac{\partial J}{\partial u_t} = 2\left(Py^*_{t+k|t} - Rw_t + Qu_t\right)\left(\frac{\partial y^*_{t+k|t}}{\partial u_t} + q_0\right) \tag{2.152}$$

Setting this derivative to zero results in the same control law as derived earlier (2.140), namely,

$$Py^*_{t+k|t} - Rw_t + Qu_t = 0 \tag{2.153}$$

From the definition of the auxiliary signal (2.141) it can be seen that (2.153) can be equivalently stated as,

$$\alpha^*_{t+k|t} = 0 \tag{2.154}$$

Inserting the expression for predicting the system output, (2.132), into (2.141) yields,

$$\alpha^*_{t+k|t} = \frac{P}{C}\left[F'_k y_t + E'_k B u_t + \gamma_k d\right] - Rw_t + Qu_t \tag{2.155}$$

and expressing the P polynomial as an explicit summation gives,

$$\alpha^*_{t+k|t} = \sum_{j=0}^{k-1} \frac{p_j}{C} \left[F'_{k-j} y_t + E'_{k-j} B u_t + \gamma_{k-j} d \right] - R w_t + Q u_t \tag{2.156}$$

Three new polynomials and a new constant are defined from the terms of (2.156) as,

$$F(z^{-1}) \triangleq \sum_{j=0}^{k-1} p_j F'_{k-j} \tag{2.157}$$

$$G(z^{-1}) \triangleq \sum_{j=0}^{k-1} p_j z^{-j} E'_{k-j} B + CQ \tag{2.158}$$

$$H(z^{-1}) \triangleq -CR \tag{2.159}$$

$$\delta \triangleq \sum_{j=0}^{k-1} p_j \gamma_{k-j} d \tag{2.160}$$

Substituting these polynomials into (2.156) yields,

$$C\alpha^*_{t+k|t} = F y_t + G u_t + H w_t + \delta \tag{2.161}$$

In (2.154) it was noted that the control action that minimizes the value of the cost functions I and J sets $\alpha^*_{t+k|t}$ to zero at each step. The desired control action is thus computed as,

$$u_t = -\frac{1}{G} \left[F y_t + H w_t + \delta \right] \tag{2.162}$$

2.2.3 Self-Tuning Generalized Minimum Variance Control

The generalized minimum variance control strategy described in the previous section can be easily adapted to the self-tuning case where only an estimate of the plant parameters is available.

From (2.161) the prediction of the auxiliary signal is given by,

$$C\alpha^{*}_{t+k|t} = Fy_t + Gu_t + Hw_t + \delta \tag{2.163}$$

From (2.147) the actual value of the auxiliary signal at time $t+k$ is equal to the predicted value plus a disturbance. This can be expressed as,

$$\alpha_{t+k} = \alpha^{*}_{t+k|t} + \epsilon_{t+k} \tag{2.164}$$

The generalized minimum variance control action sets the predicted value of the auxiliary signal to zero at each sampling step. The true value is thus equal to the disturbance component only, as in,

$$\alpha_{t+k} = \epsilon_{t+k} \tag{2.165}$$

If the C polynomial in (2.163) is equal to 1 it can be seen that the combination of (2.163) and (2.164) reduces to the form used in the derivation of the least squares identification algorithm,

$$\alpha_{t+k} = \phi_t^T\theta + \epsilon_{t+k} \tag{2.166}$$

The regressor vector is given by,

$$\phi_t^T = [\, y_t \; y_{t-1} \; \ldots \; u_t \; u_{t-1} \; \ldots \; w_t \; w_{t-1} \ldots \; 1 \,] \tag{2.167}$$

The vector of parameters to be identified is,

$$\theta^T = [\, f_0 \; f_1 \; \ldots \; g_0 \; g_1 \; \ldots \; h_0 \; h_1 \; \ldots \; \delta \,] \tag{2.168}$$

The disturbance ϵ_t is uncorrelated with the elements of the regressor, ϕ_t, so the recursive least squares identification of the parameter estimates, $\hat{\theta}_t$, will converge to the actual parameters. The control action is calculated at each sampling interval using the latest estimate of the parameter vector to set the predicted value of the auxiliary signal to zero. This is given by,

$$C\alpha^*_{t+k|t} = \hat{F}y_t + \hat{G}u_t + \hat{H}w_t + \hat{\delta} = \phi_t^T\hat{\theta}_t = 0 \tag{2.169}$$

If the C polynomial has more than a single term the elements of the regressor are not uncorrelated with the disturbance. Under these conditions the parameters identified by recursive least squares will not converge to the true parameter values. In [7] it is shown that the bias in the identified parameters is such that the control action still converges to that of the GMV controller based on the known A, B and C polynomial coefficients. In effect, the C polynomial is implicitly identified and the values are incorporated into the control strategy. An identification technique which explicitly identifies the coefficients of the C polynomial is briefly described in chapter four.

In [35] it is noted that good control action can be achieved by the self-tuning GMV controller even when identification is imprecise. If a parameter is difficult to identify because it has little effect on the prediction error of the recursive least squares identification it will have correspondingly little effect on the calculation of the control signal. An example of this is included later in this chapter.

Further analysis of the self-tuning generalized minimum variance control algorithm may be found in [55]. An analysis of the convergence properties of the multivariable implementation of the algorithm is in [56]. A recent paper by Guo and Chen [59] presents a rigorous proof of the stability and optimality of the self-tuning regulator presented in [7] and gives a proof of convergence of extended least squares adaptive trackers.

2.3 Examples Illustrating Concepts and Algorithms

2.3.1 Example of U-D Factorization

To illustrate the effectiveness and importance of U-D factorization of the covariance matrix update an example of recursive least squares identification with and without factorization was performed.

Consider the fourth-order continuous-time plant given by,

$$\frac{Y(s)}{U(s)} = \frac{180s}{s^2 + 0.1s + 100} \cdot \frac{s^2 + 0.1s + 36}{s^2 + 0.1s + 25} \tag{2.170}$$

The discrete-time ARMAX model of this plant, assuming a zero-order hold on the input and a 25 millisecond sampling interval is,

$$\begin{aligned} A(z^{-1})y(t) &= B(z^{-1})u(t) + \xi(t) \\ A(z^{-1}) &= 1.0 + 3.91732z^{-1} - 5.83082z^{-2} + 3.90754z^{-3} - 0.995012z^{-4} \\ B(z^{-1}) &= 4.45284z^{-1} - 13.2474z^{-2} + 13.2363z^{-3} - 4.44172z^{-4} \end{aligned} \tag{2.171}$$

The coefficients of the A and B polynomials are the parameters to be identified by the recursive least squares algorithms. The excitation sequence $u(t)$ and noise sequence $\xi(t)$ consist of samples from a Gaussian, zero-mean, unit-variance pseudo-random number generator. One thousand samples of the excitation sequence and the plant output sequence $y(t)$ are processed by four recursive least squares identification algorithms. The first two algorithms use a U-D factored covariance update algorithm implemented in double and single precision floating point arithmetic, respectively. Double precision arithmetic on the simulation machine has a precision of about 16 decimal digits while single precision arithmetic has a precision of about 7 decimal digits. The second two identification algorithms are double and single precision versions of the recursive least squares method employing the non-factored covariance matrix.

Figure 2.3 shows plots of the trace of the covariance matrix calculated by each

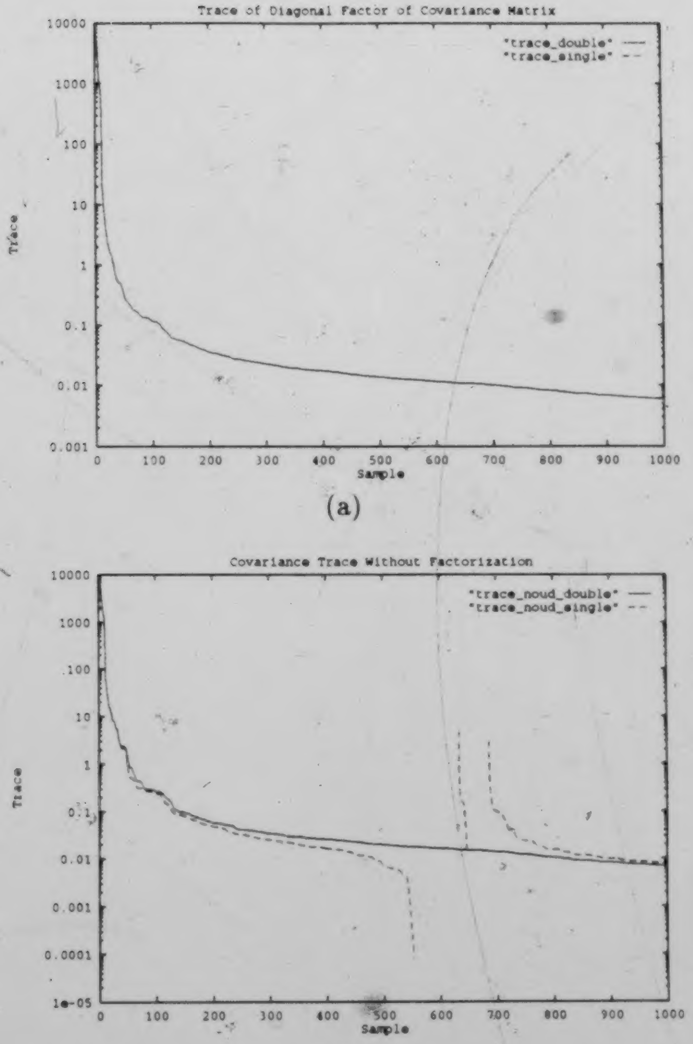

(a)

(b)

Figure 2.3: Covariance traces for factored (a) and non-factored (b) covariance updates. — Double precision - - Single precision (missing portions of plot indicate where covariance trace is negative).

of the algorithms. The single and double precision version of the factored update are virtually identical. The trace calculated by the single precision version of the non-factored updated is not monotonically decreasing and in fact becomes negative, as noted by the gaps in the plot, for considerable intervals.

The effect of numerical instability is even more dramatic on the identification of the A and B polynomial coefficients. As shown in figures 2.4 and 2.5 the parameters identified by the factored covariance update algorithm converge quickly and remain near the values used by the simulation. On the other hand, the parameters identified by the algorithm employing a non-factored covariance update make occasional bursts far from their true values. The double precision version of both the algorithms yield parameter updates virtually identical to the factored single precision algorithm.

Clearly the factored covariance update algorithm is much more numerically stable. The single-precision, non-factored update algorithm is numerically unsound even for identification of models as simple as fourth order. Algorithms which permit the use of single-precision arithmetic are very desirable since the existing digital stabilizer hardware on which the self-tuning controller was implemented imposes a considerable speed penalty for double precision calculations[45].

2.3.2 Example of Self-Tuning GMV Control

In section 2.2.3 it was noted that the self-tuning GMV control algorithm can provide good control even when system parameter identification is imprecise. This ability was investigated using a discrete-time simulation of a fourth-order continuous-time

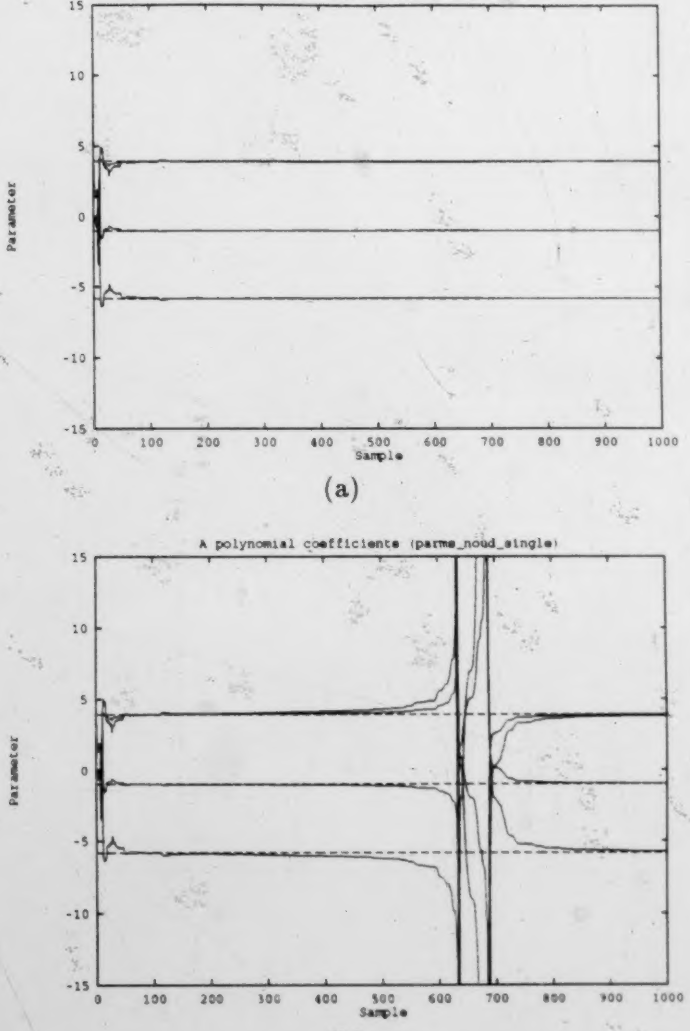

(a)

(b)

Figure 2.4: *A* polynomial coefficients identified by factored (a) and non-factored (b) covariance update algorithms.

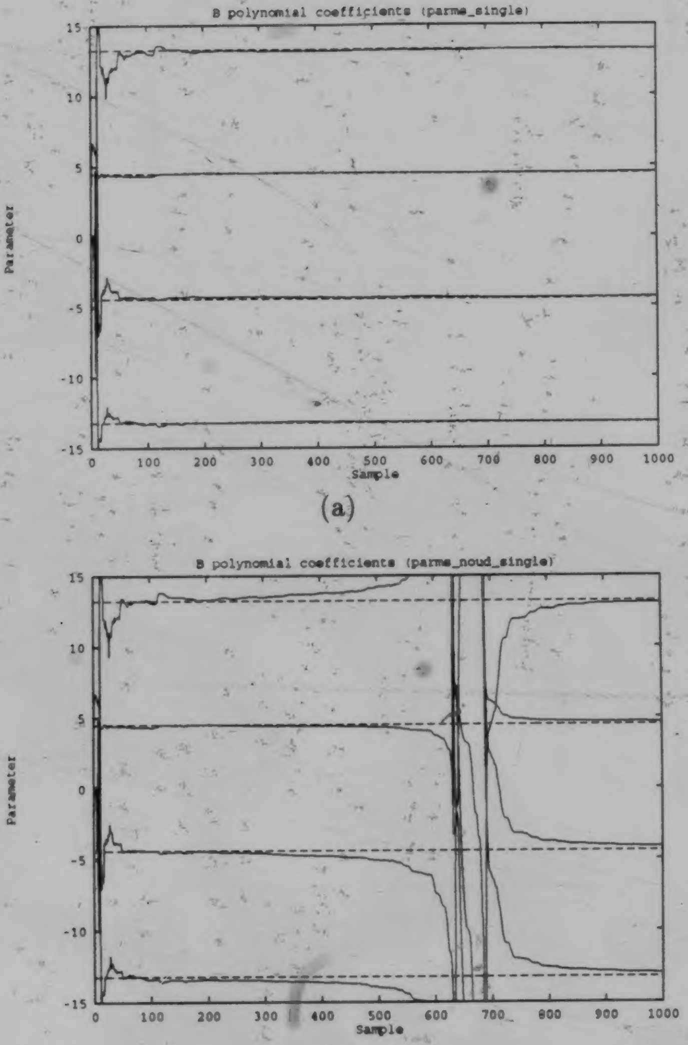

(a)

(b)

Figure 2.5: *B* polynomial coefficients identified by factored (a) and non-factored (b) covariance update algorithms.

system. The continuous-time transfer function of the system to be controlled was

$$\frac{Y(s)}{U(s)} = \frac{18s}{s^2 + 0.3s + 100} \cdot \frac{s^2 + 0.2s + 36}{s^2 + 0.4s + 16} \tag{2.172}$$

The discrete-time equivalent of this system sampled at 20 Hz can be expressed as,

$$A(z^{-1})y(t) = B(z^{-1})y(t) + C(z^{-1})\xi(t) \tag{2.173}$$

with polynomial coefficients,

$$A = [\ 1.0 \quad -3.66075 \quad 5.30778 \quad -3.59768 \quad 0.965605\ ]$$

$$B = [\ 0.0 \quad 0.856219 \quad -2.48382 \quad 2.47541 \quad -0.847804\ ]$$

$$C = [\ 1.0 \quad 0.0 \quad 0.0 \quad 0.0 \quad 0.0\ ]$$

and with $\xi(t)$ formed as samples of a zero-mean, unit-variance, Gaussian sequence.

The frequency response of the transfer function coupling the disturbance and the output, $C(z)/A(z)$, was computed and plotted. The system response with no control action is shown as the short dashed line in figures 2.6 and 2.7. The two resonant modes are clearly visible. The frequency response of the disturbance transfer function with a generalized minimum variance controller based on the true parameter values was also plotted. This response is shown as the long dashed lines in the figures. The maximum response has been suppressed by over 15 db and both resonant modes have been considerably damped. Plant output variations were given twice as much weight as control signal variations when forming the GMV control strategy. The coefficients of this controller are

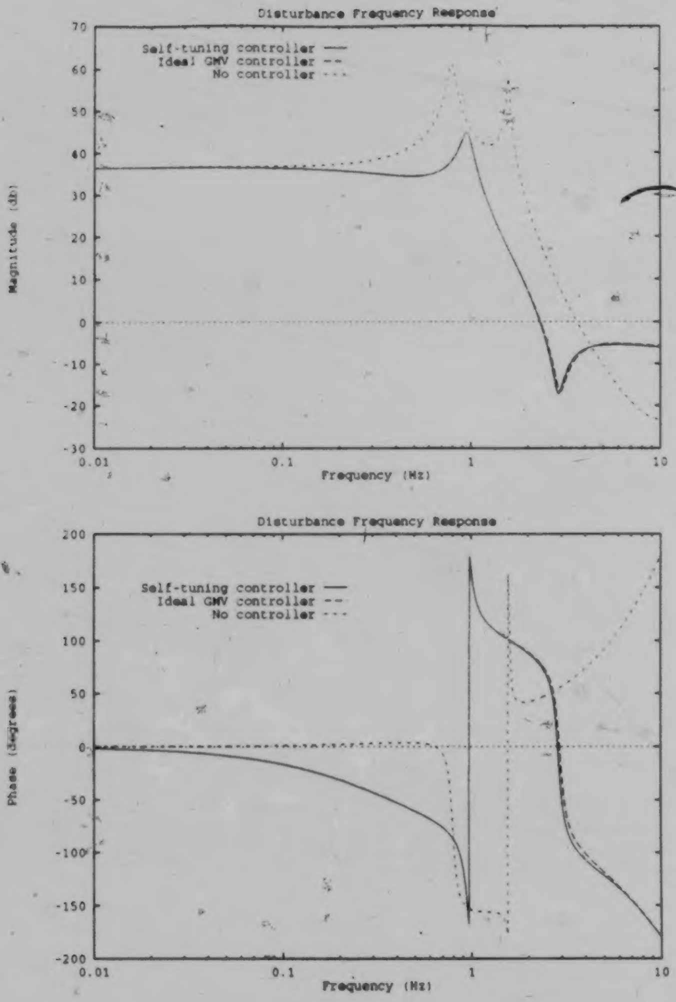

Figure 2.6: Disturbance transfer function after 2000 samples. — Controller using identified parameters. – – Controller using actual parameters. - - - No controller.

$$F = [\ 3.66075 \quad -5.30778 \quad 3.59768 \quad -0.965605\ ]$$

$$G = [\ 1.356219 \quad -2.48382 \quad 2.47541 \quad -0.847804\ ]$$

After 2000 steps the self-tuning GMV controller had adjusted its control parameters to

$$F = [\ 3.62550\ \ -4.98795\ \ 3.27592\ \ -0.759499\ ]$$

$$G = [\ 1.35578\ \ -2.38040\ \ 2.30003\ \ -0.691289\ ]$$

The first three coefficients of the F and G polynomials were identified quite closely. The final coefficient of each polynomial was somewhat farther away from the actual parameter value. The frequency response of the transfer function when the identified parameters are used in the control strategy is shown as the solid line in figure 2.6. The response is almost indistinguishable from that of the controller formed using the true parameters. This indicates that the control action is quite insensitive to the discrepancy in the final polynomial coefficients.

The variances of the control action and the plant output over the 2000 steps were computed. The square root of the variance of the plant output was 28.0 and the square root of the variance of the controller output was 55.9. These values correctly reflect the relative weights given the signals in the self-tuning component of the controller. An indication of the effectiveness of the GMV controller in damping the plant output is made by noting that the square root of the variance of the uncontrolled plant output was 137.3.

A further check on the ability of the GMV control strategy to provide good control with poorly identified parameters was made by applying the same sequence to the system but this time stopping after only 100 steps.

At this point the self-tuning GMV controller had adjusted its control parameters to,

$$F = [\ \texttt{3.16766 -3.60796 1.82135 -0.165505}\ ]$$

$$G = [\ \texttt{1.38883 -1.99010 1.43846 -0.187817}\ ]$$

Only the first coefficient of the G polynomial is close to the true parameter value. The other coefficients differ from the true values by as much as a factor of six. The frequency response of the transfer function when the identified parameters are used in the control strategy is shown as the solid line in figure 2.7. It can be seen that the control action with the identified parameters is still very close to that of the controller based on the true parameter values. In particular, the two resonant modes of the uncontrolled plant are almost identically suppressed by both controllers. The rapid convergence to an effective control strategy is evident from this test.

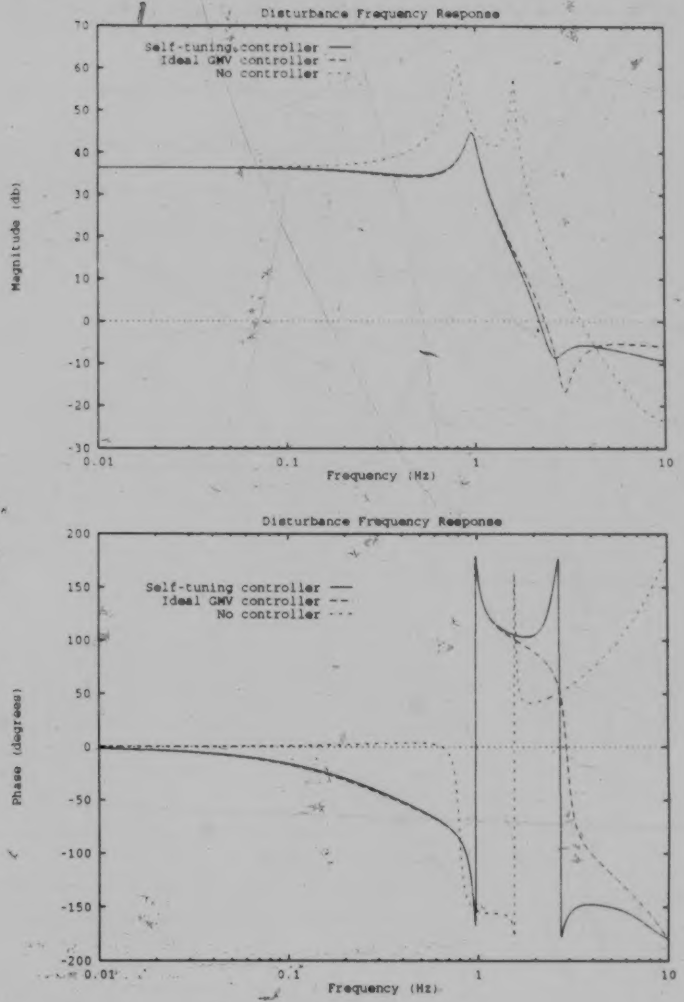

Figure 2.7: Disturbance transfer function after 100 samples. — Controller using identified parameters. - - Controller using actual parameters. - - - No controller.

Chapter 3

Model of Power System for Simulation Studies

An existing power system simulation program was used to study the operation of the self-tuning PSS. The program was originally developed with controller studies in mind thus the detailed characteristics of the power distribution network are assigned secondary importance. Features such as over-current protection, tap-changing transformers, different load representations and unsymmetrical faults are not included in the program. Several of the concepts on which the program is based are taken from an earlier program by Podmore and Fleming[106].

The following sections present the salient features of the simulation program. Each piece of equipment is modelled as an analog-computer simulation of the actual system hardware. The synchronous generator model is the most critical component of the simulation and is described in depth. The remaining components are quite simple in comparison to the generator model. These pieces of equipment are described in terms of their block and analog computer diagrams.

3.1 Mathematical Model of the Synchronous Generator

The synchronous generator model used in the transient stability program is similar to the model described by Olive [100, 101] and is based upon the $d-q-o$ variables obtained by Park's equations [103, 104] from phase quantities.

The equations of a synchronous machine can be derived from a linear two-pole model. The stator is considered to be three identical, symmetrically-placed, lumped windings called a, b and c. Two unequal lumped windings with axes 90° apart are located on the periphery of the rotor. The winding in the direct axis is called f and represents the field winding. The winding in the other axis is called g and is a fictitious winding inserted to account for transient behavior in the quadrature axis. Subtransient effects in both direct and quadrature axes are ignored. The IEEE Task Force on definitions [70] refers to a representation of this complexity as Model 1.1.

The assumptions made in the development of the model are:

1. All inductances are independent of current. This restriction is lifted in section 3.1.4 where the effects of saturation are added to the model.
2. All self and mutual inductances can be represented as constants plus a sinusoidal component based upon the rotor angle θ_r or $2\theta_r$.
3. All distributed windings can be represented as lumped windings.
4. The effects of currents flowing in the iron parts of the rotor or in a damper winding can be represented by a single lumped rotor coil g.

Park's equations for a machine with the windings noted above are,

$$v_d = -R_a i_d + \frac{d\lambda_d}{dt} - \omega_r \lambda_q \tag{3.1}$$

$$v_q = -R_a i_q + \frac{d\lambda_q}{dt} + \omega_r \lambda_d \tag{3.2}$$

$$v_0 = -R_a i_0 + \frac{d\lambda_0}{dt} \tag{3.3}$$

$$v_f = R_f i_f + \frac{d\lambda_f}{dt} \tag{3.4}$$

$$v_g = R_g i_g + \frac{d\lambda_g}{dt} = 0 \tag{3.5}$$

$$\lambda_d = -L_d i_d + L_{afm} i_f \tag{3.6}$$

$$\lambda_q = -L_q i_q + L_{agm} i_g \tag{3.7}$$

$$\lambda_0 = L_0 i_0 \tag{3.8}$$

$$\lambda_f = -\tfrac{3}{2} L_{afm} i_d + L_{ff} i_f \tag{3.9}$$

$$\lambda_g = -\tfrac{3}{2} L_{agm} i_q + L_{gg} i_g \tag{3.10}$$

For studies focussing on mechanical oscillations and transient behavior below 10 Hz the transformer voltages $\frac{d\lambda_d}{dt}$ and $\frac{d\lambda_q}{dt}$ can be neglected. The zero-sequence variables need not be considered since only symmetrical faults are considered. With these simplifications the equations become,

$$v_d = -R_a i_d - \omega_r \lambda_q \tag{3.11}$$

$$v_q = -R_a i_q + \omega_r \lambda_d \tag{3.12}$$

$$v_f = R_f i_f + \frac{d\lambda_f}{dt} \tag{3.13}$$

$$v_g = R_g i_g + \frac{d\lambda_g}{dt} = 0 \tag{3.14}$$

$$\lambda_d = -L_d i_d + L_{afm} i_f \tag{3.15}$$

$$\lambda_q = -L_q i_q + L_{agm} i_g \tag{3.16}$$

$$\lambda_f = -\tfrac{3}{2} L_{afm} i_d + L_{ff} i_f \tag{3.17}$$

$$\lambda_g = -\tfrac{3}{2}L_{agm}i_q + L_{gg}i_g \tag{3.18}$$

These equations are presented in terms of the flux linkages, currents, and inductances of the model windings. Some of the parameters can be be measured physically, but many consist of coupling between equivalent inductances and are difficult to obtain. The equations can be reformulated in terms of the direct and quadrature axis voltages and currents and the steady state and transient inductances and associated time constants. This eliminates some of the measurement problems by allowing parameter determination from a group of reasonably simple tests [17, 69] and relates the behavior to a set of more familiar variables. For transient and dynamic stability studies the deviations in frequency are small and little error results from substituting the reactance at synchronous frequence, X, for inductance, L, in the generator equations.

3.1.1 Mechanical Equations

The remaining equations needed to simulate a generator are those relating the applied torques and the position of the rotor. Assuming a rigid shaft with total coupled inertia $2H$ and linear friction D the equation is,

$$T_M - T_E = 2H\ddot{\theta} + D\dot{\theta} \tag{3.19}$$

where T_M is the externally applied mechanical torque and T_E is the electrical torque due to the interactions of the magnetic fields within the generator.

The steady-state energy balance,

$$P_e = P_m - P_l \tag{3.20}$$

states that the power delivered to the generator terminals, P_e, is equal to the applied mechanical power, P_m, minus the losses within the generator, P_l. In terms of the terminal voltage and current these values are,

$$P_e = V_t \times I_t^* \tag{3.21}$$

$$P_l = R_a \times I_t^2 \tag{3.22}$$

Since shaft speed changes are relatively small, the torques and powers can be considered to be equivalent in per-unit notation. Applying this assumption to (3.19) yields the mechanical inertia equations,

$$\dot{\omega} = \frac{P_m - P_e - P_l - D\omega}{2H} \tag{3.23}$$

$$\dot{\delta} = 2\pi f_o \omega \tag{3.24}$$

where ω is the rotor speed deviation from synchronous speed, δ is the rotor angle relative to a synchronous reference, and f_o is the synchronous frequency.

3.1.2 Air-Gap Voltage

The remaining equations consider the effects of saturation on the generator reactances and time constants. As described in section 3.1.4 the magnitude of the air-gap voltage, E_{at}, is required to determine the level of saturation within the generator. The air-gap voltage is the difference between the voltage induced by the field and q-axis damper windings and the armature reaction of the stator current. The armature reaction is equal to the stator current times the stator self-inductance reduced by the leakage inductance, L_l.

The q-axis component of the air-gap voltage is,

$$E_{aq} = E'_q - \omega_r(L'_d - L_l)i_d \tag{3.25}$$

The d-axis component of the air-gap voltage is,

$$E_{ad} = E'_d + \omega_r(L'_q - L_l)i_q \tag{3.26}$$

The total air-gap voltage is the vector sum of the components,

$$E_{at} = \sqrt{E_{ad}^2 + E_{aq}^2} \tag{3.27}$$

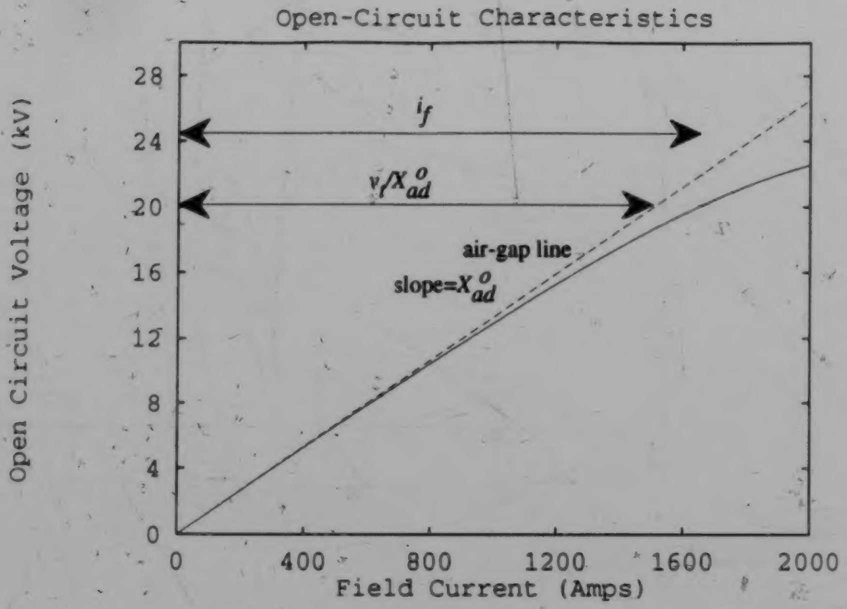

Figure 3.1: Typical synchronous generator open-circuit characteristic curve

3.1.3 Open-Circuit Saturation Curve

The field current required to produce a given open-circuit steady-state terminal voltage is given by the expression,

$$i_f = \frac{v_d}{X^o_{ad}} \tag{3.28}$$

(3.28) is derived from (3.15) by removing the armature current term, noting that the terminal voltage has the same per-unit value as the direct-axis flux and replacing the mutual inductance with X^o_{ad}, the mutual reactance. The ^{o} superscript indicates an unsaturated value.

The difference between the current given by (3.28) and the field current actually required to produce the same terminal voltage provides an indication of the degree of magnetic-circuit saturation within the generator. A typical open-circuit saturation curve is shown in figure 3.1.

To a first approximation the saturation curve can be calculated as,

$$i_f = \frac{v_t}{X^o_{ad}}(1 + Ae^{Bv_t}) \tag{3.29}$$

The saturation value as a function of the terminal voltage is then given by,

$$S(v_t) \triangleq \frac{i_f X^o_{ad}}{v_t} - 1 = Ae^{Bv_t} \tag{3.30}$$

The coefficients A and B can be determined directly from the open-circuit characteristics. If two points are selected, say $S_1(i_{f_1}, v_{t_1})$ and $S_2(i_{f_2}, v_{t_2})$, it follows from (3.30) that,

$$B = \frac{1}{v_{t_1} - v_{t_2}} \ln \frac{S_1}{S_2} \tag{3.31}$$

$$A = \frac{S_1}{e^{v_{t_1}}} \tag{3.32}$$

The measurement points S_1 and S_2 are typically taken at the machine's rated voltage and at 1.1 or 1.2 times the rated voltage, respectively.

The saturation factor, k, used to modify the unsaturated reactances and time constants is defined in terms of the air-gap voltage as,

$$k \triangleq \frac{1}{1 + S(E_{at})} = \frac{1}{1 + Ae^{BE_{at}}} \tag{3.33}$$

3.1.4 Saturation Effects

A number of assumptions are made before considering the effect of saturation on the model reactances and time constants:

1. For round-rotor machines the degree of saturation is dependent on the magnitude of the air-gap voltage and is equal in both axes.
2. For salient-pole machines the degree of saturation is dependent on the q-axis component of the air-gap voltage and affects only d-axis quantities.
3. The saturation level in a given axis exists for all rotor and stator circuits in that axis.
4. The distortion of any air-gap flux waves does not change the unsaturated reactance values or destroy the sinusoidal variations assumed for rotor and stator reactances.
5. Leakage flux paths are unaffected by saturation.

With these assumptions and the definition of the saturation factor from (3.33) the generator saturated mutual reactances vary according to the expressions,

$$X_{ad} = kX^{o}_{ad} \tag{3.34}$$

$$X_{aq} = kX^{o}_{aq} \tag{3.35}$$

The direct-axis saturated and unsaturated synchronous reactances are defined as,

$$X_d \triangleq X_{ad} + X_l \tag{3.36}$$

$$X_d^o \triangleq X_{ad}^o + X_l \tag{3.37}$$

(3.38)

Substituting (3.34) and (3.37) into (3.36) yields the expression for the direct-axis saturated synchronous reactance,

$$X_d = kX_d^o + (1-k)X_l \tag{3.39}$$

It follows that the expression for the quadrature-axis saturated synchronous reactance is,

$$X_q = kX_q^o + (1-k)X_l \tag{3.40}$$

The direct-axis saturated open circuit time constant is,

$$T'_{do} = T'^{o}_{do}\left(1 - \frac{(1-k)(X_d^o - X'_d)}{X_d^o - X_l}\right) \tag{3.41}$$

Similarly, the quadrature-axis saturated open circuit time constant is,

$$T'_{qo} = T'^{o}_{qo}\left(1 - \frac{(1-k)(X_q^o - X'_q)}{X_q^o - X_l}\right) \tag{3.42}$$

3.1.5 Generator Block Diagram

With all saturation factors applied, the set of dynamic equations governing the behavior of the synchronous generator may be summarized as follows,

- d-axis stator equation:

$$v_d = E'_d + X'_q i_q - R_a i_d \tag{3.43}$$

- q-axis stator equation:

$$v_q = E'_q - X'_d i_d - R_a i_q \tag{3.44}$$

- d-axis air-gap equation:

$$E_{ad} = E'_d + (X'_q - X_l) i_q \tag{3.45}$$

- q-axis air-gap equation:

$$E_{aq} = E'_q - (X'_d - X_l) i_d \tag{3.46}$$

- air-gap voltage equation:

$$E_{at} = \sqrt{E_{ad}^2 + E_{aq}^2} \tag{3.47}$$

- saturation equation:

$$k = \frac{1}{1 + Ae^{BE_{at}}} \tag{3.48}$$

- d-axis field equation:

$$\dot{E}'_q = \frac{kE_f - E'_q - (X_d - X'_d)i_d}{T'_{do}} \tag{3.49}$$

- q-axis damper equation:

$$\dot{E}'_d = \frac{-E'_d + (X_q - X'_q)i_q}{T'_{qo}} \tag{3.50}$$

- inertia equations:

$$\dot{\omega} = \frac{P_m - P_e - P_l - D\omega}{2H} \tag{3.51}$$

$$\dot{\delta} = 2\pi f_o \omega \tag{3.52}$$

The block diagram form of these equations is shown in figure 3.2. The P_{dist} input to the power summing junction can be used to apply a disturbance signal during simulations. The analog computer form of the equations are the basis of the transient stability program's simulation of the generator dynamics.

3.1.6 Steady-State Generator Equations

The steady-state generator equations are used to calculate the initial conditions for the simulation. The equations can be derived by considering the vector diagram for a synchronous generator under steady-state conditions as shown in figure 3.3. The

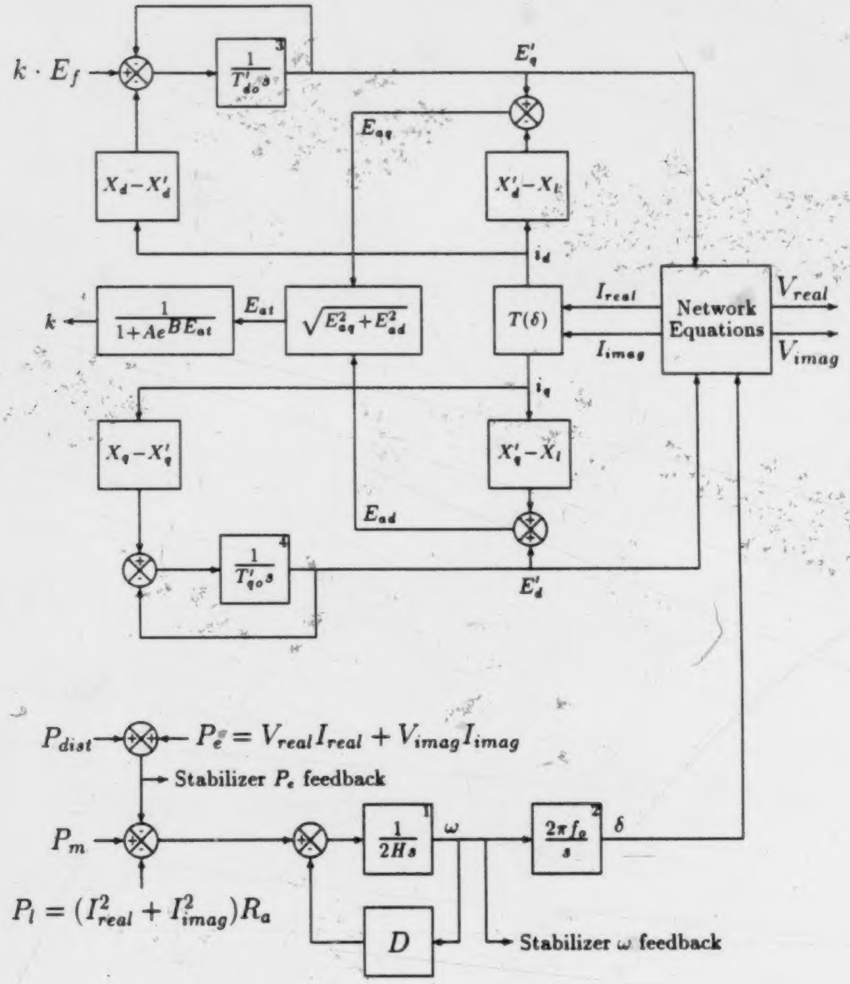
$k \cdot E_f$
$\frac{1}{T'_{do}s}$
3
E'_q
E_{aq}
$X_d - X'_d$
$X'_d - X_l$
i_d
k
$\frac{1}{1+Ae^{BE_{at}}}$
E_{at}
$\sqrt{E_{aq}^2 + E_{ad}^2}$
$T(\delta)$
I_{real}
I_{imag}
Network Equations
V_{real}
V_{imag}
i_q
$X_q - X'_q$
$X'_q - X_l$
E_{ad}
$\frac{1}{T'_{qo}s}$
4
E'_d
P_{dist}
$P_e = V_{real}I_{real} + V_{imag}I_{imag}$
Stabilizer P_e feedback
P_m
$\frac{1}{2Hs}$
1
ω
$\frac{2\pi f_o}{s}$
2
δ
$P_l = (I_{real}^2 + I_{imag}^2)R_a$
D
Stabilizer ω feedback

Figure 3.2: Synchronous generator model.

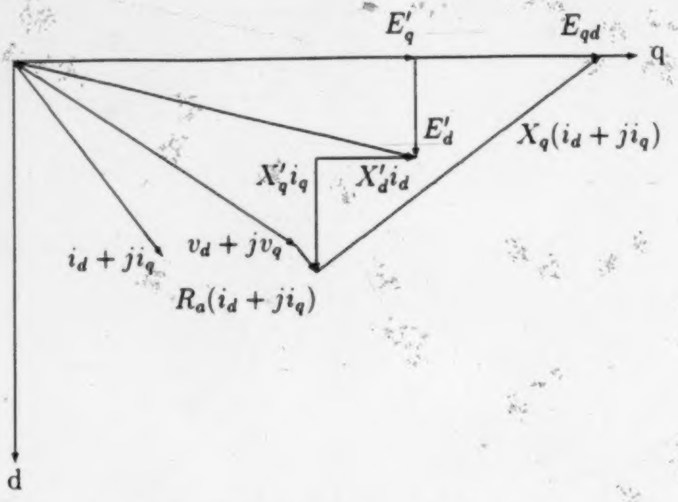
E'_q
E_{qd}
q
E'_d
$X_q(i_d + ji_q)$
$X'_q i_q$
$X'_d i_d$
$i_d + ji_q$
$v_d + jv_q$
$R_a(i_d + ji_q)$
d

Figure 3.3: Synchronous generator steady-state vector diagram.

voltage E_{qd} is defined as,

$$E_{qd} = (v_d + jv_q) + (R_a + jX_q)(i_d + ji_q) \tag{3.53}$$

Under steady-state conditions this voltage has the useful property of lying along the quadrature axis since the real part of E_{qd} is,

$$\Re(E_{qd}) = v_d + R_a i_d - X_q i_q \tag{3.54}$$

and from (3.11) and (3.16),

$$v_d + R_a i_d - X_q i_q = -\omega_r L_{agm} i_g \tag{3.55}$$

At steady state $i_g = 0$, hence $\Re(E_{qd}) = 0$. This property of E_{qd} is used to calculate the initial rotor position relative to the synchronous reference frame of the terminal voltage and current as,

$$E_{qd} = V_t + (R_a + jX_q)I_t \tag{3.56}$$

and,

$$\delta = \angle E_{qd} \tag{3.57}$$

$$\theta = \delta - \frac{\pi}{2} \tag{3.58}$$

From the steady-state vector diagram it can be seen that,

$$E'_q = |E_{qd}| - (X_q - X'_d)i_d \tag{3.59}$$

The remaining equations used to calculate the generator initial conditions are obtained by setting the derivative terms to zero in the q-axis damper equation (3.49) and the d-axis field equation (3.50), giving rise to,

$$E'_d = (X_q - X'_q)i_q \tag{3.60}$$

$$E_f = E'_q + (X_d - X'_d)i_d \tag{3.61}$$

The procedure for determining the initial conditions is in fact iterative, since saturation effects must also be considered.

3.2 Network Model and Generator Stator Equations

The final portion of the transient stability generator simulation concerns the power flow in the network to which the generator is connected and the effect of this flow on the generator terminal conditions. The variables used in the solution of the equations are the rotor electrical position θ and the internal voltages E'_q and E'_d. The values to be solved for are the complex voltages, currents and power at the generator terminals.

The transmission and load network is represented by a matrix of driving-point and transfer admittances as seen from the generator terminals. The matrix includes the system loads represented as constant impedances. The equivalent admittance matrix $\mathbf{Y_{TT}}$ can be used to write the matrix nodal equation for the reduced system as,

$$\mathbf{I} = \mathbf{Y_{TT}}\mathbf{V} \tag{3.62}$$

where,

$\mathbf{I}$ is the complex vector of generator terminal currents referred to the network synchronous reference,

$\mathbf{V}$ is the complex vector of generator terminal voltages referred to the network synchronous reference, and,

$\mathbf{Y_{TT}}$ is the admittance matrix for the reduced power system.

For each generator in the system there are two scalar equations describing the stator circuits. Written in matrix form the equations are,

$$\begin{bmatrix} v_d \\ v_q \end{bmatrix} = \begin{bmatrix} E'_d \\ E'_q \end{bmatrix} - \begin{bmatrix} R_a & -X'_q \\ X'_d & R_a \end{bmatrix} \begin{bmatrix} i_d \\ i_q \end{bmatrix} \tag{3.63}$$

In (3.63) the voltages and currents are referred to the individual d and q reference frames of each generator. In order to obtain a combined solution of (3.62) and (3.63) for all the generators, the equations must be transformed to a common reference frame. If I is the generator terminal current relative to the network reference, and θ is the angle between the generator d-axis and the network reference, then the currents are related by the expression,

$$i_d + j i_q = I e^{-j\theta} \tag{3.64}$$

If transient saliency is neglected (i.e. if $E'_d = E'_q$) the simultaneous solution of (3.62) and (3.63) is quite simple. The two scalar equations in (3.63) can be combined into a single complex equation and solved along with (3.62).

If transient saliency is not neglected, the simultaneous solution of the stator and nodal equations becomes considerably more difficult. In this case, when (3.63) is transformed into the synchronous reference frame it becomes,

$$\begin{bmatrix} V_{real} \\ V_{imag} \end{bmatrix} = \begin{bmatrix} E'_{real} \\ E'_{imag} \end{bmatrix} - \begin{bmatrix} \cos\theta & -\sin\theta \\ \sin\theta & \cos\theta \end{bmatrix} \begin{bmatrix} R_a & -X'_q \\ X'_d & R_a \end{bmatrix} \begin{bmatrix} \cos\theta & \sin\theta \\ -\sin\theta & \cos\theta \end{bmatrix} \begin{bmatrix} I_{real} \\ I_{imag} \end{bmatrix} \tag{3.65}$$

Two difficulties arise in the solution of (3.65)

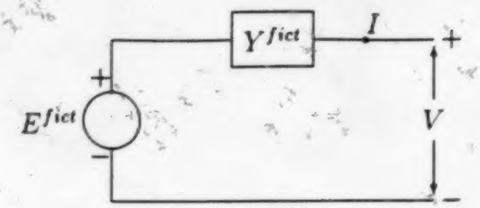

Figure 3.4: Generator equivalent circuit showing fictitious voltage and admittance for generator stator equations.

1. It can not be combined into a single complex equation and solved as part of the nodal equation.

2. The coefficients of I_{real} and I_{imag} are functions of θ and therefore change with time.

It is possible to combine (3.62) and (3.65) to obtain a set of $2N$ (N = the number of generators) real equations which can be solved directly. However, because the coefficients are time-varying, the matrix must be factored or reinverted for every integration step, which is a very time-consuming process.

An effective method for overcoming these difficulties has been presented by Dommel and Sato [46]. The method requires iterations at each integration step, but uses a matrix which is constant as long as a certain network configuration exists. Calculation of the power flows requires an iterative solution at each integration step in any case so the iterative stator equation solution does not add appreciably to the computation time. The method is based upon representing the generator as a fictitious slack voltage behind a fictitious admittance as shown in figure 3.4. The fictitious admittance is defined as,

$$Y^{fict} = \frac{R_a - j\frac{1}{2}(X'_d + X'_q)}{R_a^2 + X'_d X'_q} \tag{3.66}$$

The next step is to derive an expression for the fictitious voltage. Solving (3.63) for the direct and quadrature-axis currents yields,

$$\begin{bmatrix} i_d \\ i_q \end{bmatrix} = \frac{1}{R_a^2 + X'_d X'_q} \begin{bmatrix} R_a & X'_q \\ -X'_d & R_a \end{bmatrix} \begin{bmatrix} E'_d - v_d \\ E'_q - v_q \end{bmatrix} \tag{3.67}$$

This can be expressed as a single complex equation,

$$I_d + jI_q = \frac{1}{R_a^2 + X'_d X'_q} \left[R_a(E'_d + jE'_q) - R_a(v_d + jv_q) + X'_q(E'_q - v_q) - jX'_d(E'_d - v_d)\right] \tag{3.68}$$

Applying Kirchoff's voltage law to the circuit in figure 3.4, and using Y_{fict} from (3.66), the generator terminal current can be written as,

$$I_d + jI_q = \frac{R_a - j\frac{1}{2}(X'_d + X'_q)}{R_a^2 + X'_d X'_q} \left[(E_d^{fict} + jE_q^{fict}) - (v_d + jv_q)\right] \tag{3.69}$$

Equating the currents from (3.68) and (3.69) and solving for E_{fict} yields,

$$E_d^{fict} + jE_q^{fict} = E'_d + jE'_q + \frac{j\frac{1}{2}\left(X'_q - X'_d\right)}{R_a - \frac{1}{2}\left(X'_d + jX'_q\right)} \left[(E'_d - jE'_q) - (v_d - jv_q)\right] \tag{3.70}$$

In the manner given by (3.64) the relationship between the values on the generator reference and on the network synchronous reference is,

$$E_d^{fict} + jE_q^{fict} = E^{fict}e^{-j\theta} \tag{3.71}$$

$$E_d' + jE_q' = E'e^{-j\theta} \tag{3.72}$$

$$v_d + jv_q = Ve^{-j\theta} \tag{3.73}$$

The complex conjugates of the latter two expressions are then,

$$E_d' - jE_q' = E'^{*}e^{j\theta} \tag{3.74}$$

$$v_d - jv_q = V^{*}e^{j\theta} \tag{3.75}$$

Substituting these values into (3.70) gives the expression for calculating the value of E^{fict} as,

$$E^{fict} = E' + \frac{j\frac{1}{2}\left(X_q' - X_d'\right)}{R_a - \frac{1}{2}\left(X_d' + jX_q'\right)}\left[E'^{*} - V^{*}\right]e^{j2\theta} \tag{3.76}$$

Each time the transient stability program reads a new terminal admittance matrix, $\mathbf{Y_{TT}}$, it invokes Kron's reduction formula to absorb the fictitious generator admittances into the matrix thus forming the augmented admittance matrix, $\mathbf{Y'_{TT}}$. The nodal matrix equation is then written as,

$$\mathbf{I} = \mathbf{Y'_{TT}}\mathbf{E^{fict}} \tag{3.77}$$

The simultaneous solution of (3.76) and (3.77) at each integration step proceeds by iterating the estimate of the terminal voltage vector $\tilde{\mathbf{V}}$. The steps in this process are:

1. Set the initial estimate of $\tilde{\mathbf{V}}$ to the terminal voltage obtained in the previous time step.

2. Transform the generator internal voltages to the network synchronous reference. For each generator calculate,

$$\theta = \delta - \frac{\pi}{2} \tag{3.78}$$

$$E' = \left(E'_d + jE'_q\right) e^{j\theta} \tag{3.79}$$

3. Use (3.76) to calculate the fictitious internal voltage E^{fict} for each generator. Use the values to form the vector $\mathbf{E^{fict}}$.

4. Use (3.77) to calculate the vector $\mathbf{I}$ of generator currents.

5. Form a new estimate of the terminal voltages. For each generator calculate,

$$\tilde{V} = E^{fict} - \frac{I}{Y^{fict}} \tag{3.80}$$

6. Check for convergence. For each generator calculate,

$$I_d + jI_q = Ie^{-j\theta} \tag{3.81}$$

$$\tilde{v}_d + j\tilde{v}_q = \overline{V}e^{-j\theta} \tag{3.82}$$

If,

$$\left|\tilde{v}_q - \left(E'_q - X'_d I_d - R_a I_q\right)\right| < \epsilon \tag{3.83}$$

and,

$$\left|\tilde{v}_d - \left(E'_d + X'_q I_q - R_a I_d\right)\right| < \epsilon \tag{3.84}$$

for every generator then the solution has converged. If not, the solution has not converged and the next iteration begins at step 3.

3.3 Turbine/Governor and AVR Models

The block diagram of the turbine/governor model used in the simulation studies is shown in figure 3.5. The model represents a three-stage steam turbine and a mechanical hydraulic governor. For the simulation studies the model was used to represent a single-stage turbine by setting F_{IP} and F_{LP} to zero and F_{HP} to one.

The block diagram of the AVR model used in the simulation studies is shown in figure 3.6. The model represents a simple prototype static exciter. Although not shown in the figure, the V_{ref} signal is actually the sum of the machine voltage reference, an optional identification excitation signal and an optional disturbance signal. The parameter values used in the simulation studies are presented in table 3.1.

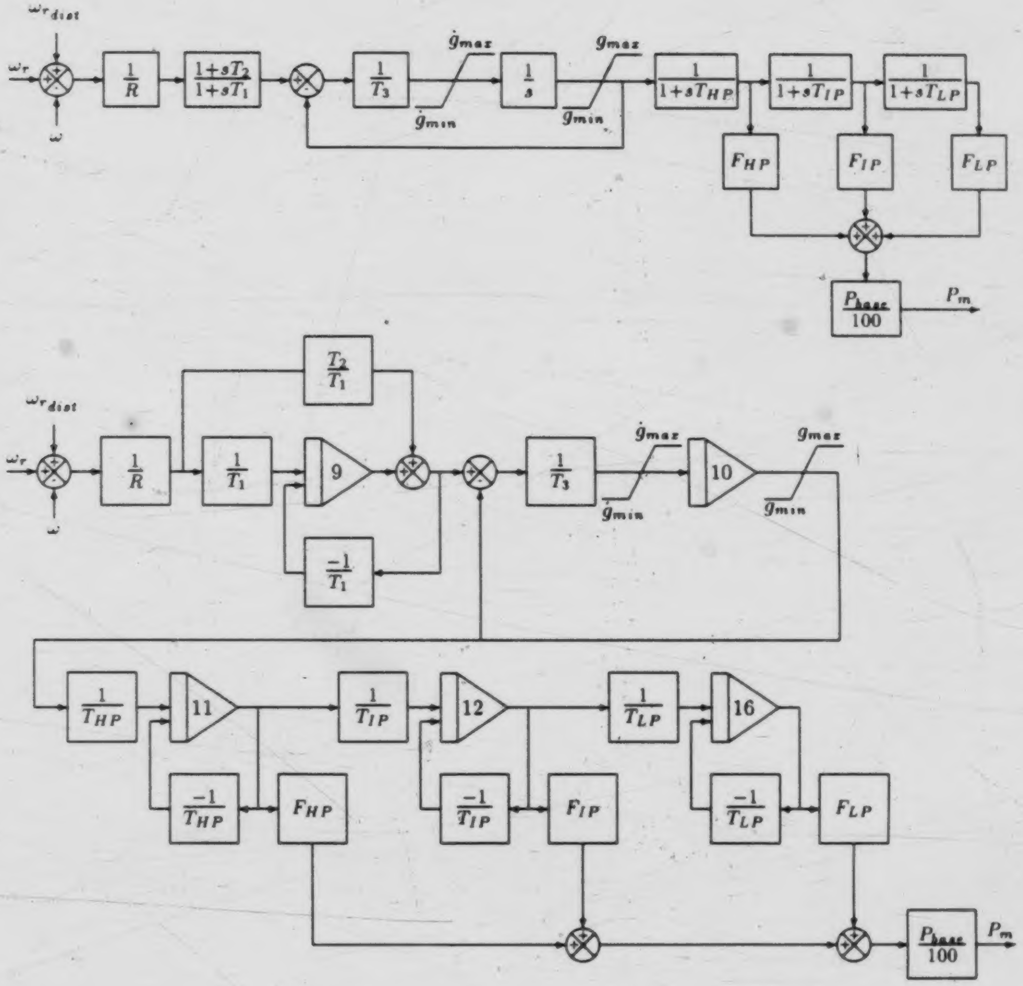
$\omega_{r_{dist}}$
ω_r
ω
$\frac{1}{R}$
$\frac{1+sT_2}{1+sT_1}$
$\frac{1}{T_3}$
$\dot{g}_{max}$
$\dot{g}_{min}$
$\frac{1}{s}$
g_{max}
g_{min}
$\frac{1}{1+sT_{HP}}$
$\frac{1}{1+sT_{IP}}$
$\frac{1}{1+sT_{LP}}$
F_{HP}
F_{IP}
F_{LP}
$\frac{P_{base}}{100}$
P_m
$\frac{T_2}{T_1}$
$\frac{1}{T_1}$
9
$\frac{-1}{T_1}$
10
$\frac{1}{T_{HP}}$
11
$\frac{-1}{T_{HP}}$
$\frac{1}{T_{IP}}$
12
$\frac{-1}{T_{IP}}$
$\frac{1}{T_{LP}}$
16
$\frac{-1}{T_{LP}}$

Figure 3.5: Block diagram and analog wiring diagram of Turbine/Governor type 3 (three-stage steam turbine and mechanical-hydraulic governor).

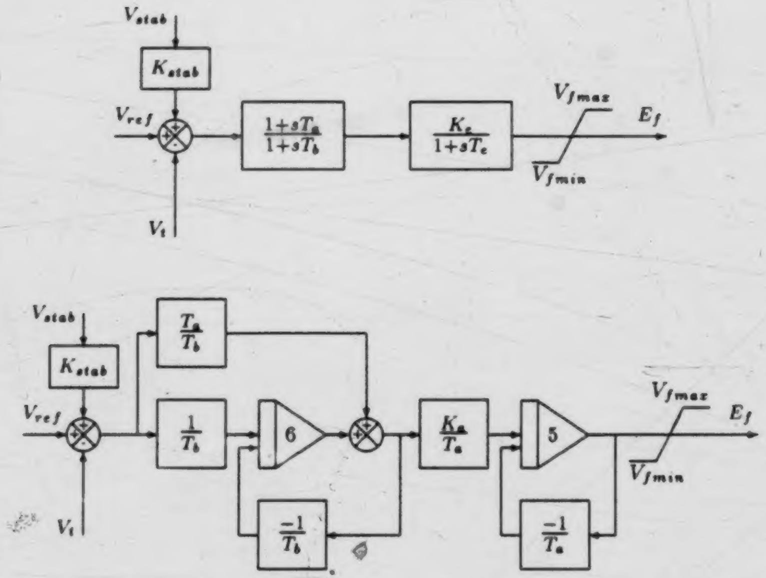
Vstab
Kstab
Vref
Vt
1+sTa / 1+sTb
Ke / 1+sTe
Vfmax
Vfmin
Ef
Ta / Tb
1 / Tb
6
Ke / Te
5
−1 / Tb
−1 / Te

Figure 3.6: Block diagram and analog wiring diagram of AVR type 2 (Simple static exciter).

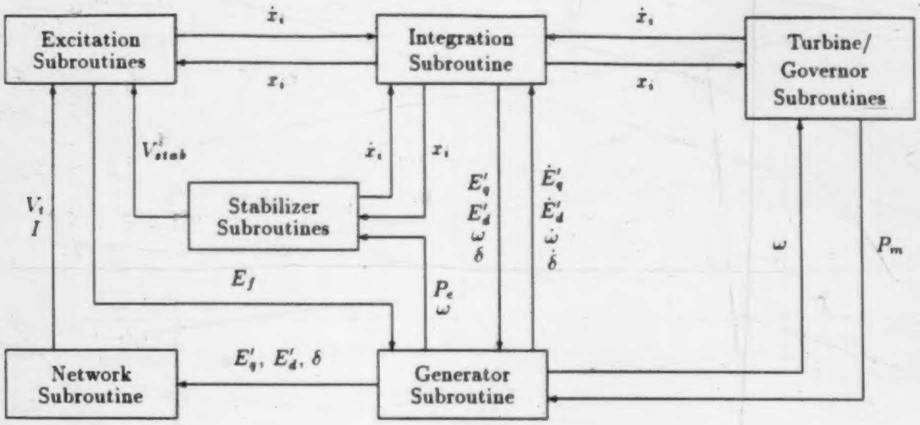
Excitation Subroutines
Integration Subroutine
Turbine/ Governor Subroutines
Stabilizer Subroutines
Network Subroutine
Generator Subroutine
$\dot{x}_i$
x_i
V_{stab}
V_t
I
E_f
E'_q
E'_d
ω
δ
$\dot{E}'_q$
$\dot{E}'_d$
$\dot{\omega}$
$\dot{\delta}$
P_e
P_m
E'_q, E'_d, δ

Figure 3.7: Data flow in transient stability program.

3.4 Program Overview

Figure 3.7 shows the flow of data within the transient stability program. At each time step a new network condition is calculated, then for each unit the stabilizer, AVR and turbine/governor subroutines are called. For each unit the generator subroutine is called and finally the integration routine is called to determine the new values of the state variables.

3.4.1 Initial Conditions

Calculation of the initial (steady-state) conditions begins with a call to the generator 'initial condition' subroutine for each unit in the simulation. This subroutine receives the terminal voltage and current with respect to the synchronous reference and produces the steady-state value of the generator state variables ω, δ, E'_q and E'_d and the steady-state field voltage and mechanical power. The procedure is iterative since the machine reactances are dependent upon the saturation factor which must also be determined. The following steps describe the procedure:

1. Set initial estimate of saturation factor $k = 1$.
2. Calculate saturated reactances X_d and X_q from (3.39) and (3.40).
3. Calculate angle of generator rotor with respect to the synchronous reference using (3.56), (3.57) and (3.58).
4. Calculate d- and q-axis components of generator terminal current from (3.64).
5. Calculate generator transient voltages and field voltage using (3.59), (3.60) and (3.61).
6. Calculate the air-gap voltage from (3.25), (3.26), and (3.27).
7. Use the air-gap voltage to calculate a new estimate of the saturation factor, (3.33).
8. If the saturation factor has converged continue to the next step, otherwise return to step 2.
9. Calculate steady-state mechanical power as the sum of the generator output and armature loss.
10. Return from the subroutine.

The 'initial conditions' subroutines for the other components of the simulation are called after the gen[illegible]or initial conditions have been determined. These subroutines calculate AVR and governor setpoints and perform other initialization specific to a given piece of equipment.

3.4.2 Step by Step Simulation

The stabilizer, excitation system and turbine-governor subroutines are called each simulation step to calculate the new value of the field voltage and mechanical power as well as the value of the state variable derivatives specific to each piece of equipment.

The generator subroutines are called after the other equipment subroutines. The saturation factor and the state variable derivatives are calculated for each generator as follows:

1. Calculate d- and q-axis components of the terminal current from (3.64).
2. Calculate the generator electrical output and losses using (3.21) and 3.22.
3. Calculate the saturated reactances X_d, X_q and time constants T'_{do}, T'_{qo} from (3.39), (3.40), (3.41), and (3.42).
4. Calculate the air-gap voltage from (3.25), (3.26), and (3.27).
5. Use the air-gap voltage to calculate the saturation factor, (3.33).
6. Calculate the time derivatives of the generator state variables using (3.49), (3.51), (3.52) and (3.50).
7. Return from the subroutine.

3.4.3 Numerical Integration Algorithm

The heart of the transient stability simulation program is the subroutine which predicts the state variable vector for the next simulation step based on the current value of the state variables and the state variable derivatives. The algorithm is referred to as the modified Euler method and is given by the expression,

$$\mathbf{X}_{t+\Delta t} = \mathbf{X}_t + \left[\dot{\mathbf{X}}_t + \frac{\dot{\mathbf{X}}_t - \dot{\mathbf{X}}_{t-\Delta t}}{2}\right]\Delta t \qquad (3.85)$$

The prediction is made on the assumption that the change of the state variable derivative from time t to time $t + \Delta t$ will be the same as from time $t - \Delta t$ to time t.

3.5 Two-Machine Infinite-Bus Test System

A block diagram of the power system used in the simulation studies is shown in figure 3.8. The system parameters are summarized in table 3.1. Parameter values are in per-unit using the generator's rated power as the power base. Time constants are in seconds.

The test system is intended to simulate a single generator connected to a large generation/load pool in turn connected to an even larger generation/load pool. The test machine parameters are those of an actual 300 MW turbogenerator on which previous AVR and PSS studies were performed[81]. The large generation/load pool is simulated as a single equivalent machine providing a response similar to that exhibited by a large interconnected system. The equivalent machine was not equipped with a

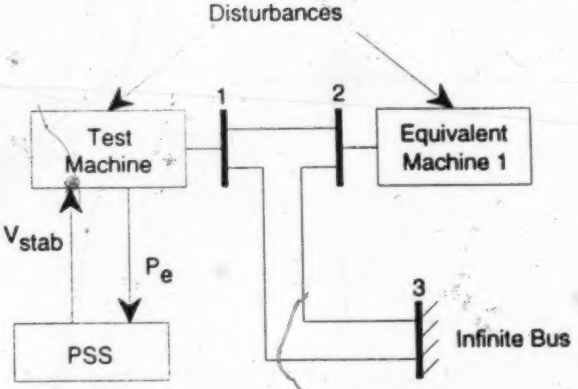
Disturbances
1
2
3
Test Machine
Equivalent Machine 1
V_stab
P_e
PSS
Infinite Bus

Z_{12}	$0.01 + j0.15$
Z_{23}	$0.01 + j0.30$
Z_{13}	$0.01 + j2.00$

Figure 3.8: Block diagram of two-machine infinite-bus test system.

Table 3.1: Two-machine infinite-bus test system parameter values.

Generator Parameters		
	Test Machine	Equivalent Machine
P_{base}	100.0	250.0
H	2.70	15.0
R_a	9.0×10^{-4}	9.0×10^{-4}
X_l	0.24	0.24
X_d	1.83	1.83
X'_d	0.29	0.29
X_q	1.78	1.78
X'_q	0.44	0.44
T'_{do}	4.60	4.60
T'_{qo}	0.373	0.373
D	2.00	3.00
A	3.0×10^{-5}	3.0×10^{-5}
B	6.00	6.00

AVR Parameters		
	Test Machine	Equivalent Machine
T_a	1.00	1.00
T_b	10.0	10.0
K_e	125.0	30.0
T_e	0.05	0.05
V_{fmax}	9.00	9.00
V_{fmin}	-9.00	-9.00
K_{stab}	1.00	—

Turbine/Governor Parameters		
	Test Machine	Equivalent Machine
P_{base}	100.0	250.0
T_{HP}	0.11	0.11
T_{IP}	5.50	5.50
T_{LP}	0.424	0.424
F_{HP}	0.28	0.28
F_{IP}	0.42	0.42
F_{LP}	0.30	0.30
R	0.047	0.047
T_1	0.18	0.18
T_2	0.00	0.00
T_3	0.15	0.15
$\dot{g}_{min}$	-1.00	-1.00
$\dot{g}_{max}$	0.10	0.10
g_{min}	0.00	0.00
g_{max}	1.10	1.10

power system stabilizer.

This simple two-machine infinite-bus test system exhibits two oscillatory modes. The first is the local oscillatory mode of the test machine itself. The second, low frequency mode is provided by the large inertia constant of the equivalent machine. In a realistic system these modes would correspond to a single machine swinging relative to a large generation pool and a group of generators interchanging power with another area. This represents the interarea mode of the generation/load pool oscillating relative to the infinite bus. Both the test machine and the equivalent machine were equipped with simple static AVR's. As described in chapter 1, the electric power signal from the test machine was used as the supplementary feedback signal for the PSS. The adaptive control strategy could also be applied to generators using accelerating power or shaft speed feedback.

Chapter 4

System Identification of the Two-Machine Infinite-Bus System

Identification of the model of the system being controlled is fundamental to the operation of the self-tuning PSS. An investigation of the identification of models of the particular system considered in this thesis was performed under varying conditions prior to studies of the self-tuning control algorithm itself. The models thus obtained provided insight into the form of the controller required to provide good damping of both the interarea and the local oscillatory modes.

A number of system identification techniques were used to determine the characteristics of the simulated two-machine infinite-bus test system shown in figure 3.8. The test system comprises a single generator connected to a large generation/load pool, in turn connected to an even larger generation/load pool. The large power pool is simulated by a single large machine and the larger pool is represented by an infinite bus. The results of the identification procedures are presented in this chapter.

Two models of the test system were obtained. The first representation of the system was the frequency response model. The model thus obtained was used to gauge the quality of the second representation which was expressed as the discrete-time transfer function model of the system. The aim was to determine the simplest transfer function representation which exhibited the same major oscillatory modes as the test system. This lower limit of model complexity indicates the order of the controller required to effectively damp both modes. A linear response around a given operating point was assumed. This assumption permits the use of the identification techniques described in chapter 2. The results presented in this chapter were obtained with the test machine supplying 0.95 p.u. real power and 0.23 p.u. reactive power to the network.

4.1 Frequency Response Model

The frequency response of the transfer functions linking the test machine's electric power output to its AVR PSS input and to the equivalent machine's electric power disturbance input were measured using Pseudo-Random Binary Sequence (PRBS) excitation and Fast Fourier Transform (FFT) analysis[12]. The excitation signal was formed by passing a 4095-point PRBS signal through a sixth-order low-pass Butterworth filter. The clock rate of the PRBS signal and the sampling rate of the test machine electrical power were fixed at 20 Hz. The low-pass filter limited the effects of the aliasing of high frequency components into the frequency range of interest. The harmonic content of the filtered PRBS excitation sequence is shown in figure 4.1. The signal has a uniform harmonic content over the frequency range of interest[16, 127]. The filtered 4095-point excitation signal was applied to the test simulation three consecutive times but only the final 4095 samples of the test machine electrical power were recorded. The two 'pre-acquisition' cycles of excitation provide

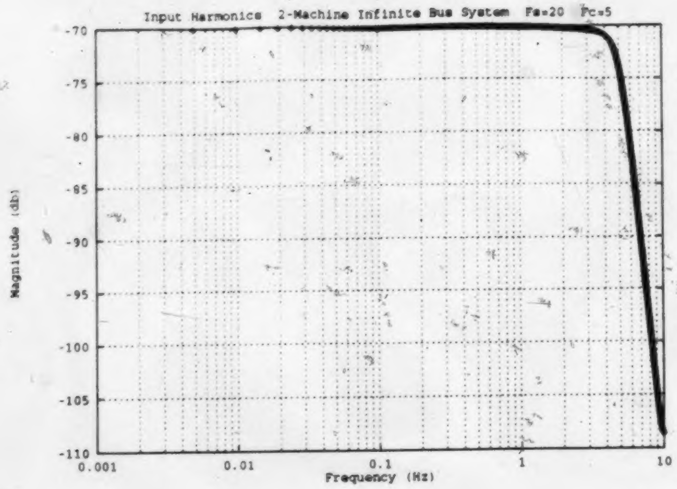

Figure 4.1: Harmonic content of filtered PRBS excitation signal.

time for the initial transient response of the system to decay. No shaping window was applied to the samples of excitation or electrical power since harmonic analysis, rather than spectral analysis, was used to determine the frequency responses.

Two tests were performed to obtain the frequency response models. The first test determined the frequency response between the test machine's AVR stabilizer input and the electrical power output by the test machine (P_e/V_{stab}). This is the response of the 'external plant' seen by the self-tuning PSS. The second test measured the frequency response between the equivalent machine's electric power disturbance input and the electrical power produced by the test machine ($P_e/P_{dist_{equiv}}$). This response shows the coupling between the test machine electrical power output and disturbances within the power pool represented by the equivalent machine.

The two frequency response models are shown in figures 4.2 and 4.3, respectively.

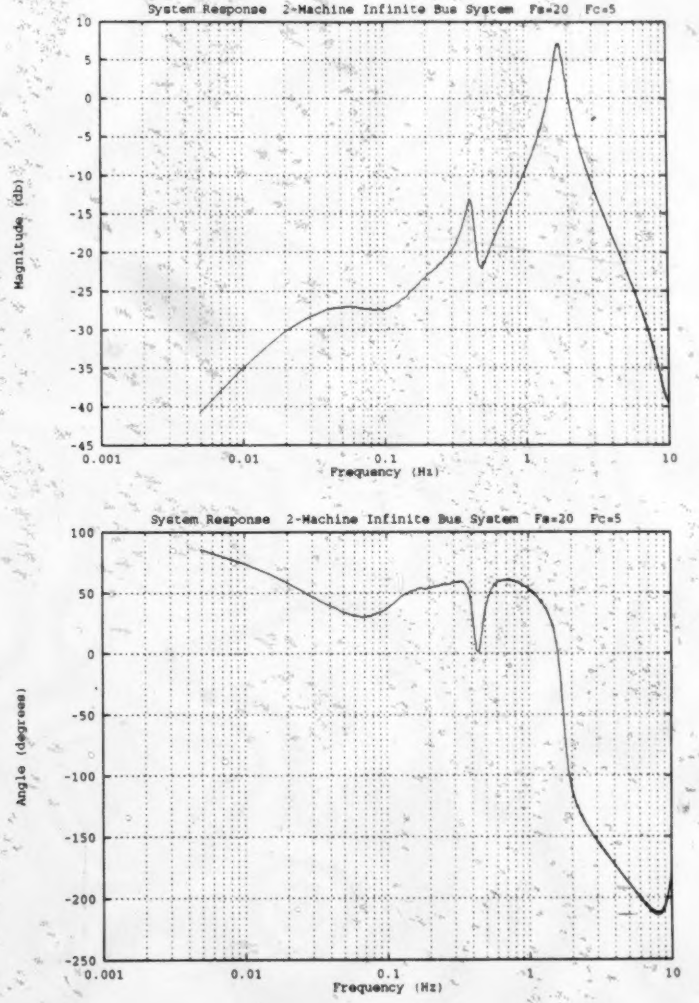

Figure 4.2: Frequency response (P_e/V_{stab}) of two-machine infinite-bus test system.

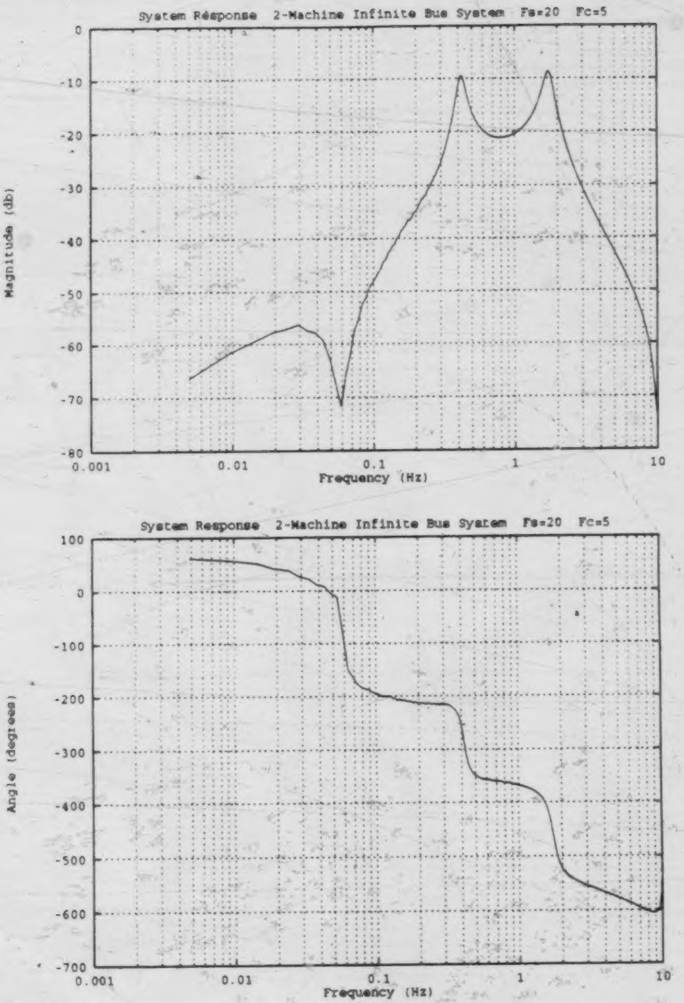

Figure 4.3: Frequency response ($P_e/P_{dist_{equiv}}$) of two-machine infinite-bus test system.

The two oscillatory modes are clearly evident in both responses. The local mode of the test machine can be seen at 1.75 Hz and the interarea oscillatory mode can be seen at 0.4 Hz. The challenge of damping the interarea mode with a PSS attached to the test machine can be seen by comparing the two responses. The coupling of both modes from the disturbance input is nearly identical, while the coupling of the interarea mode from the AVR input is over 20 db lower than the coupling of the local mode. A PSS attached to the test machine will thus be able to provide only a limited amount of damping of the interarea mode. One of the difficulties in providing significant damping at low frequencies is that the machine's AVR attempts to 'correct' the terminal voltage difference induced by the PSS.

The magnitude and phase information in figure 4.2 can be used to deduce the form of the discrete-time (z-plane) model of the 'external plant' seen by the PSS. At low frequencies the response approaches derivative action, indicating a zero near the $(1,0)$ point in the z-plane and a corresponding pole inside the unit circle on the real axis. The resonant peak of the interarea mode then shows the presence of a complex pole-pair. The presence of only a temporary drop in the phase angle near the interarea mode shows that a complex zero-pair is present at a frequency slightly higher than the interarea complex pole-pair. Finally, the resonant peak of the local mode indicates the presence of another complex pole-pair. A fifth-order discrete-time model should thus be able to represent the dynamics of the local and interarea modes. Identification of the parameters of such a discrete-time model is the subject of the following section.

4.2 Off-Line Time-Domain Identification

Several attempts to identify the parameters of a fifth-order discrete-time model of the two-machine infinite bus test system were made. In all cases a record of input/output samples was obtained by applying a filtered PRBS sequence to the test machine's AVR stabilizer input and recording samples of the electrical power produced by the test machine. This method is similar to that used by the first frequency response measurement described in the previous section (P_e/V_{stab}) except that only one PRBS record was applied and the electric power was recorded immediately rather than waiting for the initial transients to decay. This matches the assumption of the time-domain identification techniques that the system being identified is initially operating under steady-state conditions.

4.2.1 Least Squares Identification

The first identification technique applied to the data was the batch least squares algorithm given by (2.9). The Fortran LINPACK library[47] provides numerically-stable subroutines for computing this expression.

A comparison of the magnitude response of the discrete-time model obtained using the batch least squares method and the response obtained in the previous section is shown in figure 4.4. The method was able to accurately identify the local mode, but was unable to identify the poles and zeros of the interarea mode. In fact the complex pole/zero-pairs corresponding to the interarea mode suffer almost complete cancellation.

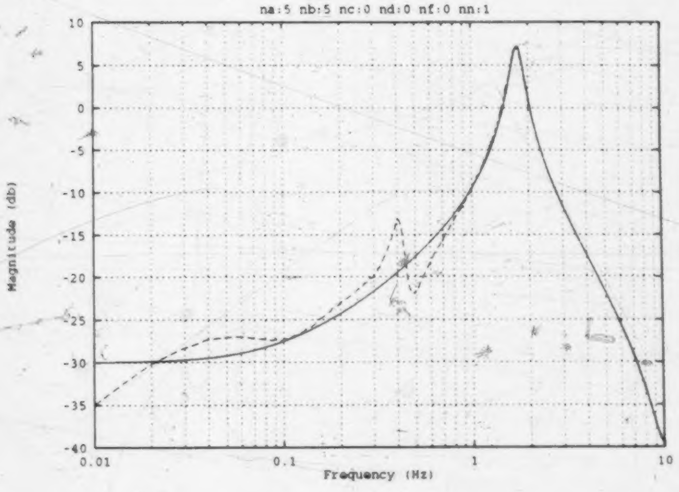

Figure 4.4: Comparison of frequency response (P_e/V_{stab}) of two-machine infinite-bus test system and 5-th order model obtained using batch least squares (— Response of fifth-order model, - - True response).

4.2.2 Generalized Least Squares Identification

The second identification method employed is referred to as the Generalized Least Squares (GLS) technique. This is a more complex prediction error technique which attempts to identify the coefficients of the C polynomial as well as the coefficients of the A and B polynomials of the ARMAX model. The method is briefly described below with full descriptions presented in [87], [95] and [118].

The parameter vector consists of the coefficients of the A, B and C polynomials as follows,

$$\theta^T = [a_1 \ldots a_{na}\, b_1 \ldots b_{nb}\, c_1 \ldots c_{nc}] \tag{4.1}$$

The cost function $V(\theta)$ is a nonlinear function of the parameters so an iterative numerical search technique is required to perform the minimization. A typical minimization technique is the *Gauss-Newton* algorithm which is expressed algebraically as,

$$\theta^{(k+1)} = \theta^k + \alpha_k \times \tag{4.2}$$
$$\left[\sum_{t=1}^{N} \psi(t,\theta^k)\psi^T(t,\theta^k)\right]^{-1} \left[\sum_{t=1}^{N} \psi(t,\theta^k)e(t,\theta^k)\right]$$

Here, α_k is an acceleration factor used to improve the convergence of the algorithm, θ^k is the old parameter estimate, $\theta^{(k+1)}$ is the new parameter estimate, and $\psi(t,\theta)$ is the vector of gradients of the error $e(t)$ with respect to the parameters, given by,

$$\psi(t,\theta) = -\left(\frac{\partial e(t,\theta)}{\partial \theta}\right)^T \tag{4.3}$$

A comparison of the expression for performing the batch least squares operation (2.9), and (4.2) shows that the second line of (4.2) can be computed by the same subroutine used to compute the batch least squares.

The vector of gradients required by (4.2) is computed by first forming the filtered signals,

$$y^F(t) = \frac{y(t)}{C(q^{-1})} \tag{4.4}$$

$$u^F(t) = \frac{u(t)}{C(q^{-1})} \tag{4.5}$$

$$e^F(t) = \frac{e(t)}{C(q^{-1})} \tag{4.6}$$

from the system output y, input u and the prediction error between model and system output e. Then $\psi(t,\theta)$ is given by

$$\begin{aligned} \psi^T(t,\theta) = -[&y^F(t-1) \ldots y^F(t-n)\ u^F(t-1) \\ &\ldots u^F(t-n)\ e^F(t-1) \ldots e^F(t-n)] \end{aligned} \tag{4.7}$$

The GLS method permits models with non-unit C polynomials to be accurately identified. In this case, though, the model identified by the GLS method was almost identical to that identified by the batch least squares method in the previous section. The local mode was accurately identified but the interarea mode was not.

4.2.3 Excitation Shaping

The inability of the preceding two attempts to identify the interarea mode arises from the fact that the energy in the output spectrum in the frequency range of the interarea mode is much lower than that in range of the local mode. A solution to this problem is to prefilter the excitation sequence to provide a more uniform harmonic content of output signal. This was performed as follows.

1. A record of input/output data was acquired using the filtered PRBS signal shown in figure 4.1.
2. A third-order model was identified using the batch least squares method.
3. The numerator and denominator of the third order discrete-time transfer function obtained above were interchanged to form a 'prewhitening' filter.
4. A new excitation sequence was formed by passing the PRBS signal through both the low-pass Butterworth filter and the prewhitening filter.

The harmonic content of the resulting excitation sequence is shown in figure 4.5. The corresponding output harmonics are shown in figure 4.6. The harmonic content of the output signal is more or less constant over the 0.2 Hz to 3.0 Hz frequency range of interest. In particular, the local mode resonant peak is no longer present in the output signal. Prediction errors over the frequency range of interest are thus given equal weight.

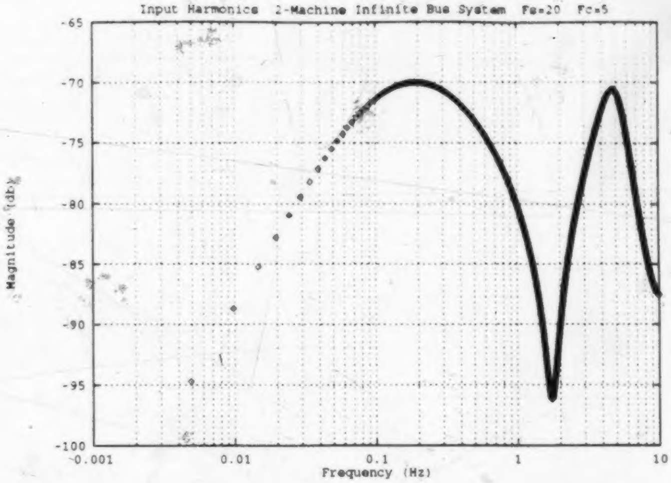

Figure 4.5: Harmonic content of filtered, prewhitened PRBS excitation signal.

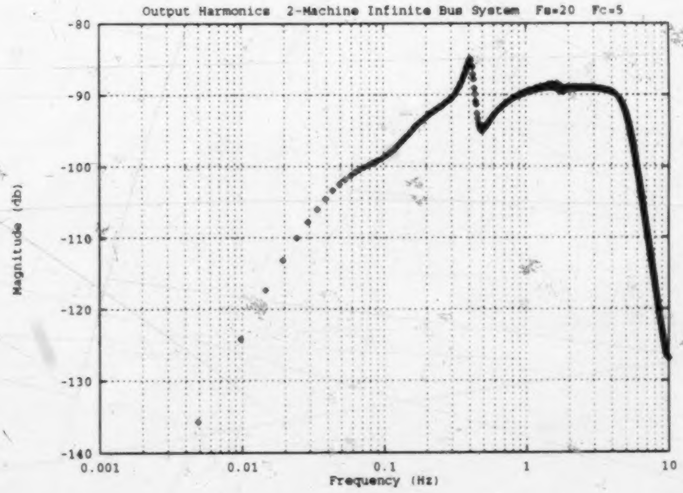

Figure 4.6: Harmonic content of electric power signal with filtered, prewhitened PRBS excitation.

When this prewhitened and filtered excitation sequence was applied to the system, and the GLS identification algorithm was applied to the recorded data, both the local and interarea modes were successfully identified. A comparison of the frequency response of the discrete-time model obtained using the generalized least squares method and the response obtained using FFT techniques is shown in figure 4.7.

The z-plane pole-zero plot of the identified system is shown in figure 4.8. The interarea complex pole-zero combination are very close together. It is the proximity of these poles and zeros that makes their identification difficult. The zero on the negative real axis of the z-plane is a result of the zero-order hold present in the excitation signal.

The basic least squares algorithm was unable to identify the interarea mode even with the prewhitening filter employed. This indicates that the C polynomial is required to allow identification of the interarea mode. As described previously, the RLS algorithm combined with the GMV control strategy implicitly consider the coefficients of the C polynomial and so should be able to identify the interarea mode, and damp it as much as possible.

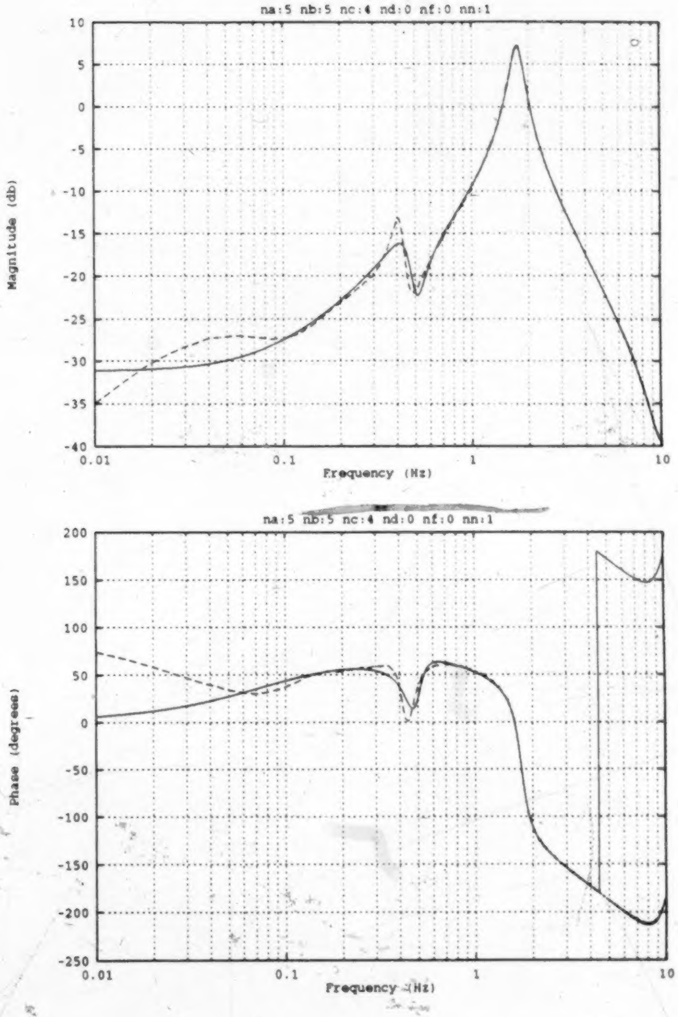

Figure 4.7: Comparison of frequency response (P_e/V_{stab}) of two-machine infinite-bus test system and 5-th order model obtained using generalized least squares (— Response of fifth-order model, – – True response).

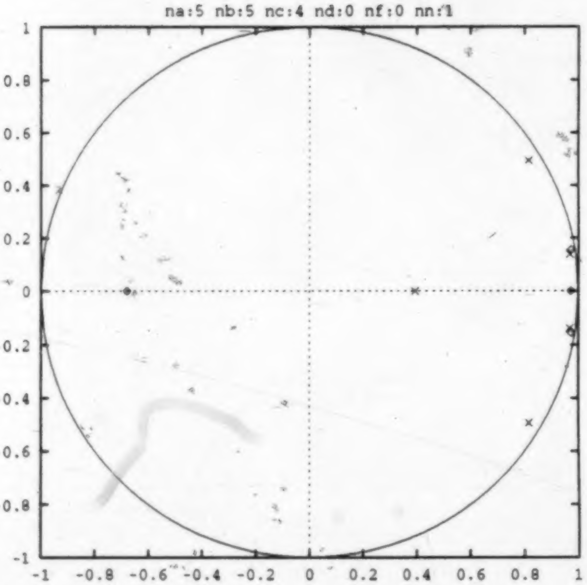

Figure 4.8: z-plane poles and zeros (P_e/V_{stab}) of 5-th order model obtained using generalized least squares.

Chapter 5

Performance Studies of the Self-Tuning Power System Stabilizer

A number of studies were performed to determine the characteristics of the self-tuning power system stabilizer when applied to the simulated two-machine infinite-bus system described in section 3.5. Results of a number of these tests are presented in this chapter. Particular attention was paid to the ability of the stabilizer to damp both the local and interarea oscillatory modes of the simulated power system.

The first series of tests investigated the parameter convergence provided by the identification algorithm of the self-tuning PSS while Gaussian noise was applied to the equivalent machine. This would be the typical operating conditions encountered by the PSS in a real power system. The damping provided by a controller derived from the identified parameters was noted.

The second group of tests examined the tracking of changes in the generator parameters arising from a change in the operating point of the test generator. The combination of the first and second groups of tests demonstrates the ability of the self-tuning portion of the algorithm to converge quickly to a good control strategy and yet remain alert to changes in the parameters arising from changes in the operating conditions.

Multimode damping provided by the self-tuning PSS in response to a step change in the load connected to the test machine and to a transient fault condition is the focus of the next group of tests. These tests demonstrate the stable operation of the PSS under major system disturbances. The use of additional feedback signals to provide improved damping was also studied.

The final series of simulation studies investigated the operation of the self-tuning PSS when the input/output signals of the PSS were quantized as they would be by an analog to digital and digital to analog converter.

The self-tuning PSS algorithm was implemented on a commercial digital PSS. Results of preliminary field tests of this version of the self-tuning PSS are included at the end of this chapter. The stabilizer was tested briefly on both steam and hydro-power generators.

5.1 Identification Convergence Using Gaussian Load Disturbances Applied to the Equivalent Machine

The first series of simulation studies investigated the operation of the self-tuning PSS with a Gaussian load disturbance applied to the equivalent machine. This would be the normal operating condition encountered by a PSS connected to a real generator since the equivalent machine represents a pool of generators and loads and the effect of a large number of small random load changes within this pool can be approximated by a Gaussian disturbance. The simulation conditions are shown schematically in

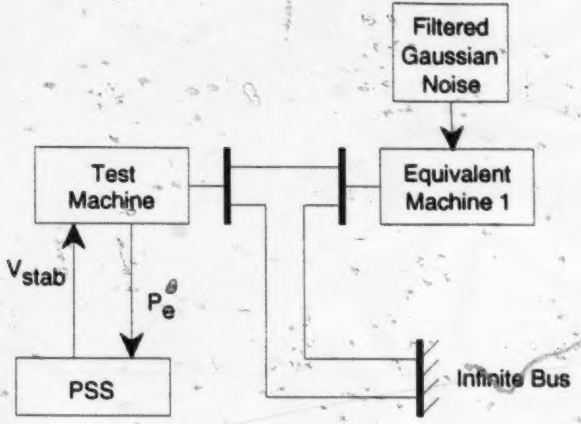

Figure 5.1: Simulation conditions for self-tuning PSS tests with Gaussian noise applied to equivalent machine.

figure 5.1.

The random disturbance applied to the equivalent machine was formed by passing the output of a zero-mean, normally-distributed random number generator through a lowpass filter with a cutoff frequency of 10 Hz.

The response of the test system with no PSS was determined by performing a simulation run with the self-tuning PSS disabled. The simulation consisted of 5 minutes of simulation time. This is equivalent to 240,000 steps of the transient stability simulation program (1.25 msec per step) or 6000 samples applied to the self-tuning PSS algorithm (20 Hz sampling). The spectra of the electric power and terminal voltage of the test machine are shown in figure 5.2. Spectral analysis was performed on the Hamming-windowed set of samples from the entire simulation interval. The local and interarea oscillatory modes can be seen in the spectrum of the test machine

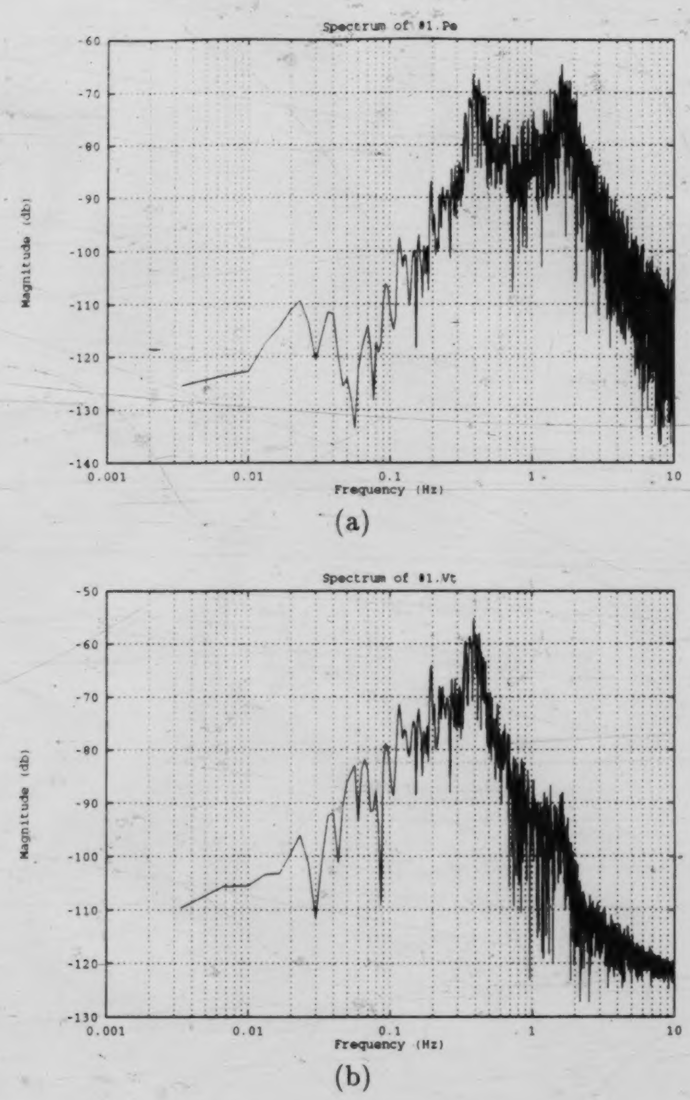

Figure 5.2: Spectrum of test machine electric power (a) and terminal voltage (b) with Gaussian noise applied to equivalent machine (PSS disabled).

electric power signal. The interarea mode dominates the spectrum of the test terminal machine terminal voltage.

The simulation was then repeated with the self-tuning PSS enabled. The control action weighting parameter, λ, was set to assign control action, u_t, one-fifth the weight of plant output variations, y_t, in the generalized minimum variance cost function (2.111). This value was chosen based on reports of prior studies of the GMV self-tuning PSS [57]. The variable forgetting factor employed by the parameter identification portion of the PSS was computed using the method presented by Kulhavý [80]. The method is described in section 2.1.3.

The results of several simulation runs made it apparent that this method of computing the value of the variable forgetting factor was producing 'bursting' of the parameter estimates after several thousand samples had been processed by the recursive least squares identification portion of the self-tuning PSS algorithm. The bursting became more pronounced as time progressed. A plot of the value of the first element of the estimated parameter vector is shown in figure 5.3a. The characteristics of the disturbance applied to the test system remained constant over the entire simulation. The parameter estimate is converging well until approximately 6000 samples have been processed. By sample number 10000 the parameter estimate becomes very erratic. The corresponding forgetting factor is shown in figure 5.3b. Again, the forgetting factor is well-behaved until about sample number 6000. By sample number 10000 the forgetting factor has become very erratic as well.

This pattern of erratic forgetting factor values after several thousand samples had been processed was observed under a number of simulation conditions including different types of disturbances, different control action weighting, and different generator operating points. In all cases the forgetting factor computation became

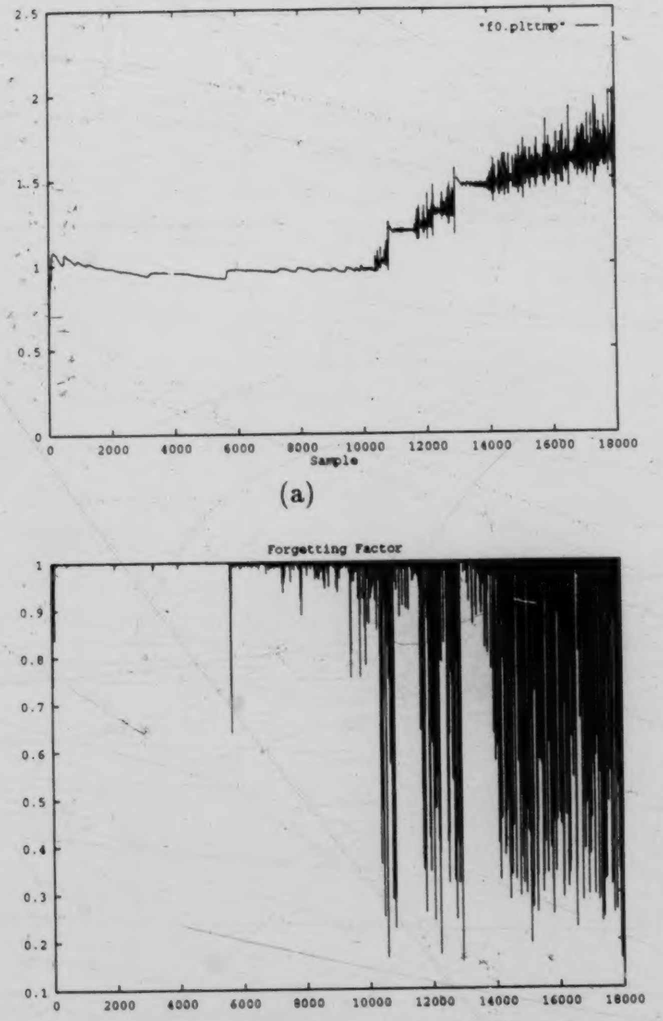

(a)

(b)

Figure 5.3: First element of parameter vector (a) and forgetting factor (b) from RLS using Kulhavý's variable forgetting factor.

unstable after several thousand simulation steps. The cause of this instability was not determined. Numerical instability seemed unlikely, as all calculations were performed using double precision arithmetic and none of the numbers involved seemed disproportionately large or small. As well, the onset of instability in the calculation of forgetting factor was very abrupt. For several thousand samples the forgetting factor remained between 0.995 and 1.0, and then dropped suddenly to less than 0.6 for several samples.

As a result of the above difficulties the algorithm for calculating the value of the variable forgetting factor was replaced with a method proposed by Sripada and Fisher [120]. The method is described in section 2.1.3 of this thesis. No problems with parameter bursting, even with simulation runs consisting of as many as 25,000 samples, were noted with this forgetting factor algorithm. Long term stability is critical for application of the self-tuning PSS to real generating systems.

The response of the self-tuning PSS using Sripada and Fisher's [120] variable forgetting factor is shown on the following pages. The plots represent 5 minutes of simulation time. In figure 5.4a the trace of the covariance matrix is seen to drop rapidly at the beginning of the simulation and then to decrease slowly. The prediction error, shown in figure 5.4b, exhibits some large excursions near the beginning of the simulation but settles down quickly. The quality of the parameter identification is verified by the plot of the frequency spectrum of the prediction error, in figure 5.4d, which is relatively flat, indicating that there are no resonant modes that have not been identified. The forgetting factor, shown in 5.4c, is small at the beginning of the simulation so that the initial estimate of the parameter values is quickly forgotten. As the simulation proceeds the forgetting factor approaches unity reflecting the fact that the characteristics of the disturbance applied to the system and the true parameter values are not changing with time.

The values of the elements of the estimated parameter vector are shown in figures 5.5 and 5.6. Rapid convergence of most of the parameters can be seen in these plots. The parameters which show slower convergence (f_2, f_3, f_4) have less effect on the response of the self-tuning PSS and so the fact that their values keep changing throughout the simulation does not greatly affect the computed control action. An example of this combined insensitivity to identification and computation of control action is shown in section 2.3.2. The g parameters, which form the denominator of the control algorithm and, hence, are the coefficients of the characteristic equation of the PSS, converge quickly. The g_0 parameter can be thought of as the parameter which sets the gain of the PSS (see equation 2.162). This element of the estimated parameter vector converges very quickly.

Observation of the spectrum of the test machine electrical power and terminal voltage, shown in figure 5.7, shows the effectiveness of the self-tuning PSS in damping both oscillatory modes. The local mode resonance of the electrical power has been suppressed by 20 db compared to the response shown in figure 5.2. The interarea mode resonance is seen to have been decreased by about 5 db. The spectrum of the terminal voltage shows that the interarea resonance of this signal has also been decreased by 5 db.

The variance of the test machine electrical power and terminal voltage, with and without the self-tuning PSS, are given in table 5.1. The self-tuning PSS has considerably reduced the variance of both signals. The energy in the electrical power variations has been reduced by more than a factor of 6.

Table 5.1: Test machine variances with and without self-tuning PSS.

Variance (per unit)		
	P_e	V_t
Without PSS	9.79×10^{-5}	1.79×10^{-4}
With PSS	1.50×10^{-5}	1.03×10^{-4}

The improvement in the damping of both oscillatory modes was verified by repeating the frequency response measurements described in section 4.1 but this time equipping the test machine with a fixed PSS using the parameter values taken at the end of the simulation described above. Fixing the parameters in this way is necessary to obtain a true frequency response. If the parameters were allowed to continue their self-tuning they would attempt to adapt to minimize the effects of the identification excitation signal and a true frequency response would not be obtained. The response of the system with this fixed PSS in place is shown in figure 5.8. The response of the system without the PSS is shown by the dashed line. The plots show that the local oscillatory mode has been completely suppressed and that the interarea oscillatory mode has been decreased by about 5 db. The energy in the interarea oscillatory mode has thus been reduced to about one-third of its previous value. Greater damping at frequencies in the range of the interarea mode and below is difficult to obtain since

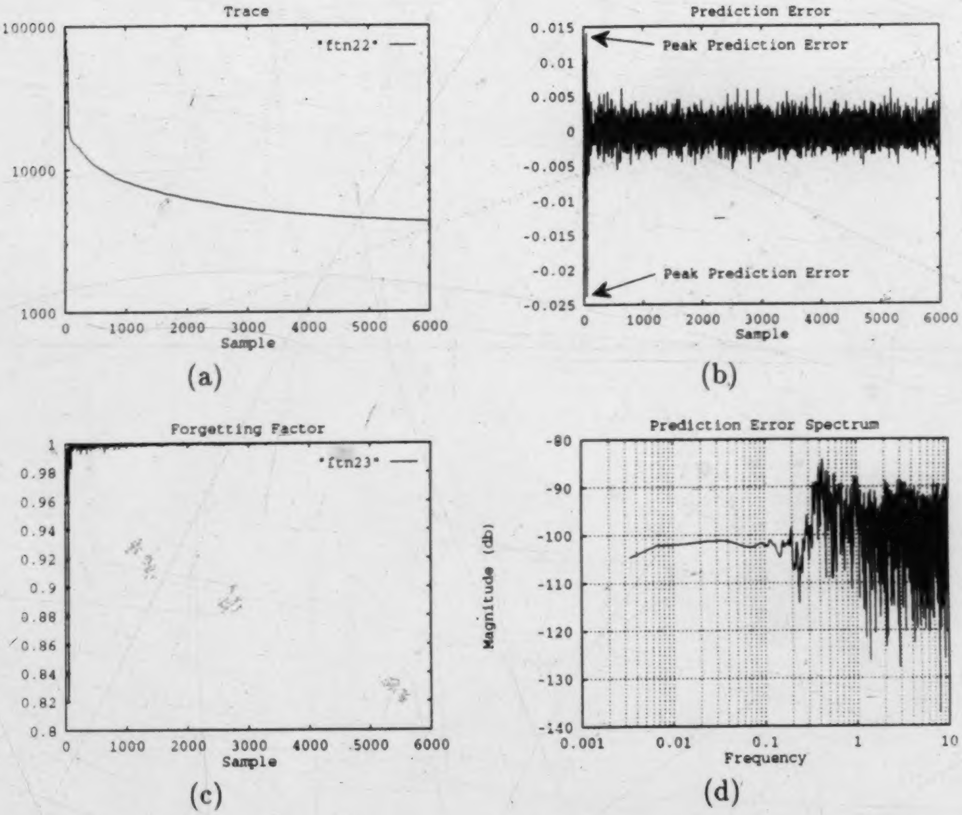

Figure 5.4: Results of self-tuning PSS simulation with Gaussian noise applied to equivalent machine. a–Trace of covariance matrix, b–Prediction error, c–Forgetting factor, d–Spectrum of prediction error.

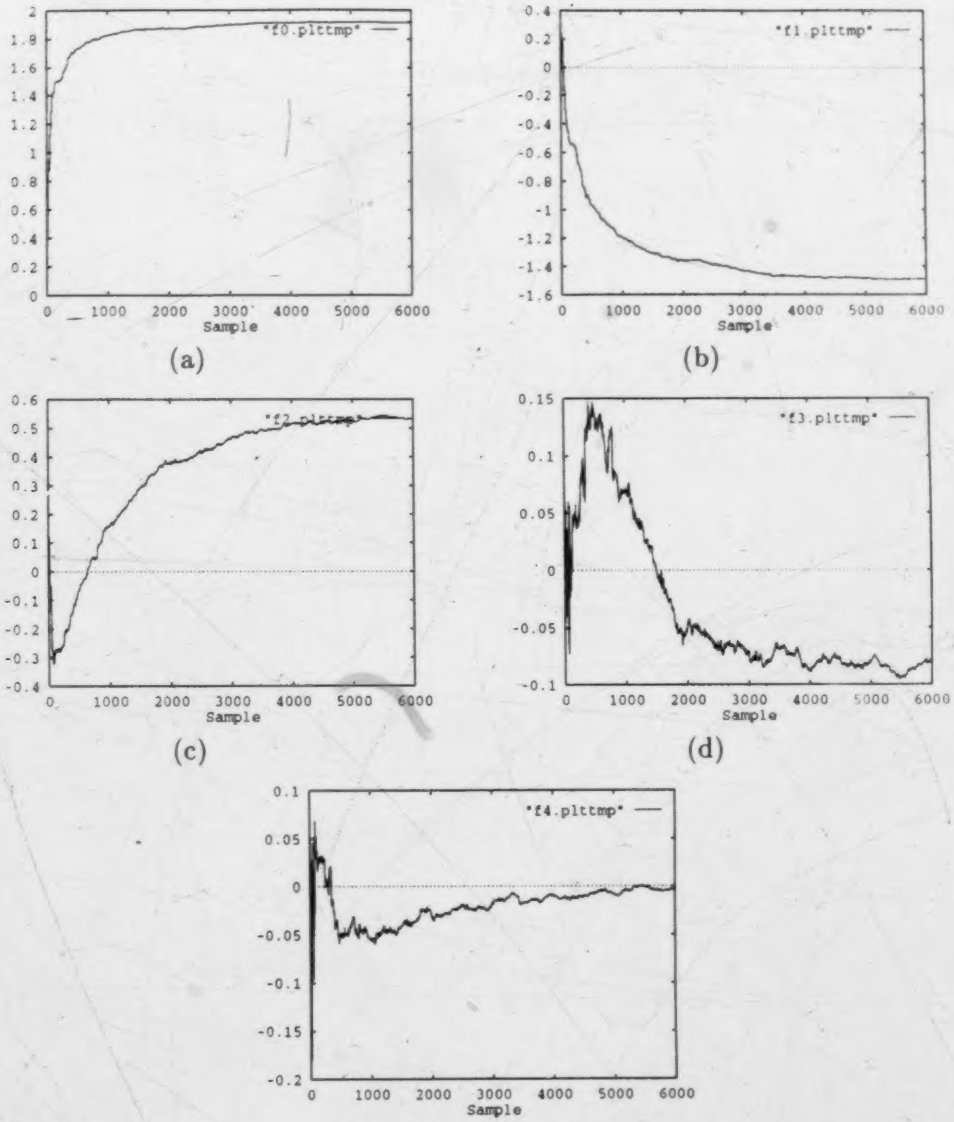

(a) (b) (c) (d) (e)

Figure 5.5: Parameter identification of self-tuning PSS simulation with Gaussian noise applied to equivalent machine. a–f_0, b–f_1, c–f_2, d–f_3, e–f_4.

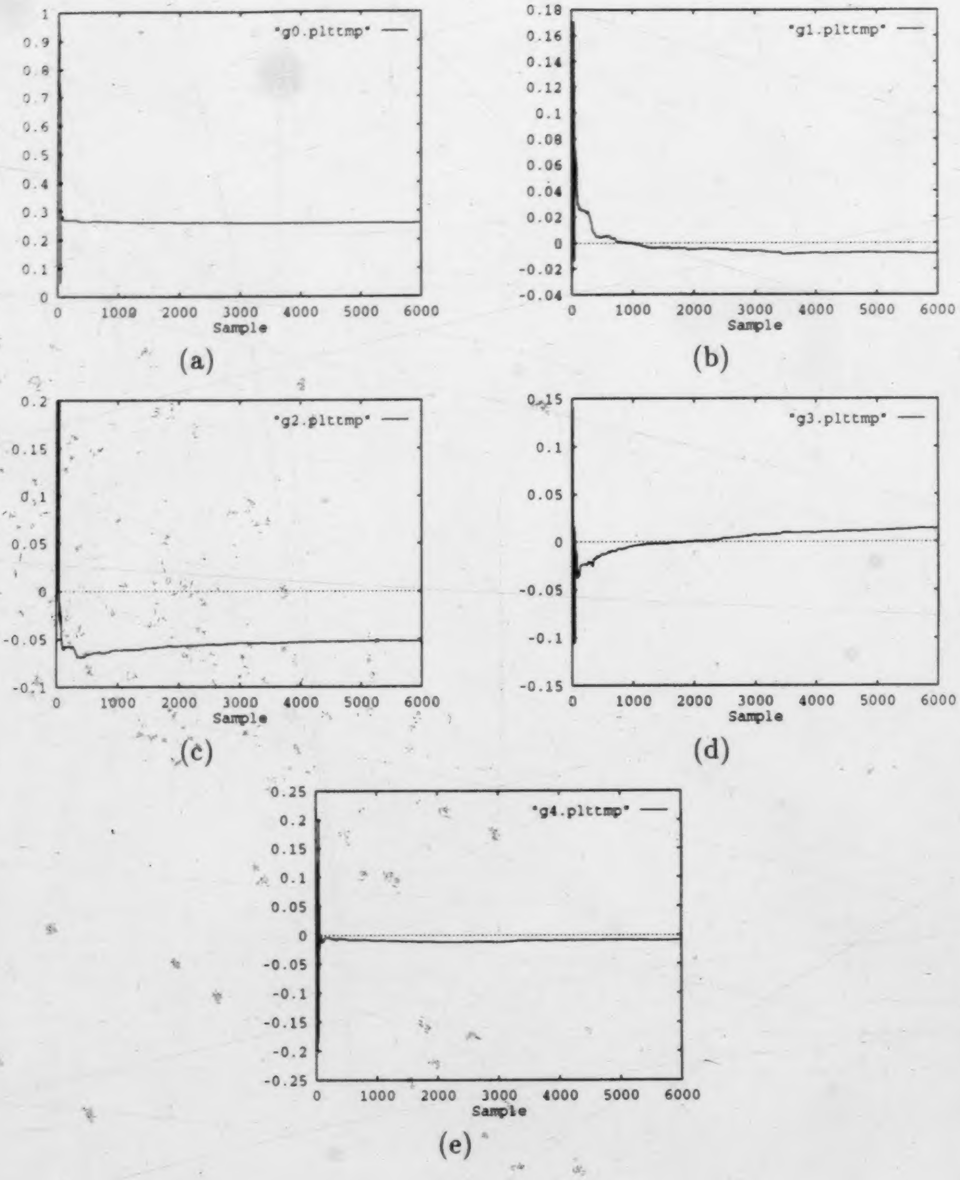

(a) (b) (c) (d) (e)

Figure 5.6: Parameter identification of self-tuning PSS simulation with Gaussian noise applied to equivalent machine. a–g_0, b–g_1, c–g_2, d–g_3, e–g_4.

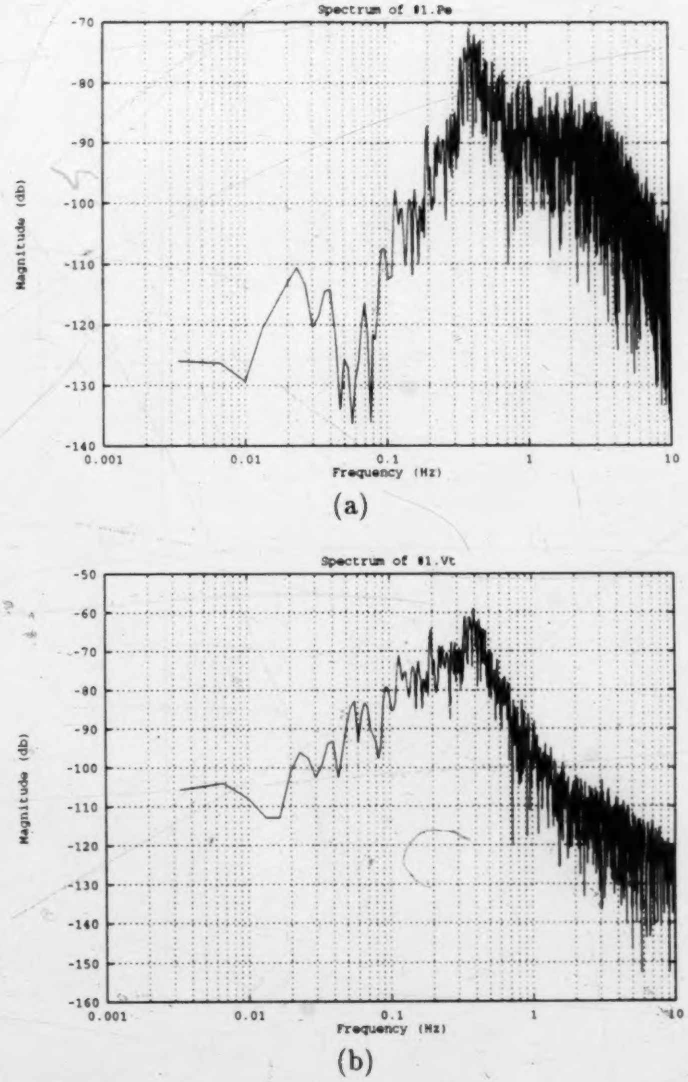

(a)

(b)

Figure 5.7: Spectrum of test machine electric power (a) and terminal voltage (b) with Gaussian noise applied to equivalent machine (PSS enabled).

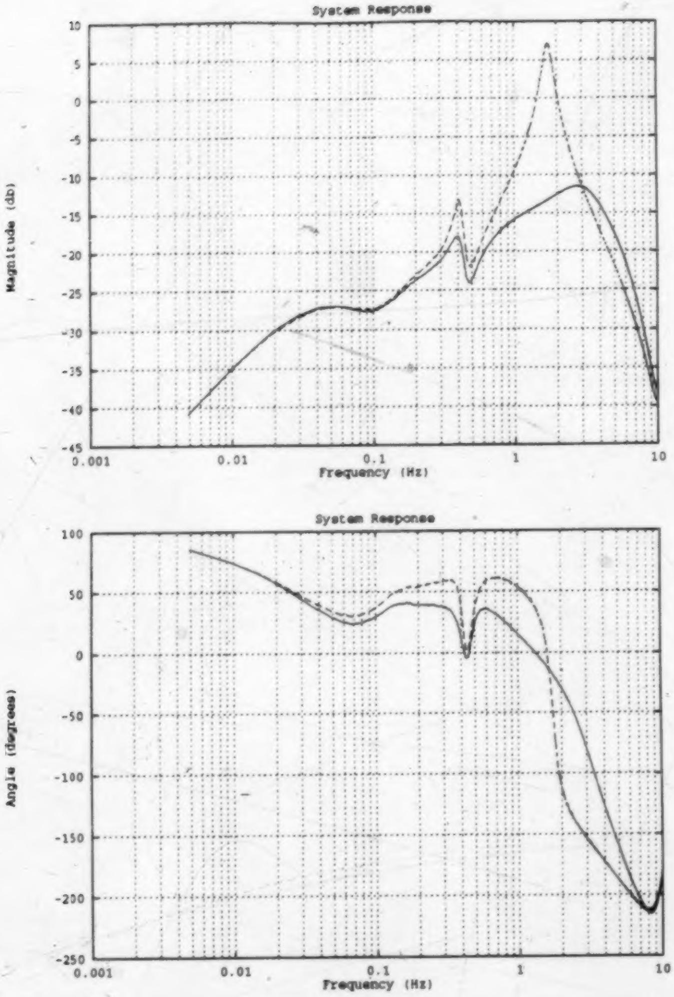

Figure 5.8: Frequency response (P_e/V_{stab}) of two-machine infinite-bus test system with fixed PSS (— with PSS, - - without PSS).

the AVR attempts to "correct" the terminal voltage offset introduced by the PSS at these lower frequencies.

5.2 Parameter Tracking During Change in Test Machine Operating Point

The second series of tests investigated the ability of the self-tuning PSS to adapt to a change in the operating point of the test machine in the two-machine infinite-bus simulation. The test results illustrate the ability of the self-tuning portion of the PSS to adapt quickly to a change in the generator operating conditions even after a considerable period of operation at the original operating conditions.

The operating point of the test machine was changed by reducing the AVR reference signal and hence changing the reactive power produced by the machine. The initial operating point, as described in section 4, had the test machine producing 0.23 p.u. reactive power. The new operating point has the test machine absorbing 0.08 p.u. reactive power. The real power output of the test machine remained unchanged. The self-tuning PSS was initialized with the parameter and covariance matrix taken from the last sample of the simulations described in the previous section. The change in operating point thus appears to the self-tuning algorithm to have occurred after 6000 samples at the original operating point.

The response of the simulated test machine to the change in operating point is shown in figure 5.9. The response of the system with no PSS attached is given by the dotted line on the plots. The test machine is stable both before and after the change in operating point, but the local and interarea modes are both quite lightly damped. The improved damping of the local and interarea oscillatory modes when the PSS is operating can be seen in the plot of the real power output (P_e) of the test machine.

The presence of both oscillatory modes is even more apparent in the plot of the shaft speed (ω) of the test machine when not equipped with a PSS. The local oscillatory mode can be seen superimposed on the lower-frequency, more lightly-damped, interarea mode. The interarea oscillation persists for almost the entire simulation.

The damping provided by the self-tuning PSS is readily seen in the plots of the electric power and shaft speed of the test machine. The initial excursion of both signals is less than half of the same machine not equipped with a stabilizer. The nearly total suppression of the local oscillatory mode is apparent from the plot of the test machine shaft speed. The reduction in the amplitude and duration of the interarea mode oscillation in the test machine shaft speed can also be seen.

The plot of the field voltage (E_f) of the test machine shows that the initial excursion of this value is also reduced when the machine is fitted with the self-tuning PSS.

The forgetting factor computed by the recursive least squares identification portion of the self-tuning PSS is shown in figure 5.10. Prior to the change in the test machine operating point the forgetting factor is near unity, as it was at the end of the simulation shown in figure 5.4. At the time of the change in the operating point the forgetting factor drops and the identification algorithm discounts the old data it has used to form the parameter estimate.

The memory time constant beyond which old data is effectively forgotten is given

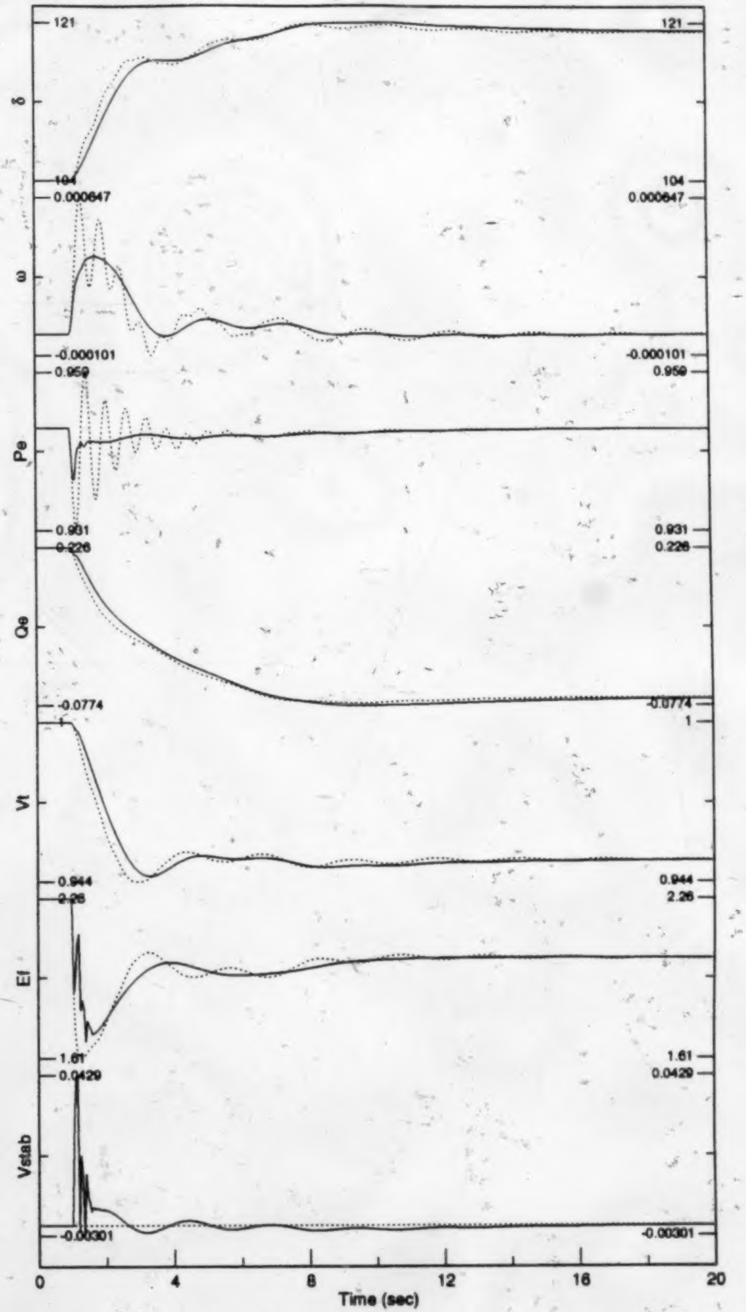

Figure 5.9: Test machine transient response following change in test machine operating point (··· No PSS, — Self-tuning PSS).

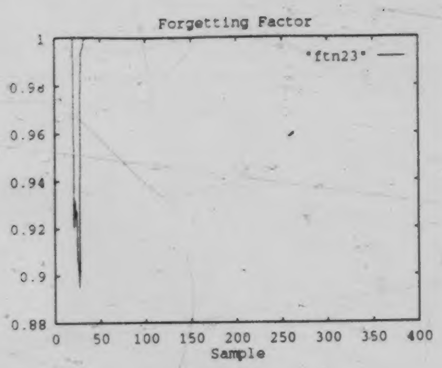

Figure 5.10: Forgetting factor computed in response to change in test machine operating point.

by,

$$\text{Memory time constant} = \frac{1}{1-\gamma} \tag{5.1}$$

where γ is the value of the forgetting factor. A fixed forgetting factor of 0.95 thus corresponds to a memory time constant of 20 samples, or in the simulation study presented here, 1 second. The plot of the forgetting factor in figure 5.10 shows that the factor is well below 0.95 for several samples which indicates that the old information from which the parameters were estimated is being rapidly discounted.

The identified parameter values are shown in figures 5.11 and 5.12. The rapid change in the parameters at the time of the change in the operating point reflects the effectiveness of the variable forgetting factor in keeping the identification algorithm alert even after several thousand samples at the original operating point. All the parameters settle to their new values very quickly and have ceased changing within about 30 samples (1.5 seconds) of the change in the reference signal to the AVR of the test machine.

The results presented in the above two sections show that the identification portion of the self-tuning PSS provides stable parameter estimates during long periods of small disturbances while still remaining alert to changes in the generator operating conditions. The self-tuning PSS is shown to be capable of damping the local oscillatory mode and to provide some suppression of interarea oscillations in response to both random and deterministic disturbances.

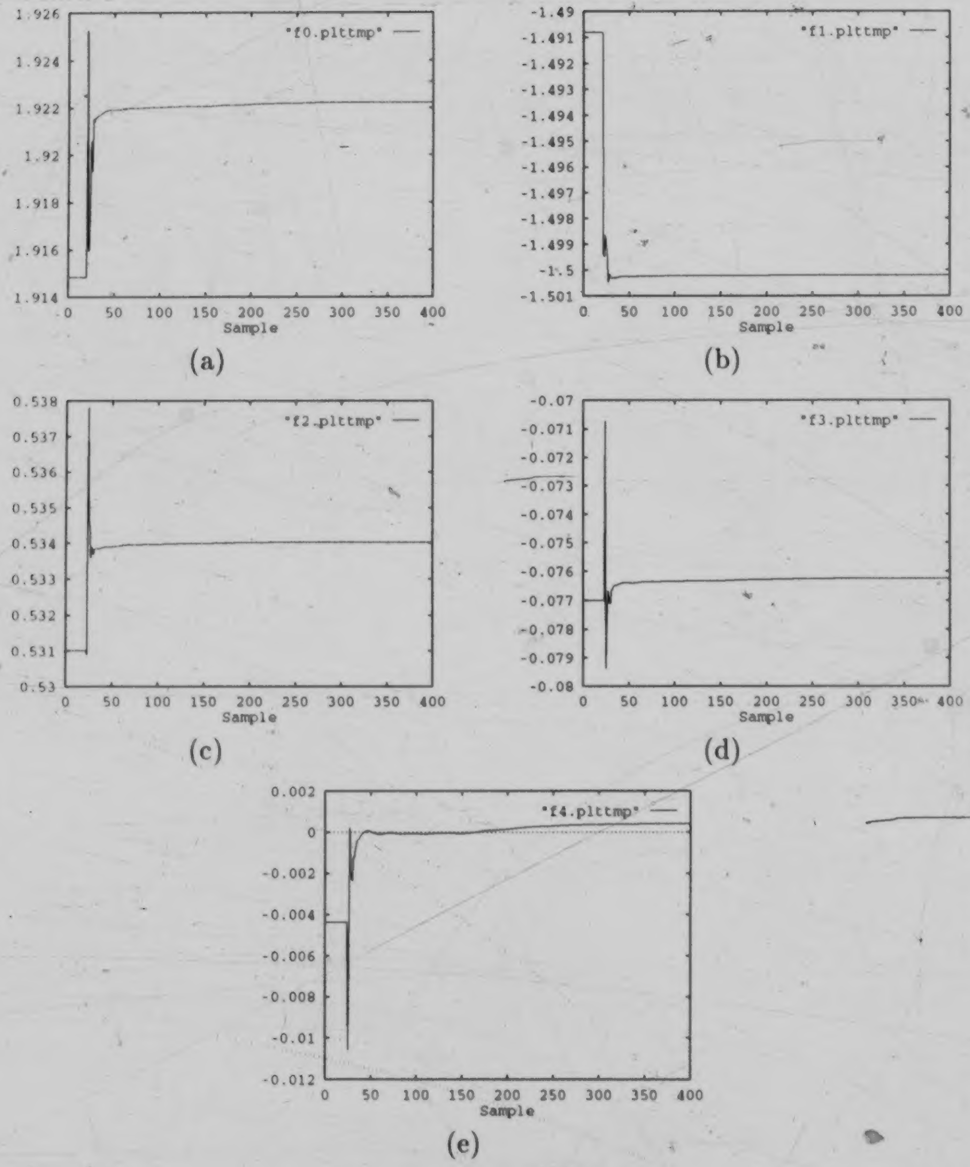

(a)

(b)

(c)

(d)

(e)

Figure 5.11: Parameter identification of self-tuning PSS simulation with change in operating point of test machine. a–f_0, b–f_1, c–f_2, d–f_3, e–f_4.

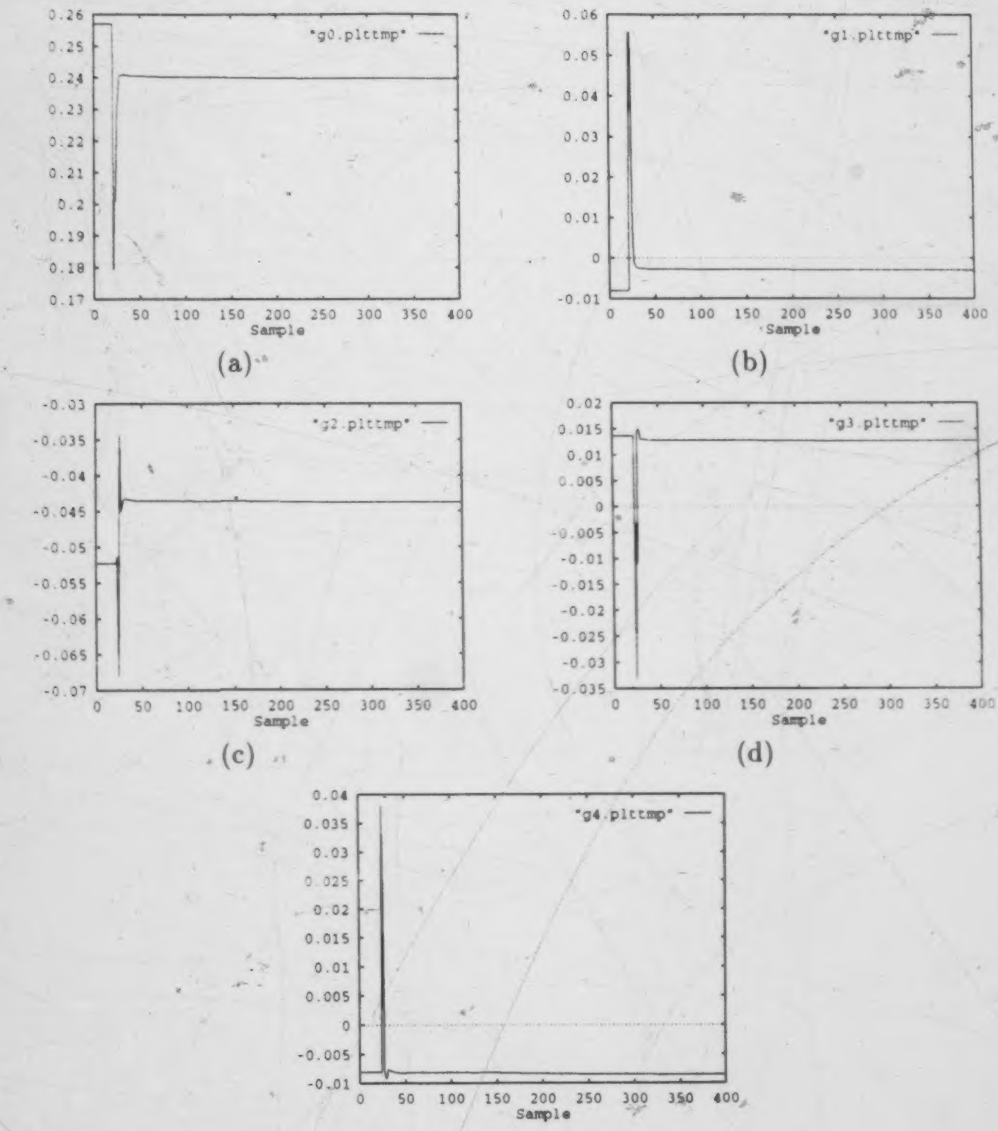

(a)

(b)

(c)

(d)

(e)

Figure 5.12: Parameter identification of self-tuning PSS simulation with change in operating point of test machine. a–g_0, b–g_1, c–g_2, d–g_3, e–g_4.

5.3 Suppression of Local and Interarea Modes Following Step Load Change

The response of the self-tuning PSS to a large disturbance was investigated by applying a -0.2 p.u. step disturbance to the P_{dist} input of the test machine model shown in figure 3.2. This disturbance represents the sudden loss of a local load. The test results illustrate the ability of the PSS to adapt quickly to an abrupt change in the generator operating conditions. As described in the previous section the self-tuning PSS is initialized with parameter and covariance values from the last sample of the simulations described in section 5.1. This has the effect of applying the electric power disturbance after a considerable period of operation at the original operating conditions.

The response of the simulated test machine to the step power disturbance is shown in figure 5.13. The response of the system with no PSS attached is given by the dotted line on the plots.

The presence of both local and interarea oscillatory modes is apparent in the plot of the shaft speed (ω) of the test machine when not equipped with a PSS. The local oscillatory mode can be seen in the first few seconds of the transient superimposed on the lower-frequency, more lightly-damped, interarea mode.

The damping provided by the self-tuning PSS is readily seen in the plots of the electric power and shaft speed of the test machine. The initial excursion of the electric power is the same both with and without the PSS enabled. The reason for this behavior is apparent by noting that the disturbance injection point in the

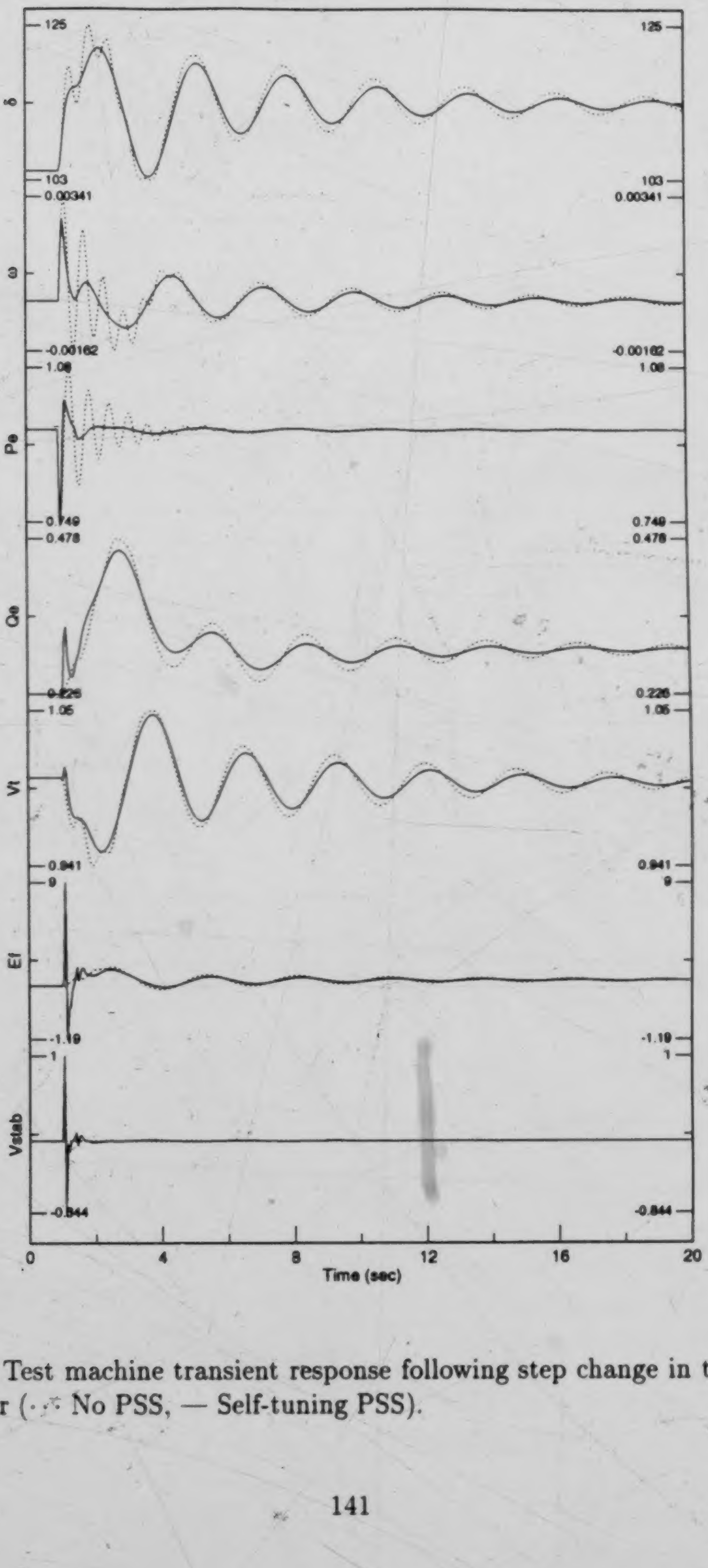

Figure 5.13: Test machine transient response following step change in test machine electric power (··· No PSS, — Self-tuning PSS).

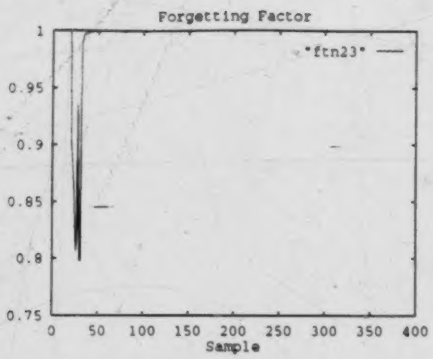

Figure 5.14: Forgetting factor computed in response to step change in test machine electric power.

simulation model of the generator simulation model is coupled directly to the electric power. A synchronous generator has no instantaneous coupling path between the PSS input to the AVR and the electric power produced by the machine, so a step power disturbance will result in the same initial excursion no matter what type of PSS is employed. The second excursion of the electric power is reduced by about one-half by the self-tuning PSS and the electric power is almost completely damped within one second of the disturbance. The nearly total suppression of the local oscillatory mode is apparent from the plot of the test machine shaft speed. The amplitude of the initial excursion is reduced by about one-third by the PSS. The reduction in the amplitude and duration of the interarea mode oscillation in the test machine shaft speed can also be seen.

The forgetting factor computed by the recursive least squares identification portion of the self-tuning PSS is shown in figure 5.14. Prior to the change in the test machine operating point the forgetting factor is near unity, as it was at the end of the simulation shown in figure 5.4. At the time of the change in the operating point the forgetting factor drops and the identification algorithm discounts the old data it has used to form the parameter estimate.

The identified parameter values are shown in figures 5.15 and 5.16. The rapid change in the parameters at the time of the step disturbance in the electric power of the test machine reflects the effectiveness of the variable forgetting factor in keeping the identification algorithm alert even after several thousand samples under the original operating conditions. All the parameters settle to their new values very quickly and have ceased changing within about 50 samples (2.5 seconds) of the electric power disturbance.

The results presented in this section emphasize the ability of the self-tuning PSS to damp the local oscillatory mode and to provide some suppression of interarea oscillations in response to a fairly large disturbance applied to the test machine.

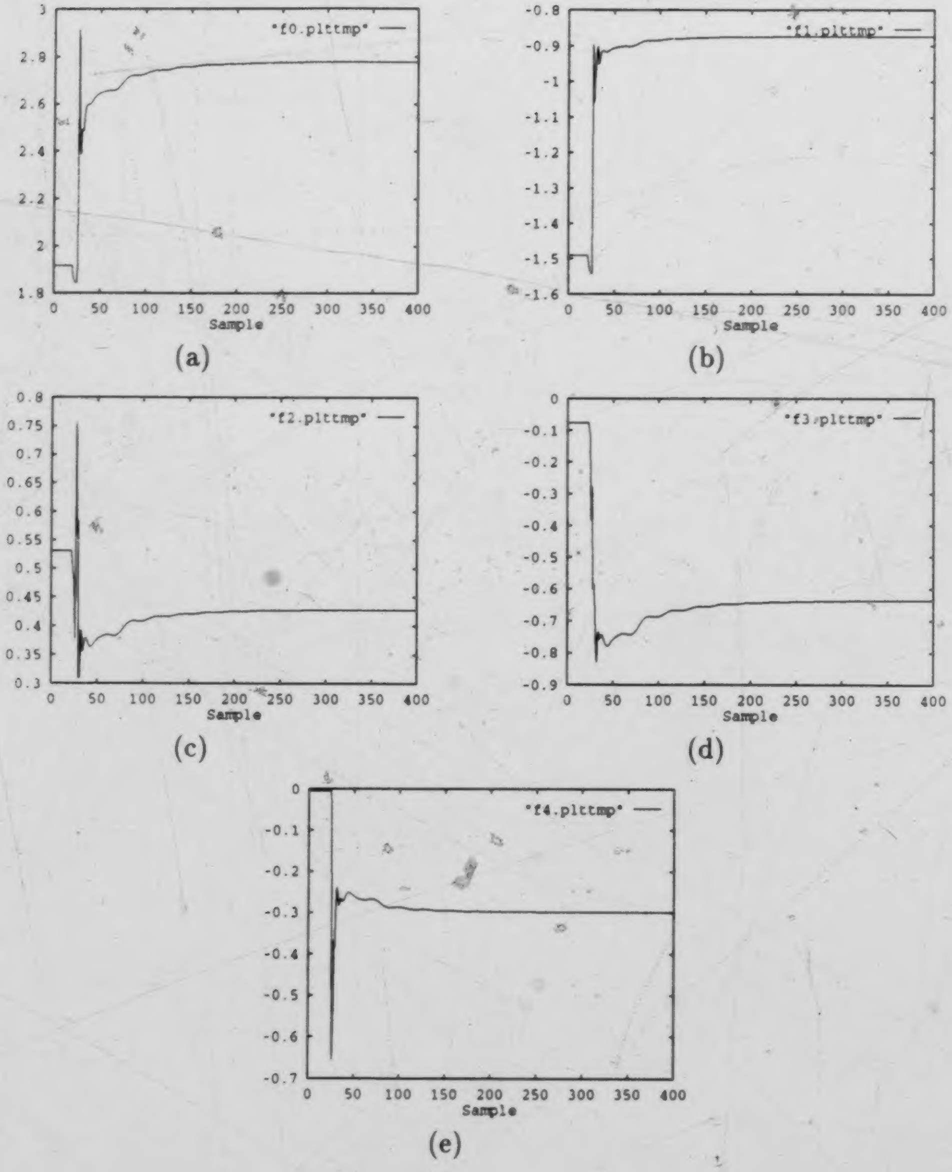

Figure 5.15: Parameter identification of self-tuning PSS simulation with change in electric power of test machine. a–f_0, b–f_1, c–f_2, d–f_3, e–f_4.

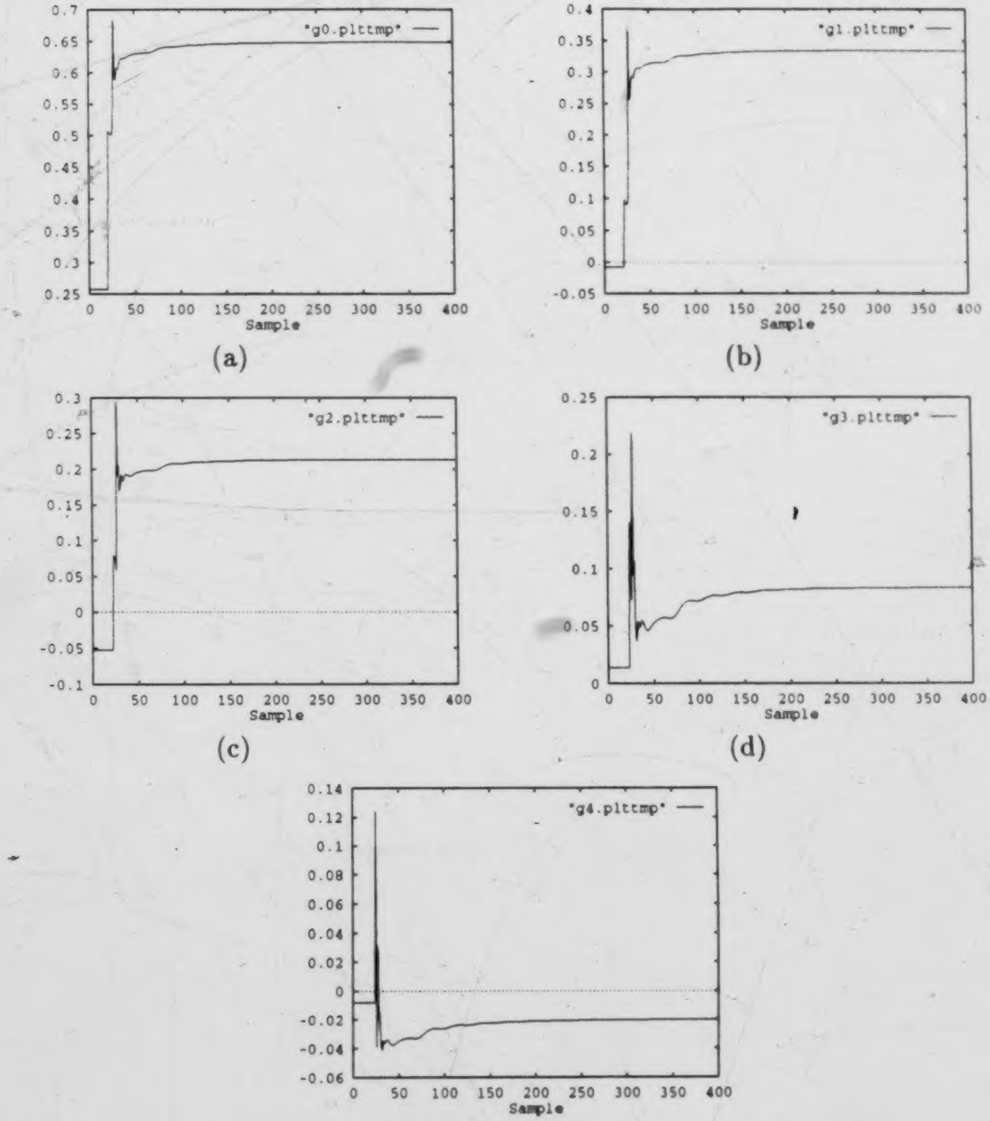

(a) (b) (c) (d) (e)

Figure 5.16: Parameter identification of self-tuning PSS simulation with change in electric power of test machine. a–g_0, b–g_1, c–g_2, d–g_3, e–g_4.

5.4 Suppression of Local and Interarea Modes Following Transient Fault Condition

Operation of the self-tuning PSS during, and immediately following, a transient fault condition was investigated by applying a three-cycle, three-phase short circuit to the line joining the test machine and the equivalent machine. As was the case for the results presented in the previous two sections, the self-tuning PSS was initialized with the parameter vector and covariance matrix from the final sample of the simulation described in section 5.1. The fault was located on the line joining the machines one-fifth of the distance from the test machine.

The response of the test machine, with and without the self-tuning PSS, is shown in figure 5.17. The response of the system with no PSS attached is given by the dotted line on the plots.

The presence of both local and interarea oscillatory modes is most apparent in the plot of the rotor angle (δ) of the test machine when not equipped with a PSS. The local oscillatory mode can be seen in the first few seconds of the transient superimposed on the interarea oscillation. The interarea oscillation persists for the remainder of the simulation.

The self-tuning PSS remains stable during the fault even though the field voltage is held at its upper limit. After the fault has been cleared the local mode oscillations in the electric power are damped more quickly when the generator is equipped with the self-tuning PSS. The terminal voltage and reactive power of the test machine show

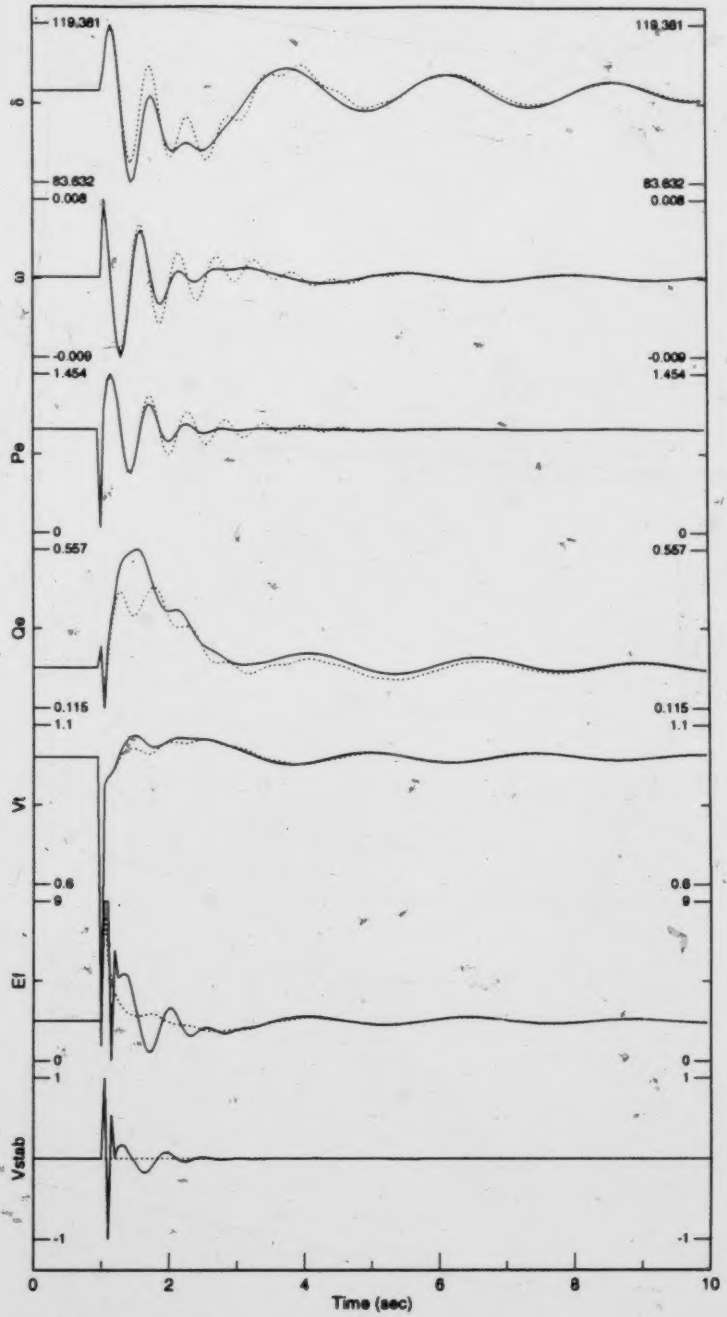

Figure 5.17: Test machine transient response following transient fault condition (··· No PSS, — Self-tuning PSS).

the presence of the interarea oscillation even though the electric power oscillations have been almost completely suppressed. The use of additional feedback signals to the self-tuning PSS may allow better damping of the terminal voltage and reactive power oscillations while still retaining the good damping of the real power produced by the machine. The following section describes the operation of the self-tuning PSS when additional feedback signals are employed.

5.5 Suppression of Local and Interarea Modes Following Transient Fault Condition Using Self-Tuning PSS with Multivariable Feedback

The use of multivariable feedback was studied by modifying the self-tuning PSS algorithm to accept two output signals from the generator to be stabilized. The cost function to be minimized by the control action is then,

$$I = E\left\{(P_1 y_1(t+k))^2 + (P_2 y_2(t+k))^2 + (Qu(t))^2\right\} \tag{5.2}$$

where $y_1(t+k)$ and $y_2(t+k)$ are the two plant outputs, $u(t)$ is the controller output and P_1, P_2 and Q are weighting polynomials in the backwards shift operator. The w_t term in (2.111) has been deleted since the presence of a washout filter on the PSS feedback signals yields a zero reference to which the control algorithm attempts to drive the feedback signals. For the simulation studies described in this section the weighting polynomials are simply constants,

$$P_1(z^{-1}) = \lambda_1 \tag{5.3}$$

$$P_2(z^{-1}) = \lambda_2 \tag{5.4}$$

$$Q(z^{-1}) = 1 \tag{5.5}$$

The results presented here used the real and reactive power of the test machine as the feedback signals to the self-tuning PSS. Similar results were obtained when the real power and the terminal voltage of the test machine were used. The terminal voltage may often be a more appropriate signal to include as a feedback signal since the stability of the terminal voltage directly reflects the quality of the generated power. For this particular simulation the reactive component of the power supplied by the generator also provided good damping when used as an additional feedback signal. Results of tests using reactive power feedback are presented here to emphasize that the self-tuning PSS algorithm can provide good results with a wide selection of feedback signals.

The initial parameter vector and covariance matrix for the transient fault tests were obtained as described in section 5.1. A Gaussian disturbance was applied to the P_{dist} point of the equivalent machine and the self-tuning PSS was given 6000 samples (5 minutes of simulation time) to adapt to the system. With these initial values in place the response of the self-tuning PSS to a three-cycle, three-phase short circuit along the line joining the test machine and the equivalent machine was obtained.

The response of the test machine, with and without the self-tuning PSS, is shown in figure 5.18. The response of the system with no PSS attached is shown as the dotted line on the plots. The response shows little improvement over the results obtained using the electric power only of the test machine as the feedback signal.

A possible explanation for the poor response is that the parameters identified by the recursive least squares algorithm make large changes while the fault is present and do not return to their prefault values quickly enough to produce a control action capable of providing good damping. A technique whereby this improper identification can be avoided was described by Fan, Ortmeyer and Mukundan in a paper describing an adaptive PSS [50]. The method simply inhibits parameter updates when the terminal voltage of the generator is more than 30% below its nominal value. The change affects only the parameter identification portion of the self-tuning PSS. The control action is calculated and fed to the AVR the same way regardless of the value of the terminal voltage. As shown below, this modification makes the self-tuning PSS considerably more robust in the presence of system fault conditions.

The response of the test machine, with the above modification to the self-tuning PSS algorithm, is shown in figure 5.19. The dotted line shows the response of the system with no PSS attached.

The results show much better damping of the local mode oscillation in the real electric power signal as well as better damping of the interarea oscillation present in the reactive power signal. The improved damping of both modes is apparent in the plot of the rotor angle of the test machine as well. The local mode oscillation

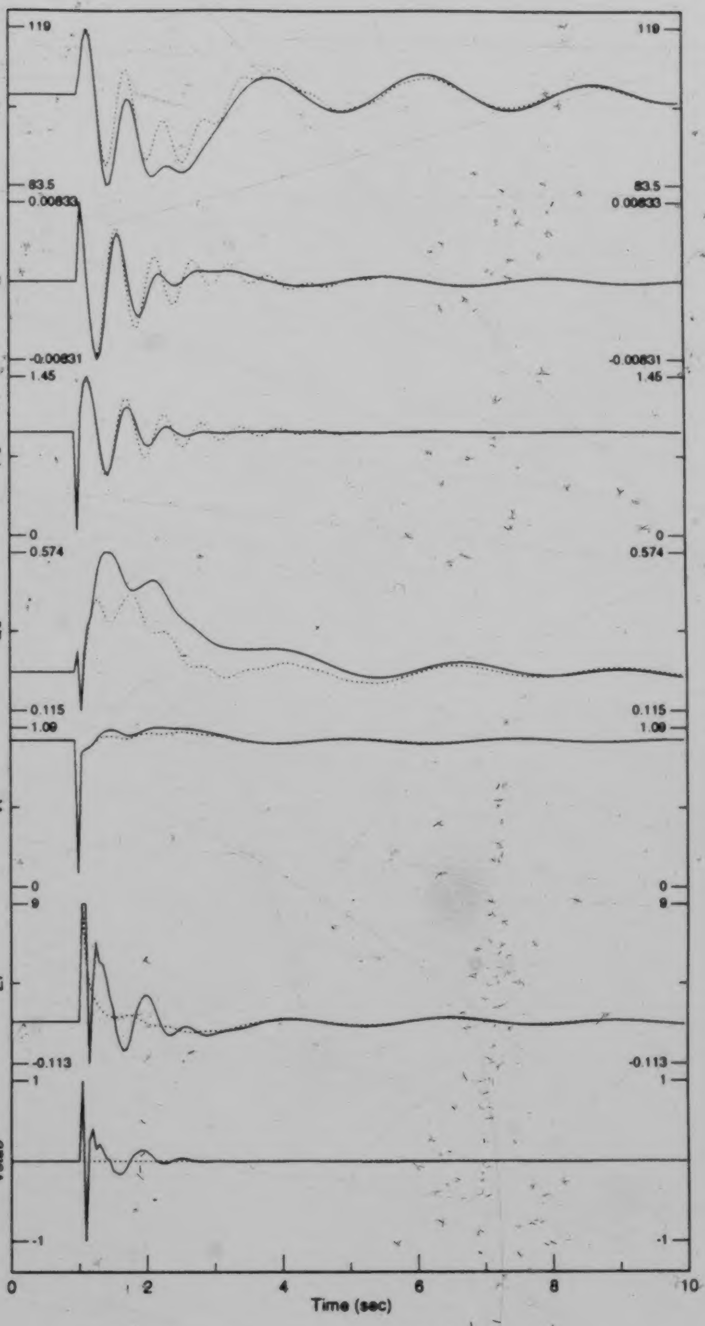

Figure 5.18: Test machine transient response following transient fault condition (··· No PSS, — Self-tuning PSS using P_e and Q_e feedback).

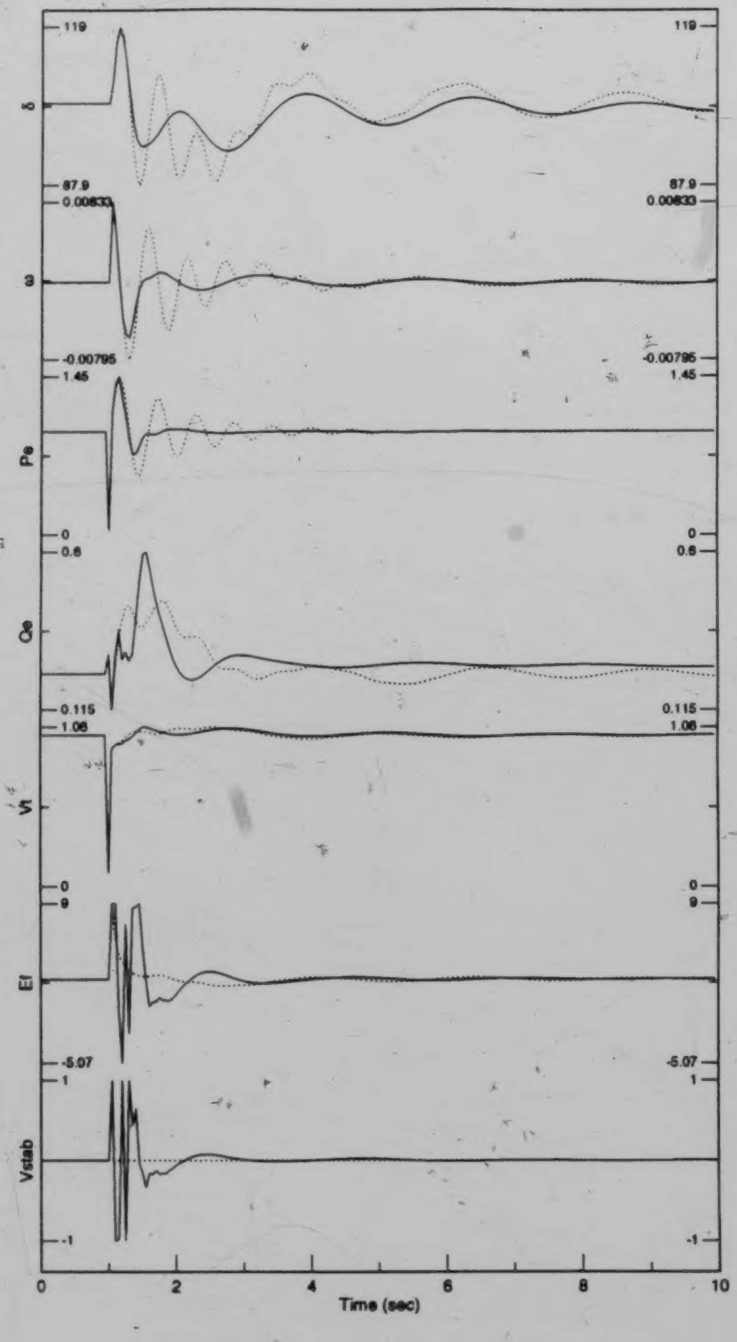

Figure 5.19: Test machine transient response following transient fault condition (··· No PSS, — Self-tuning PSS using P_e and Q_e feedback and parameter identification inhibited while terminal voltage out of range).

prominent in the rotor angle plot of the unstabilized generator is suppressed within one second and the amplitude of the lower frequency interarea oscillation is also reduced.

5.6 Effect of Analog to Digital and Digital to Analog Quantization on PSS Performance

The self-tuning PSS used in the simulation studies described in the previous sections used double precision floating point values to communicate with the transient stability simulation program. This corresponds to a quantization level of around 1 part in 10^{16}. The resolution of the analog to digital and digital to analog converters commonly used in existing digital stabilizers is 1 part in 4096. The effect of the quantization errors introduced by such converters on the operation of the self-tuning stabilizer is described in this section.

The tests described in section 5.1 were repeated with the self-tuning PSS input/output signals quantized to steps of 0.001 per unit. The quantized control signal was fed to the identification portion of the self-tuning PSS. Use of the quantized control signal in this way makes the parameter identification insensitive to the quantization imposed by the digital to analog converter. The quantization of the electric power signal by the analog to digital is then the only change seen by the parameter identification algorithm.

The parameter identification results obtained from the application of a filtered

Table 5.2: Test machine variances with and without quantization of PSS signals.

Variance (per unit)		
	P_e	V_t
Without PSS	9.79×10^{-5}	1.79×10^{-4}
With PSS (no quantization)	1.50×10^{-5}	1.03×10^{-4}
With PSS (quantized I/O)	1.57×10^{-5}	1.05×10^{-4}

Gaussian disturbance to the P_{dist} of the equivalent machine are shown in figures 5.20 and 5.21.

The parameter values identified from the quantized signals are nearly identical to those identified from the non-quantized input/output values and shown in figures 5.5 and 5.6. This result is very good considering that the RMS value of the electric power signal over the duration of the simulation is on the order of just 5 quantization levels.

The variance of the test machine electrical power and terminal voltage over the entire simulation, with and without the self-tuning PSS, are given in table 5.2. The variance of the electric power of the test machine is only slightly greater when the quantized signals are used.

The damping provided by the self-tuning PSS with input/output quantization was determined by repeating the frequency response measurements described in section 5.1 using a fixed-parameter PSS with input/output quantization based on the parameter values from the end of the simulation described above. The response of the system with this fixed PSS in place is shown in figure 5.22. The response of the system the PSS formed from the non-quantized input/output signals is shown by the dashed line. The noise added by the quantization of the input/output signals is most apparent

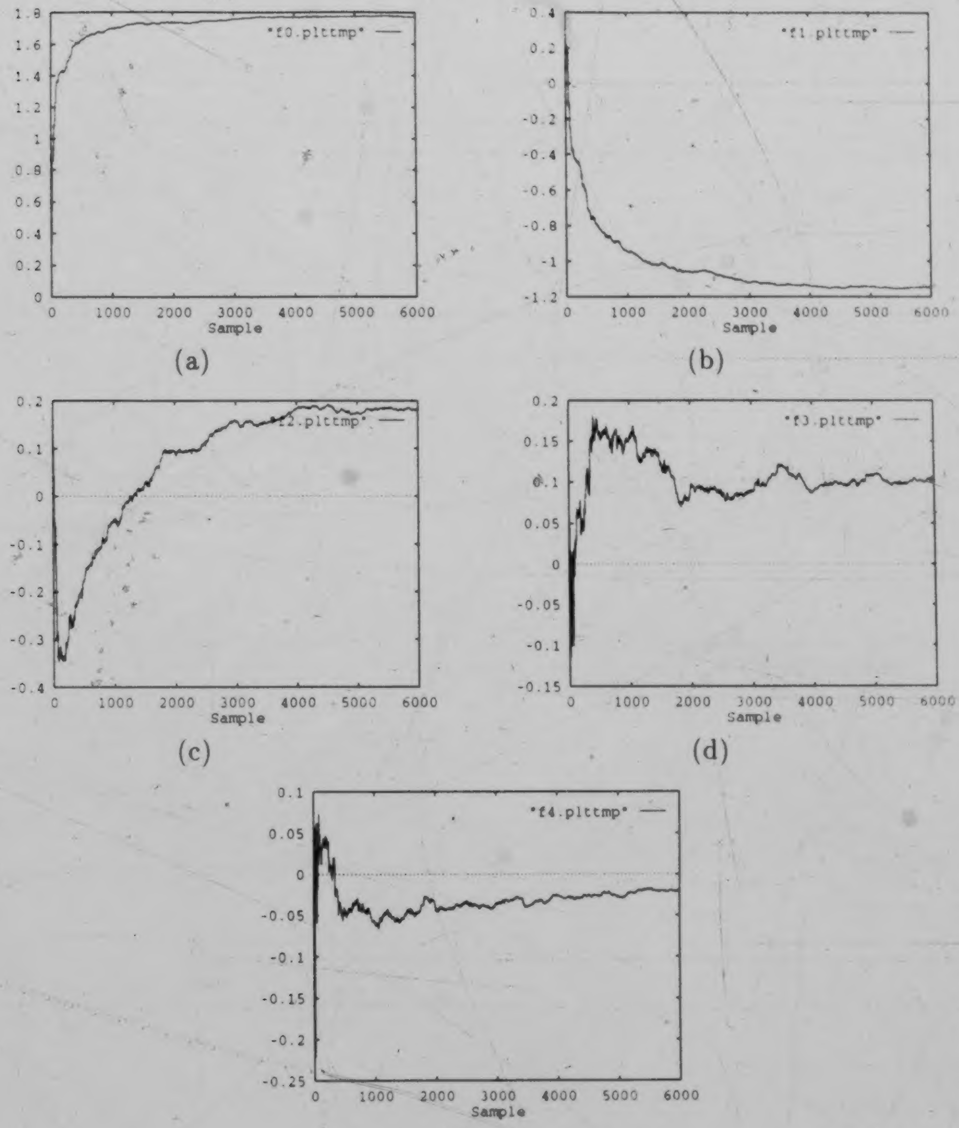

(a) (b)

(c) (d)

(e)

Figure 5.20: Parameter identification of self-tuning PSS simulation with Gaussian noise applied to equivalent machine and quantization of PSS input/output signals. a–f_0, b–f_1, c–f_2, d–f_3, e–f_4.

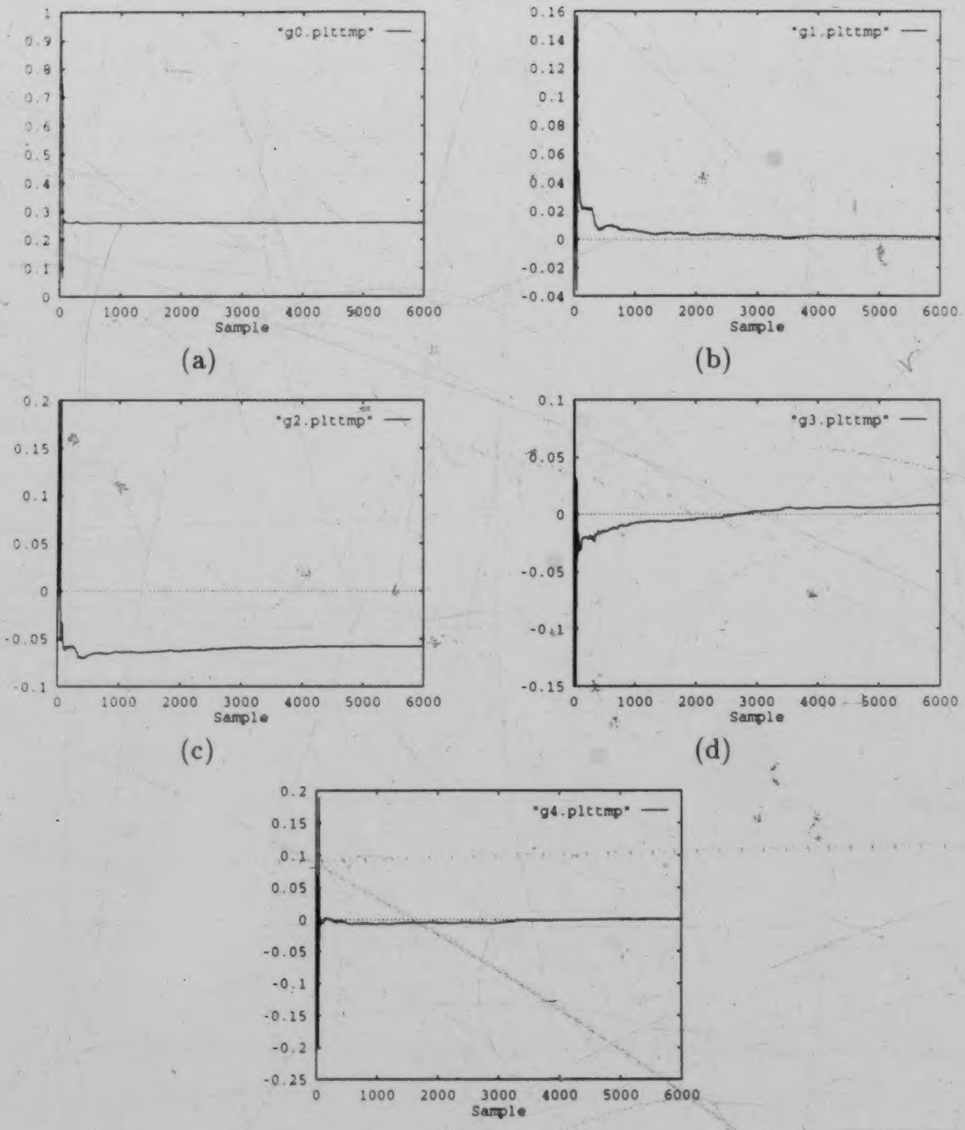

(a) (b)

(c) (d)

(e)

Figure 5.21: Parameter identification of self-tuning PSS simulation with Gaussian noise applied to equivalent machine and quantization of PSS input/output signals. a–g_0, b–g_1, c–g_2, d–g_3, e–g_4.

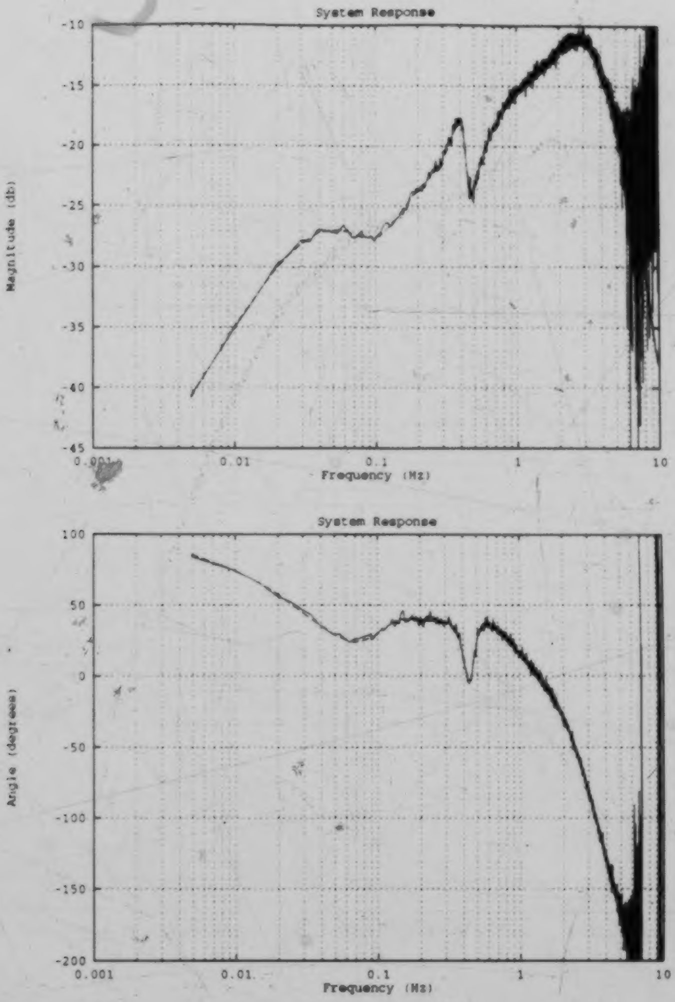

Figure 5.22: Frequency response (P_e/V_{stab}) of two-machine infinite-bus test system with fixed PSS (— PSS with input/output quantization, - - PSS without quantization).

at higher frequencies where the energy in the electric power signal is low. The low energy at higher frequencies is a result of the low pass filter applied to the excitation signal used to form the frequency response as well as the low-pass filtering effect of the generator itself.

The overall frequency response is quite similar to that provided by the PSS with no quantization. In particular the interarea and local mode resonant peaks are suppressed almost equally well by both stabilizers. The self-tuning PSS is able to provide good damping even when the constraints imposed by practical analog to digital and digital to analog converters are present.

5.7 Field Test Results

5.7.1 Implementing the Self-Tuning Algorithm on an Existing Digital PSS

Field tests of the self-tuning PSS were enabled by implementing the algorithms on a commercial digital PSS computer system. The recursive least squares identification and generalized minimum variance control algorithms required no changes to allow them run on the PSS computer. The source code for these algorithms was merely recompiled and the subroutines joining the algorithms to the transient stability program were replaced with calls to subroutines driving analog to digital and digital to analog converters. Algorithms providing smooth transfer between the standby and operating states were also added to the self-tuning PSS program.

The digital PSS systems used for the field tests are based on the PDP-11 processor family. Bench studies of the self-tuning PSS were performed on a system using the PDP-11/23 processor. This implementation required about 45 milliseconds to perform the calculations required by a fourth order self-tuning controller. Field tests of the self-tuning PSS employed a more powerful PDP-11/73 processor. This version required about 5 milliseconds to perform the same calculations. The simulation studies described earlier in this chapter indicate that satisfactory results can be obtained with sampling rates as low as 20 Hz so the computer used for the field tests can be used to implement high order self-tuning PSS's or, perhaps more complex self-tuning control algorithms.

The analog to digital and digital to analog converters on the digital PSS system had a resolution of 1 part in 4096. The effect of this degree of quantization is described in section 5.6.

The digital PSS system has a number of other features such as output limiters and watchdog timers that are necessary for secure operation. These features are important to the long-term unattended operation of the stabilizer but were not used in the field test results described here.

5.7.2 Results of Preliminary Tests of the Self-Tuning PSS on a Coal-Fired Generator

Preliminary field tests of the self-tuning PSS were performed as extra activity during the commissioning and tuning of a conventional digital PSS by Professor K. E. Bollinger. Time constraints made more extensive testing impossible but preliminary results obtained show that the self-tuning PSS can operate reasonably when operating with a real generator.

The self-tuning PSS was connected to one of two 400 Megawatt coal-fired generators at the power plant. A block diagram of the equipment used for the tests is shown in figure 5.23. The electric power signal used as the feedback signal for the self-tuning PSS was isolated, filtered and amplified before being applied to the analog to digital converter of the PSS. The analog output signal of the self-tuning PSS was isolated and fed to the stabilizer input of the AVR. A disturbance signal was generated by a manually-operated switch which applied a step change in the terminal voltage reference of the generator. This disturbance is similar to that used in the simulation studies presented in section 5.2. The electric power produced by the generator and the field voltage provided by the excitation system were recorded on a strip-chart recorder.

The analog to digital and digital to analog converters have a range of ±10 volts and a resolution of 1 part in 4096. In section 5.6 it was shown that the self-tuning PSS algorithm is only slightly affected by the quantization errors introduced by converters with this resolution.

At the time of the tests the generator was supplying 393 Megawatts (0.98 p.u.) of real power and −17 Megawatts (0.04 p.u.) of reactive power Because the generator was being operated near capacity the applied disturbance was quite small. Nevertheless the effect of the disturbance on the electric power produced by the generator was quite apparent.

The response of the generator with no PSS to the step change in the AVR reference voltage is shown in figure 5.24. The upper trace shows the electric power produced by the generator and the lower trace shows the generator field voltage. The chart

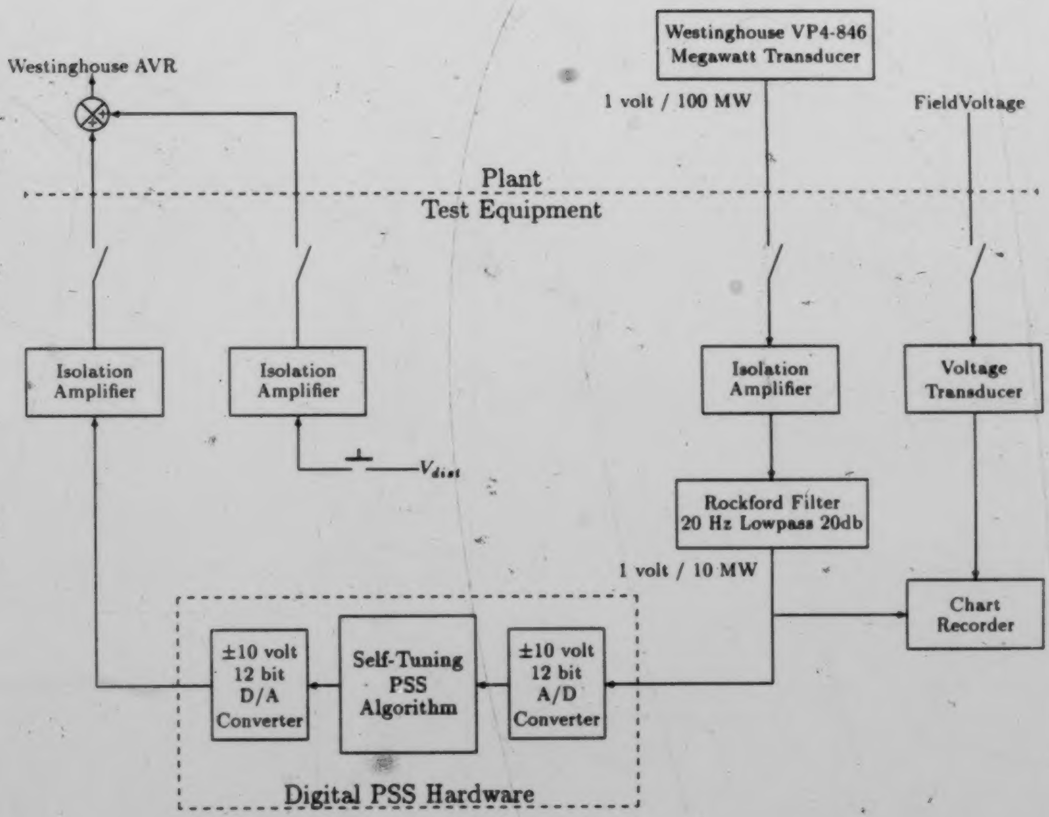
Westinghouse VP4-846
Megawatt Transducer
Westinghouse AVR
1 volt / 100 MW
FieldVoltage
Plant
Test Equipment
Isolation Amplifier
Isolation Amplifier
Isolation Amplifier
Voltage Transducer
V_{dist}
Rockford Filter
20 Hz Lowpass 20db
1 volt / 10 MW
Chart Recorder
±10 volt
12 bit
D/A
Converter
Self-Tuning
PSS
Algorithm
±10 volt
12 bit
A/D
Converter
Digital PSS Hardware

Figure 5.23: Block diagram of equipment used for field tests of self-tuning PSS.

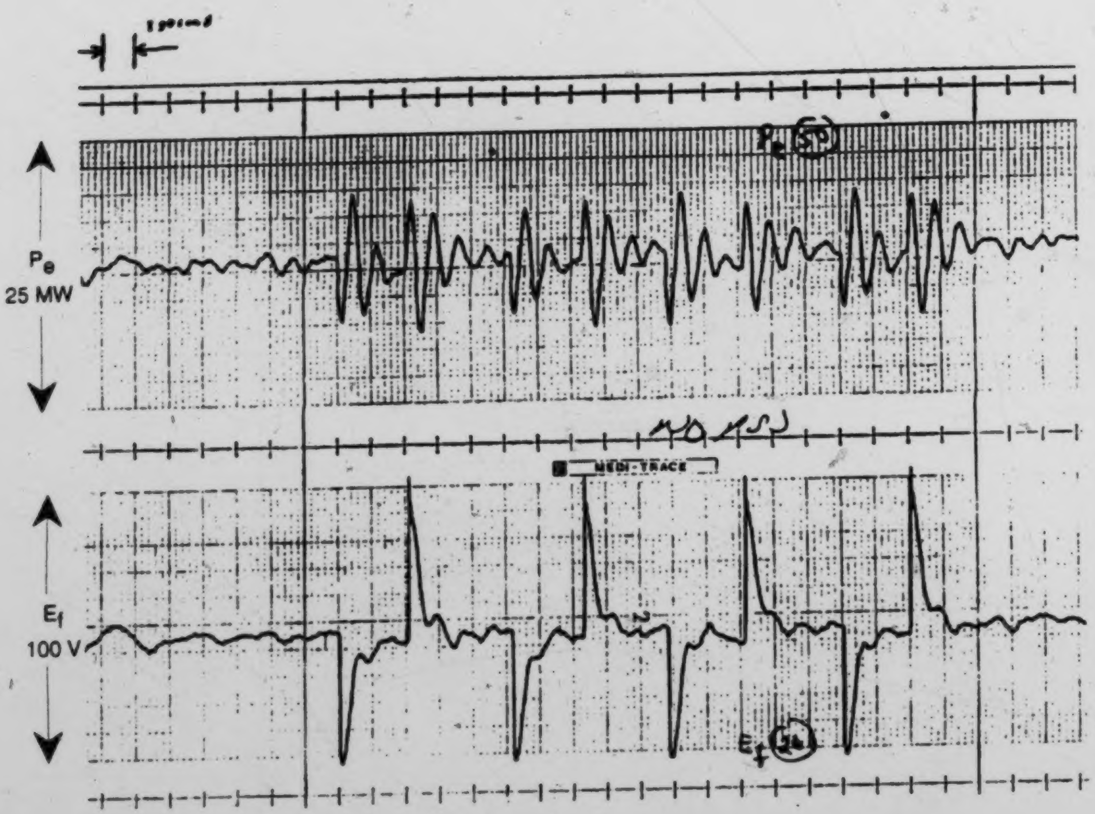

Figure 5.24: Generator electric power and field voltage transients with no PSS. 5 mm per second. Upper trace–Electric power. Lower trace–Field voltage.

speed was 5 mm per second so the tick marks along the sides of the chart correspond to a time interval of one second. The initial transients of the electric power are about 11 Megawatts peak-to-peak and are rather poorly damped.

The self-tuning PSS was then connected and the same disturbance was applied to the generator. The self-tuning PSS remained stable during the entire test even though the identification algorithm was given no initial information about the coefficients of the plant model. Improved damping of the electric power was noted as early as the

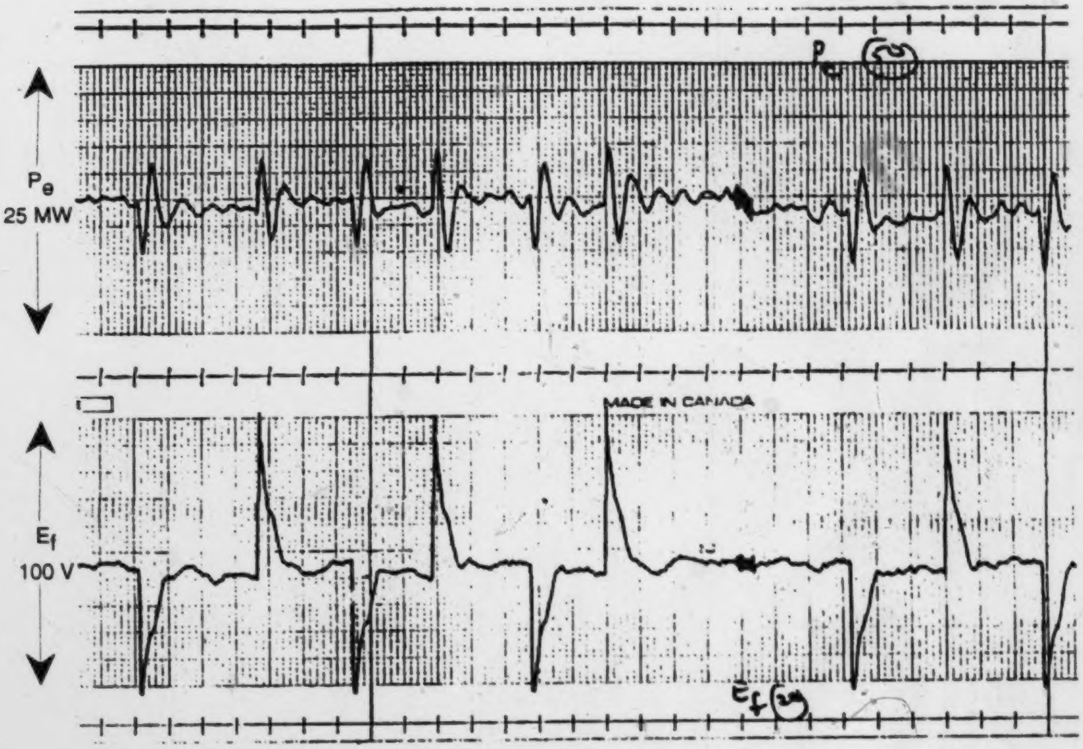

Figure 5.25: Generator electric power and field voltage transients with self-tuning PSS. 5 mm per second. Upper trace–Electric power. Lower trace–Field voltage.

application of the second step disturbance. After about a dozen disturbances had been applied to give the PSS time to tune itself the electric power and field voltage signals appeared as shown in figure 5.25. The improved damping provided by the self-tuning PSS is apparent from these traces. The initial transients of the electric power have been reduced to about 7 Megawatts peak-to-peak and are nearly completely damped after two cycles of oscillation.

These initial results are very encouraging but additional work is required to incorporate practical constraints imposed by the power system and to ensure fail-safe operation of the adaptive PSS. Among the requirements for long term, unattended operation are supervisory checks for PSS hardware failures or loss of feedback signals from the generator. Upon detection of such failure conditions the PSS must smoothly drive the control output to zero and generate an alarm condition.

Chapter 6

Summary and Conclusions

The main thrust of this research project was to develop techniques that would allow the generalized minimum variance self-tuning PSS to damp multiple oscillatory modes of a generator connected to a power generation and load pool. Several key areas were investigated and specific goals were attained.

The importance of a numerically stable method of updating the covariance matrix in the recursive least-squares parameter identification was illustrated. The UD-factorized covariance matrix update using single-precision calculations was found to give good results for covariance matrices as large as 10 × 10 elements. Covariance matrices of this size arise when forming fifth-order models of the plant to which the PSS is attached. The ability to perform calculations using single-precision values was critical to the practical implementation of the self-tuning PSS on existing digital stabilizer hardware.

A number of models of the two-machine infinite-bus simulated power system were formed and frequency response analysis of the simulated power system provided insight into the dynamics of the system as well as a standard against which the results of the time domain identification techniques could be compared. The frequency response of the simulated power system was determined using pseudo-random binary sequence excitation and harmonic, as opposed to spectral, analysis. The duration of these studies limit the practicality of the technique in field test conditions where the operating point of the generator or transmission and distribution network may well change during the course of the excitation and data acquisition. For example, the frequency response results presented in section 4.1 required a simulation run of over ten minutes of simulation time.

The offline time domain identification studies of the simulated power system, presented in section 4.2, showed that the bimodal nature of the system could be accurately identified if the excitation signal was filtered so as to provide a relatively flat power spectrum of the generator over the frequency range of interest. It was found that time domain identification using the basic least squares method was not able to identify the poles and zeros giving rise to the interarea oscillatory mode due to the low residues of this combination. Use of the generalized least squares method, which estimates the coefficients of all three polynomials in the ARMAX system model, produced a model exhibiting both the local and interarea modes. Neither of these points should adversely affect the application of the least squares identification algorithm in the self-tuning PSS since both points are addressed by the characteristics of the PSS itself. The filtering of the excitation signal is addressed by the action of the PSS which quickly tunes itself to damp the local oscillatory mode which would otherwise dominate the power spectrum of the generator output. The bias in the parameter estimates introduced by the basic least squares identification algorithm is exactly that required to produce the generalized minimum variance control action that would result from the generalized least squares identification of the full ARMAX model. This characteristic is an important feature of the self-tuning algorithm since the identification can be carried out using the simpler basic least squares method and yet the control action is that which would result from the identification, by the generalized least squares method, of the unbiased coefficients of the A and B polynomials and the true values of the C polynomial.

The results of simulation studies of the self-tuning PSS applied to the two-machine infinite-bus system are presented in sections 5.1 through 5.6. A noteworthy result was that the forgetting factor calculation proposed by Kulhavý [80] became unstable after several thousand steps. Calculation of the forgetting factor using a technique proposed by Sripada and Fisher [120], combined with the restricted exponential forgetting algorithm proposed by Hägglund [60] and Kulhavý [79], described in section 2.1.3 of this thesis, was found to remain stable over simulation studies as long as 25,000 samples, or over twenty minutes of simulation time, while still remaining alert to changes in the generator or network. A modification to the identification algorithm which inhibited the update of the parameter estimate when the generator terminal voltage had dropped by more than 30% from its nominal value was shown to be useful in preventing large, erroneous, parameter changes in response to major fault conditions. Modifications of this type to make the self-tuning PSS more robust are necessary for the practical implementation on real power systems.

The simulation studies indicated that the self-tuning PSS was capable of providing excellent damping of the local oscillatory mode and always contributed to some lessening of the lower frequency interarea oscillations. The self-tuning PSS was found to adapt promptly to the generator to which it was connected and to quickly provide good damping of the local oscillatory mode. A reduction in the magnitude of the interarea oscillation was also observed. This multimode damping was noted in simulation studies involving a number of different disturbances applied to the system. Damping of the interarea mode following a transient fault condition was shown to be improved by the use of additional feedback signals to the self-tuning PSS.

A practical result of the research presented here was the implementation of the self-tuning PSS algorithm on an existing commercial digital stabilizer system. The software development system allowed the program written for use with the transient stability program to be used on the digital stabilizer hardware with no changes to the source code implementing the generalized minimum variance control algorithm or the recursive least squares parameter identification. Simulation results presented in section 5.6 show that the control and parameter identification algorithms are not adversely affected by the quantization introduced by the 12-bit analog to digital and digital to analog converters employed by the digital stabilizer hardware.

The contribution of the research presented in this thesis is summarized as follows:

1. Techniques were developed and evaluated for a self-tuning PSS connected to a generator exhibiting both local and interarea oscillatory modes. Damping of both modes was noted in response to various system disturbances.

2. A number of methods for keeping the parameter identification alert by discount-

ing old information were evaluated. One particular method was found to give good results in both short and long simulation studies.

3. The effect of the quantization imposed by practical analog to digital and digital to analog converters was evaluated and shown to have little effect on the operation of the self-tuning PSS.

4. The algorithms were implemented on a commercial digital PSS system and were shown to operate reasonably well under field test conditions.

6.1 Recommendations for Further Research

Studies of the self-tuning PSS have shown a number of areas where further research is advisable.

The generalized minimum variance control algorithm exhibits good damping properties but is not completely self-tuning since the control action weighting factor, λ, has to be selected. Investigation into the use of more advanced control strategies, such as generalized predictive control [37, 38], may lead to true self-tuning action.

The encouraging preliminary results point to the need for more exhaustive field tests of the self-tuning PSS. Addition of supervisory and protection routines are necessary to allow secure unattended operation of the self-tuning PSS.

Operation of the self-tuning PSS when a number of machines are equipped with such stabilizers is also another area requiring further study.

Bibliography

[1] O. H. Abdalla, S. A. Hassan, and N. T. Tweig. Coordinated Stabilization of a Multimachine Power System. *IEEE Transactions on Power Apparatus and Systems*, 103:483–494, March 1984.

[2] S. Abe and A. Doi. A New Power System Stabilizer Synthesis in Multimachine Power Systems. *IEEE Transactions on Power Apparatus and Systems*, PAS-102(12):3910–3918, December 1983.

[3] Fernando L. Alvarado and Claudio Cañizares. Synchronous Machine Parameters from Sudden-Short Tests by Back-Solving. *IEEE Transactions on Energy Conversion*, EC-4(2):224–236, June 1989.

[4] K. J. Åström. Maximum Likelihood and Prediction Error Methods. In Peter Eykhoff, editor, *Trends and Progress in System Identification*, chapter 5, pages 145–168. Pergamon Press, 1981.

[5] K. J. Åström. Theory and Applications of Automatic Control—A Survey. *Automatica*, 19(5):471–486, May 1983.

[6] K. J. Åström, U. Borisson, L. Ljung, and B. Wittenmark. Theory and Application of Self-Tuning Regulators. *Automatica*, 13(5):457–476, September 1977.

[7] K. J. Åström and B. Wittenmark. On Self Tuning Regulators. *Automatica*, 9(2):185–198, February 1973.

[8] K. J. Åström and B. Wittenmark. Analysis of a Self-Tuning Regulator for Nonminimum Phase Systems. In *Proceedings of the IFAC Stochastic Control Symposium*, pages 165–173, Budapest, Hungary, 1974.

[9] J. C. Balda, R. E. Fairbairn, R. G. Harley, J. L. Rodgerson, and E. Eitelberg. Measurement of Synchronous Machine Parameters by a Modified Frequency Response Method — Part II: Measured Results. *IEEE Transactions on Energy Conversion*, EC-2(4):652–657, December 1987.

[10] J. C. Balda, M. F. Hadingham, R. E. Fairbairn, R. G. Harley, and E. Eitelberg. Measurement of Synchronous Machine Parameters by a Modified Frequency Response Method — Part I: Theory. *IEEE Transactions on Energy Conversion*, EC-2(4):646–651, December 1987.

[11] Ph. Barret, Y. Colot, M. Herouard, J. P. Meyer, J. Michard, and J. P. Monville. Modelling and Tests at Fessenheim Power Station of a 1080 MVA Turbogenerator and of its Excitation System. *IEEE Transactions on Power Apparatus and Systems*, 100:3993–4006, February 1981.

[12] Julius S. Bendat and Allan G. Piersol. *Random Data: Analysis and Measurement Procedures.* Wiley-Interscience, New York, 1971.

[13] Arthur R. Bergen. *Power Systems Analysis.* Prentice-Hall, Englewood Cliffs, NJ, 1986.

[14] G. J. Bierman. *Factorization Methods for Discrete Sequential Estimation.* Academic Press, New York, 1977.

[15] Gerald J. Bierman. Measurment Updating Using the U-D Factorization. *Automatica*, 12:375–382, 1976.

[16] Richard E. Blahut. *Theory and Practice of Error Control Codes.* Addison-Wesley, Reading, Mass., 1983.

[17] E. S. Boje, J. C. Balda, R. G. Harley, and R. C. Beck. Time-Domain Identification of Synchronous Machine Parameters From Simple Standstill Tests. *IEEE Transactions on Energy Conversion*, 5(1):164–175, March 1990.

[18] K. E. Bollinger. Field Verification of Exciter Models. Technical Report 304 T 639, Canadian Electrical Association, May 1990.

[19] K. E. Bollinger, R. Gilchrist, and E. Norum. A Digital Controller for Testing Control Strategy at Power Plants. In *1979 Power Industry Computer Applications Conference*, pages 260–266, March 1979.

[20] K. E. Bollinger, Wenyan Gu, and W. E. Norum. Accelerating Power Versus Electrical Power as Input Signals to Power System Stabilizers. In *IEEE/PES Winter Meeting*, February 1991. 91 WM 151-1 EC.

[21] K. E. Bollinger, H. S. Khalil, L. C. C. Li, and W. E. Norum. A Method for On-Line Identification of Power System Model Parameters in the Presence of Noise. *IEEE Transactions on Power Apparatus and Systems*, PAS-101(9):3105–3111, September 1982.

[22] K. E. Bollinger, H. S. Khalil, and W. E. Norum. Practical Identification Techniques for Excitation Systems. In *CEA Spring Meeting Part 5*, March 1980. 80-SP-170.

[23] K. E. Bollinger, A. Laha, R. Hamilton, and T. Harras. Power Stabilizer Design Using Root Locus Methods. *IEEE Transactions on Power Apparatus and Systems*, PAS-94(5):1484–1488, September 1975.

[24] K. E. Bollinger, A. K. Laha, and R. A. Winsor. System Models From Transient Stability Programs. In *IEEE PICA, New Orleans, Proceedings*, pages TP X11–6 330–334, July 1976.

[25] K. E. Bollinger and R. Lalonde. Tuning Synchronous Generator Voltage regulators Using On-Line Generator Models. *IEEE Transactions on Power Apparatus and Systems*, PAS-96(1):32–37, January 1977.

[26] K. E. Bollinger and J. C. Mathur. Identifying Power System Models Using State Space Techniques. *IEEE Transactions on Power Apparatus and Systems*, PAS-90(6):2598–2603, November 1971.

[27] K. E. Bollinger and A. F. Mistr Jr. PSS Tuning at the Virginia Electric and Power Co. Bath County Pumped Storage Plant. *IEEE Transactions on Power Systems*, 4(2):566–574, May 1989.

[28] K. E. Bollinger and R. Saunders. A Comparison of Power System Stabilizer Tuning Methods. Stabilizer tuning notes, 1979.

[29] K. E. Bollinger, R. Winsor, and A. Campbell. Frequency Response Methods for Tuning Stabilizers to Damp Out Tie-Line Power Oscillations: Theory and Field-Test Results. *IEEE Transactions on Power Apparatus and Systems*, PAS-98(5):1509–1515, September 1979.

[30] K. E. Bollinger, R. Winsor, and D. Cotcher. Power System Identification Using Noise Signals. *IEEE/PES Summer Meeting*, pages A76 339–2/1–7, July 1976.

[31] U. Borisson and R. Syding. Self-Tuning Control of an Ore Crusher. In *Proceedings of the IFAC Stochastic Control Symposium*, pages 491–495, Budapest, Hungary, 1974.

[32] F. Cameron and D. E. Seborg. A Self-Tuning Controller with a PID Structure. In *Proceedings of the IFAC Real Time Digital Control Applications Symposium*, pages 613–622, Guadalajara, Mexico, 1983.

[33] Shi-jie Cheng, Y. S. Chow, O. P. Malik, and G. S. Hope. An adaptive synchronous machine stabilizer. *IEEE Transactions on Power Systems*, PWRS-1(3):101–109, August 1986.

[34] Shi-jie Cheng, O. P. Malik, and G. S. Hope. Self-tuning stabiliser for a multimachine power system. *IEE Proceedings*, 133 Part C(4):176–185, May 1986.

[35] D. W. Clarke and P. J. Gawthrop. Self-tuning controller. *IEE Proceedings*, 122(9):929–934, September 1975.

[36] D. W. Clarke and R. Hastings-James. Design of digital controllers for randomly disturbed systems. *IEE Proceedings*, 118(10):1503–1506, October 1971.

[37] D. W. Clarke, C. Mohtadi, and P. S. Tuffs. Generalized Predictive Control—Part I. The Basic Algorithm. *Automatica*, 25(2):137–148, 1987.

[38] D. W. Clarke, C. Mohtadi, and P. S. Tuffs. Generalized Predictive Control—Part II. Extensions and Interpretations. *Automatica*, 25(2):149–160, 1987.

[39] W. D. J. Davies. *System Identification for Self-Adaptive Control.* Wiley-Interscience, New York, 1970.

[40] F. P. de Mello and L. N. Hannett. Determination of Synchronous Machine Electrical Characteristics by Test. *IEEE Transactions on Power Apparatus and Systems*, PAS-102(12):3810–3815, December 1983.

[41] F. P. de Mello, L. N. Hannett, D. W. Parkinson, and J. S. Czuba. A Power System Stabilizer Design Using Digital Control. *IEEE Transactions on Power Apparatus and Systems*, PAS-101(8):2860–329, August 1982.

[42] F. P. de Mello, L. N. Hannett, and J. M. Undrill. Practical Approaches to Supplementary Stabilizing from Accelerating Power. *IEEE Transactions on Power Apparatus and Systems*, PAS-97(5):1515–1522, September/October 1978.

[43] F. P. de Mello, P. J. Nolan, T. F. Laskowski, and J. M. Undrill. Coordinated application of stabilizers in multi-machine power systems. *IEEE Transactions on Power Apparatus and Systems*, PAS-99(3):892–901, May/June 1980.

[44] Fransisco P. de Mello and Charles Concordia. Concepts of Synchronous Machine Stability as Affected by Excitation Control. *IEEE Transactions on Power Apparatus and Systems*, PAS-88(4):316–329, April 1969.

[45] Digital Equipment Corporation. *Microcomputers and Memories.* Maynard, Massachusetts, 1981.

[46] H. W. Dommel and N. Sato. Fast Transient Stability Solutions. *IEEE Transactions on Power Apparatus and Systems*, PAS-91:1643–1650, July/August 1972.

[47] J. J. Dongarra, C. B. Moler, J. R. Bunch, and G. W. Stewart. *LINPACK Users' Guide.* Society for Industrial and Applied Mathematics, Philadelphia, 1979.

[48] P. Eykhoff. A Bird's Eye View on Parameter Estimation and System Identification. *Automatisierungstechnik*, 36(11):413–420, November 1988.

[49] Peter Eykhoff, editor. *Trends and Progress in System Identification.* Pergamon Press, 1981.

[50] J. Y. Fan, T. H. Ortmeyer, and R. Mukundan. Power System Stability Improvement with Multivariable Self-Tuning Control. *IEEE Transactions on Power Systems*, 5(1):227–234, February 1990.

[51] T. R. Fortescue, L. S. Kershenbaum, and B. E. Ydstie. Implementation of Self-Tuning Regulators with Variable Forgetting Factors. *Automatica*, 17(6):831–835, June 1981.

[52] J. J. Sanchez Gasca, C. J. Bridenbaugh, C. E. J. Bowler, and J. S. Edmonds. Trajectory Sensitivity Based Identification of Synchronous Generator and Excitation System Parameters. *IEEE Transactions on Power Systems*, 3(4):1814–1822, November 1988.

[53] Nezih C. Geçkinli and Davras Yavuz. *Discrete Fourier Transformation and its Applications to Power Spectra Estimation.* Elsevier Scientific Publishing Company, Amsterdam, 1983.

[54] A. Ghosh, G. Ledwich, O. P. Malik, and G. S. Hope. Power system stabilizer based on adaptive control techniques. *IEEE Transactions on Power Apparatus and Systems*, PAS-103(8):1983–1989, August 1984.

[55] G.C. Goodwin and R.L. Payne. *Dynamic System Identification: Experiment Design and Data Analysis.* Academic Press, New York, 1977.

[56] Wenyan Gu. *Multivariable Self-Tuning Control of Synchronous Generator Systems.* PhD thesis, University of Alberta, Edmonton, Alberta, 1989.

[57] Wenyan Gu and K. E. Bollinger. A Self-Tuning Power System Stabilizer for Wide-Range Synchronous Generator Control. *IEEE Transactions on Power Systems*, 4(3):1191–1199, August 1989.

[58] Lei Guo. Estimating Time-Varying Parameters by the Kalman Filter Based Algorithm: Stability and Convergence. *IEEE Transactions on Automatic Control*, 35(2):141–147, February 1990.

[59] Lei Guo and Han-Fu Chen. The Åström–Wittenmark Self-Tuning Regulator Revisited and ELS-Based Adaptive Trackers. *IEEE Transactions on Automatic Control*, 36(7):802–812, July 1991.

[60] T. Hägglund. The Problem of Forgetting Old Data in Recursive Estimation. In I. D. Landau, editor, *Proceedings of the IFAC Workshop on Adaptive Systems in Control and Signal Processing*, pages 213–214, San Francisco, USA, 1983. Pergamon Press.

[61] J. F. Hauer, C. J. Demeure, and L. L. Scharf. Initial Results in Prony Analysis of Power System Response Signals. *IEEE Transactions on Power Systems*, 5(1):80–89, February 1990.

[62] J. F. Hauer and F. Vakili. An Oscillation Detector Used in the BPA Power System Disturbance Monitor. *IEEE Transactions on Power Systems*, 5(1):74–79, February 1990.

[63] J. Hetthéssy and L. Keviczky. Some Innovations to the Minimum Variance Control. In *Proceedings of the IFAC Stochastic Control Symposium*, pages 353–361, Budapest, Hungary, 1974.

[64] Takashi Hiyama. Rule-Based Stabilizer for Multi-Machine Power System. *IEEE Transactions on Power Systems*, 5(2):403–411, May 1990.

[65] Yuan-Yih Hsu and Chao-Rong Chen. Tuning of Power Systems Stabilizers Using and Artificial Neural Network. In *IEEE/PES Winter Meeting*, pages 91 WM 152-9 EC, February 1991.

[66] Pei-Hwa Huang and Yuan-Yih Hsu. Eigenstructure Assignment in a Longitudinal Power System via Excitation Control. *IEEE Transactions on Power Systems*, 5(1):96–101, February 1990.

[67] IEEE Standard 100. *Standard Dictionary of Electrical and Electronics Terms.* IEEE, New York, NY, fourth edition, November 1988.

[68] IEEE Standard 115. *Test Procedures for Synchronous Machines.* IEEE, New York, NY, September 1983.

[69] IEEE Task force on Definitions. Supplementary definitions and associated test methods for obtaining parameters for synchronous machine stability study for simulations. *IEEE Transactions on Power Apparatus and Systems*, PAS-99(4):1625–1633, July/August 1980. P. L. Dandeno, Chair.

[70] IEEE Task force on Definitions. Current usage & suggested practices in power system stability simulations for synchronous machines. *IEEE Transactions on Energy Conversion*, EC-1(1):77–93, March 1986. P. L. Dandeno, Chair.

[71] F. Irving, J. P. Barret, C. Charcossey, and J. P. Monville. Improving Power Network Stability and Unit Stress with Adaptive Generator Control. *Automatica*, 15(1):31–46, January 1979.

[72] F. Ishiguro, S. Tanaka, M. Shimomura, T. Maeda, K. Matsushita, and H. Sugimoto. Coordinated stabilizing control of exciter, turbine and braking resistor. *IEEE Transactions on Power Systems*, PWRS-1(3):74–80, August 1986.

[73] I. Kamwa, P. Viarouge, and E. J. Dickinson. Optimal Estimation of the Generalized Operational Impedances of Synchronous Machines from Short-Circuit Tests. In *IEEE/PES Winter Meeting*, February 1990. 90 WM 088-5 EC.

[74] Jagannathan Kanniah, O. P. Malik, and G. S. Hope. Excitation control of synchronous generators using adaptive control–parts i and ii. *IEEE Transactions on Power Apparatus and Systems*, PAS-103(5):897–910, May 1984.

[75] E. Ya. Kazovskii and L. G. Lerner. Procedure for Determining the Electromagneteic Parameters of a Synchronous Machine Operating under Load. In *Scientific Council on Theoretical and Electrophysical Problems of Electric Power Engineering.* Academy of Sciences of the USSR in Leningrad, December 1974.

[76] A. Keyhani and S. M. Miri. Obervers for Tracking of Synchronous Machine Parameters and Detection of Incipient Faults. *IEEE Transactions on Energy Conversion*, EC-1(2):184–192, June 1986.

[77] Ali Keyhani, Shangyou Hao, and Richard P. Schulz. Maximum Likelihood Estimation of Generator Stability Constants using SSFR Test Data. In *IEEE/PES Winter Meeting*, February 1990. 90 WM 005-9 EC.

[78] R. Kulhavý. Restricted Exponential Forgetting in Real-Time Identification. In *Proceedings of the 7th IFAC/IFORS Symposium on Identification and System Parameter Estimation*, pages 1143–1148, York, UK, 1985.

[79] R. Kulhavý and M. Kárný. Tracking of Slowly Varying Parameters by Directional Forgetting. In *Proceedings of the IFAC 9th Triennial World Congress*, pages 687–692, Budapest, Hungary, 1984.

[80] Rudolf Kulhavý. Restricted Exponential Forgetting in Real-Time Identification. *Automatica*, 23(5):589–600, 1987.

[81] A. K. Laha and K. E. Bollinger. Power-Stabiliser Design using Pole-Placement Techniques on Approximate Power-System Modles. *IEE Proceedings*, 122(9):903–907, September 1975.

[82] R. D. Lang, M. A. Hutchison, and H. Yee. Microprocessor-based identification system applied to synchronous generators with voltage regulators. *IEE Proceedings*, 130 Pt. C(5):257–265, September 1983.

[83] E. V. Larsen and D. A. Swann. Applying Power System Stabilizers, Parts I, II and III. *IEEE Transactions on Power Apparatus and Systems*, PAS-100(6):3017–3046, June 1981.

[84] L. X. Le and W. J. Wilson. Synchronous Machine Parameter Identification: A Time Domain Approach. *IEEE Transactions on Energy Conversion*, 3(2):241–248, June 1988.

[85] C. C. Lee and Owen T. Tan. A Weighted-Least-Square Parameter Estimator for Synchronous Machines. *IEEE Transactions on Power Apparatus and Systems*, PAS-96(1):97–101, January/February 1977.

[86] Choo-Min Lim and S. Elangovan. A New Stabilizer Design Technique for Multimachine Power Systems. *IEEE Transactions on Power Apparatus and Systems*, 104(9):2393–2400, September 1985.

[87] L. Ljung. *System Identification—Theory for the User*. Prentice-Hall, Englewood Cliffs, N.J., 1987.

[88] Lennart Ljung. Analysis of a General Recursive Prediction Error Identification Algorithm. *Automatica*, 17(1):89–99, January 1981.

[89] Lennart Ljung and Björn Wittenmark. Analysis of a Class of Adaptive Regulators. In *Proceedings of the IFAC Stochastic Control Symposium*, pages 431–437, Budapest, Hungary, 1974.

[90] Lennart Ljung and Keith Glover. Frequency Domain Versus Time Domain Methods in System Identification. *Automatica*, 17(1):71–86, January 1981.

[91] C. Maffezzoni and V. Marchese. Structural Parameter Estimation in Power Systems. *Automatica*, 17(1):263–279, January 1981.

[92] O. P. Malik, G. S. Hope, and A. A. M. El-Ghandakly. A Technique for Coordinated On-Line Control of Exciter and Governor. *Journal of Applied Science and Engineering*, 3:39–55, 1978.

[93] Gerald Manchur, David C. Lee, M. E. Coultes, J. D. A. Griffin, and Wilfred Watson. Generator Models Established by Frequency Response Tests on a 555 MVA machine. *IEEE Transactions on Power Apparatus and Systems*, 91:2077–2084, 1972.

[94] Yakout Mansour. Application of Eigenanalysis to the Western North American Power System. In *Eigenanalysis and Frequency Domain Methods for System Dynamic Performance*, pages 97–103. IEEE Power Engineering Society, 1990. 90TH0292-3-PWR.

[95] The MATH WORKS Inc., 21 Eliot Street, South Natick, MA. *MATLAB User's Guide*, 3.5f edition, June 1989.

[96] Jean-Claude Maun. Comparison Between Identification Methods of Synchronous Machine Dynamic Parameters. In *Proceedings of the 1987 Summer Computer Simulation Conference*, pages 145–150, Montreal, Quebec, July 1987.

[97] Hamdy A. M. Moussa and Yao-nan Yu. Optimal Power System Stabilization Through Excitation and/or Governor Control. *IEEE Transactions on Power Apparatus and Systems*, 91(3):1166–1174, May/June 1972.

[98] M. Namba, T. Nishiwaki, S. Yokokawa, and K. Ohtsuka. Identification of Parameters for Power System Stability Analysis Using Kalman Filter. *IEEE Transactions on Power Apparatus and Systems*, PAS-100(7):3304–3311, July 1981.

[99] E. H. Okongwu, W. J. Wilson, and J. H. Anderson. Microalternator stabilization using a physically realizable optimal output feedback controller. *IEEE Transactions on Power Apparatus and Systems*, PAS-101(10):3771–3779, October 1982.

[100] D. W. Olive. New Techniques for the Calculation of Dynamic Stability. *IEEE Transactions on Power Apparatus and Systems*, PAS-85(7):767–777, July 1966.

[101] D. W. Olive. Digital Simulation of Synchronous Machine Transients. *IEEE Transactions on Power Apparatus and Systems*, PAS-87(8):1669–1675, August 1968.

[102] F. Luis Pagola, Luis Rouco, and Ignacio J. Pérez-Arriaga. Analysis and Control of Small Signal Stability in Electric Power Systems by Selective Modal Analysis. In *Eigenanalysis and Frequency Domain Methods for System Dynamic Performance*, pages 77–96. IEEE Power Engineering Society, 1990. 90TH0292-3-PWR.

[103] R. H. Park. Two-Reaction Theory of Synchronous Machines, Generalized Method of Analysis — Part I. *Transactions of the American Institute of Electrical Engineers*, 48(3):716–730, 1929.

[104] R. H. Park. Two-Reaction Theory of Synchronous Machines — II. *Transactions of the American Institute of Electrical Engineers*, 52(2):352–355, 1933.

[105] D. A. Pierre. A perspective on adaptive control of power systems. *IEEE Transactions on Power Systems*, PWRS-2(2):387–396, May 1987.

[106] R. Podmore and R. J. Fleming. Power-System Dynamic Simulation Program. *IEE Proceedings*, 121(10):1165–1167, October 1974.

[107] V. H. Quintana, M. A. Zohdy, and J. H. Anderson. On the Design of Output Feedback Excitation Controllers of Synchronous Machines. *IEEE Transactions on Power Apparatus and Systems*, 95:954–961, May/June 1976.

[108] J. Richalet. The Model Method. In Peter Eykhoff, editor, *Trends and Progress in System Identification*, chapter 1, pages 5–28. Pergamon Press, 1981.

[109] G. J. Rogers and P. Kundur. Small Signal Stability of Power Systems. In *Eigenanalysis and Frequency Domain Methods for System Dynamic Performance*, pages 5–16. IEEE Power Engineering Society, 1990. 90TH0292-3-PWR.

[110] P. A. E. Rusche, G. J. Brock, L. N. Hannett, and J. R. Willis. Test and Simulation of Network Dynamic Response Using SSFR and RTDR Derived Synchronous Machine Models. *IEEE Transactions on Energy Conversion*, 5(1):145–155, March 1990.

[111] Mario E. Salgado, Graham C. Goodwin, and Richard H. Middleton. Modified Least Squares Algorithm Incorporating Exponential Resetting and Forgetting. *International Journal of Control*, 47(2):477–491, 1988.

[112] P. W. Sauer, C. Rajagopalan, and M. A. Pai. An Explanation and Generalization of the AESOPS and PEALS Algorithms. In *IEEE/PES Winter Meeting*, Atlanta, Georgia, February 1990. 90 WM 239-4 PWRS.

[113] Dale E. Seborg, Thomas F. Edgar, and Duncan A. Mellichamp. *Process Dynamics and Control*. John Wiley and Sons, New York, 1989.

[114] Sirish L. Shah and William R. Cluett. Recursive Least Squares Based Estimation Schemes for Self-Tuning Control. *Canadian Journal of Chemical Engineering*, 69:89–96, February 1991.

[115] M. M. Sharaf and B. W. Hogg. Evaluation of Online Identification Methods for Optimal Control of a Laboratory Model Turbogenerator. *IEE Proceedings*, 128 Part D(2):65–73, March 1981.

[116] S. M. Z. Sharaf, B. W. Hogg, O. H. Abdalla, and M. L. El-Sayed. Multivariable Adaptive Controller for a Turbogenerator. *IEE Proceedings Part D*, 133(2):83–89, March 1986.

[117] K. S. Sin and G. C. Goodwin. Checkable Conditions for Identifiability of Linear Systems Operating in Closed Loop. *IEEE Transactions on Automatic Control*, 25(4):722–729, August 1980.

[118] T. Söderström and P. Stoica. *System Identification*. Prentice-Hall International, London, 1989.

[119] S. Sriharan and K. W. Hiong. Synchronous Machine Modelling by Standstill Frequency Response Tests. *IEEE Transactions on Energy Conversion*, EC-2(2):239–245, June 1987.

[120] N. Rao Sripada and D. Grant Fisher. Improved Least Squares Identification. *International Journal of Control*, 46(6):1889–1913, 1987.

[121] P. Stoica and A. Nehoria. On the Uniqueness of Prediction Error Models for Systems with Noisy Input-Output Data. *Automatica*, 23:541–543, 1987.

[122] Vladimír Strejc. Trends in Identification. *Automatica*, 17(1):7–21, January 1981.

[123] V. Subbarao, R. E. Burridge, and R. D. Findlay. Mathematical Models of Synchronous Machines for Dynamic Studies. In *IEEE PES Winter Meeting*, February 1979. A 79 011-8.

[124] E. Swidenbank, I. Boyd, and B. W. Hogg. On-Line Identification of Large Turbogenerators. *6th European Conference on Electrotechnics, Eurocon 84—Computers in Communication and Control*, pages 74–78, 1984.

[125] Catherine L. Thornton and Gerald J. Bierman. UDU^T Covariance Factorization for Kalman Filtering. In C. T. Leondes, editor, *Control and Dynamic Systems Advances in Theory and Application*, pages 177–258. Academic Press, 1980.

[126] D. J. Trudnowski, J. R. Smith, T. A. Short, and D. A. Pierre. An Application of Prony Methods in PSS Design for Multimachine Systems. In *IEEE/PES Winter Meeting*, Atlanta, Georgia, February 1990. 90 WM 117-2 PWRS.

[127] H. B. Verbruggen. Pseudo Random Binary Sequences. *Journal A*; 16(4):205-207, 1975.

[128] Peter E. Wellstead. Non-Parametric Methods of System Identification. *Automatica*, 17(1):55–69, January 1981.

[129] W. J. Wilson, V. M. Raina, and J. H. Anderson. Nonlinear Output Feedback Excitation Controller Design Based on Nonlinear Optimal Control and Identification Methods. *IEEE/PES Summer Meeting*, pages A76 343-4/1-9, July 1976.

[130] Daozhi Xia and G. T. Heydt. Self-tuning controller for generator excitation control. *IEEE Transactions on Power Apparatus and Systems*, PAS-102(6):1877-1885, June 1983.

[131] Peter Young. Parameter Estimation for Continuous-Time Models—A Survey. *Automatica*, 17(1):23–39, January 1981.

[132] Yao-nan Yu and Qing-hua Li. Pole-Placement Power System Stabilizers Design of an Unstable Nine-Machine System. *IEEE Transactions on Power Systems*, 5(2):353–358, May 1990.

[133] Yao-nan Yu and Hamdy A. M. Moussa. Optimal Stabilization of a Multi-Machine System. *IEEE Transactions on Power Apparatus and Systems*, 91(3):1174–1182, May/June 1972.